Nanophotonics of Organic Molecular Waveguides: Towards Active Optical Antenna

A thesis

submitted in partial fulfilment of the requirements
for the degree of Doctor of Philosophy

by

Ravi P.N. Tripathi
(Reg ID: 2012-3217)

INDIAN INSTITUTE OF SCIENCE EDUCATION AND RESEARCH,
PUNE

CERTIFICATE

Certified that the work incorporated in the thesis entitled ("Nanophotonics of Organic Molecular Waveguides: Towards Active Optical Antenna") Submitted by **Ravi P. N. Tripathi** was carried out by the candidate, under my supervision. The work presented here or any part of it has not been included in any other thesis submitted previously for the award of any degree or diploma from any other University or institution.

Date: (Supervisor)

Declaration

I declare that this written submission represents my research work in my own words and where others' ideas or works have been included, I have adequately cited and referenced the original sources. I also declare that I have adhered to all principles of academic honesty and integrity and have not misrepresented or fabricated or falsified any idea/data/fact/source in my submission. I understand that violation of the above will be cause for disciplinary action by the Institute and can also evoke penal action from the sources which have thus not been properly cited or from whom proper permission has not been taken when needed.

Date: (Signature)

Ravi P.N. Tripathi

Reg. No: 2012-3217

Abstract

Photons resides at the heart of nanophotonics and controlling freely propagating photons at nanoscale is an important aspects in these applications. This effective control over optical field at nanoscale has relevance in all scientific domains such as optical communications, biomedical and quantum computing etc. All these nanophotonic applications bank on photons as an information carrier. At the same time, an additional challenge has appeared for practical realization of nanoscale information technology: how to effectively communicate the optical energy to other coupled nanostructures. In recent years, micro- and nanowire antenna have been investigated to explore this aspect, however most of these investigations are confined to plasmonic nanostructures. There are few concerns (heating and propagation loss, CMOS compatibility, efficiency and flexibility etc.) associated with conventional plasmonic materials therefore, organic nanostructures have been explored as an alternative candidates for photonic applications. To utilize organic nanostructures for signal processing devices both in active and passive domains, it is imperative to investigate directional emission of out-coupled photons. Additionally, it is vital to study the influence of plasmonic/dielectric coupling on directional emission of the individual organic nanostructures .

To address all these issues, herein, we explore the directional emission from one dimensional organic nanostructures in different operational regime. We further extend our investigation on the influence of dielectric microstructure coupling for directing the out-coupled photon emission and demonstrate how to use dielectric microsphere as an active element for tuning the spectral feature of out-coupled photon. Moreover, we vertically couple organic nanowire (1D) with plasmonic substrate (2D) to efficiently channelling of exciton-polaritons to a leaky plasmonic substrate. Finally, we demonstrate the effect of near-field coupling on plasmons assisted directional emission.

List of Publications

Included in thesis:

- Optics of an individual organic molecular mesowire waveguide : Directional light emission and anomalous refractive index; **Ravi P.N. Tripathi**, Arindam Dasgupta, Rohit Cikkaraddy, Partha. P. Patra, Adarsh B.Vasista and G.V. Pavan Kumar, *Journal of Optics (IOP)*, 18, 065002 (2016). (Chosen for Paper of the week)

- Directional exciton-polariton photoluminescence emission from terminals of a microsphere-coupled organic waveguide; **Ravi P.N. Tripathi**, Rohit Cikkaraddy, Arindam Dasgupta and G. V. Pavan Kumar, *Applied Physics Letters*, 108, 031102 (2016).

- Radiative Channelling of Nanowire Frenkel Exciton-Polaritons through Surface Plasmons; **Ravi P.N. Tripathi**, Adarsh B. Vasista, Rohit Cikkaraddy and G. V. Pavan Kumar, *Advanced Optical Materials*, in press(2016).

Not included in thesis:

- Plasmon-controlled Excitonic Emission from Vertically-Tapered Organic Nanowires; Rohit Cikkaraddy, Partha P. Patra, **Ravi P.N. Tripathi**, Arindam Dasgupta and G.V. Pavan Kumar, *Nanoscale*, 8, 14803-14808 (2016).

- Directional Fluorescence Emission Mediated by Chemically-Prepared Plasmonic Nanowire Junctions; Arindam Dasgupta, Danveer Singh, **Ravi P.N. Tripathi**, and G. V. Pavan Kumar, *J. Phys. Chem. C*, 120 ,17692-17698 (2016).

- Large-scale dynamic assembly of metal nanostructures in plasmofluidic field; G. V. Pavan Kumar, Danveer Singh, Partha Pratim Patra and **Ravi P.N. Tripathi**, *Faraday Discussion*, 186, 95-106 (2016).

- Directional Out-Coupling of light from Plasmonic Nanowire-Nanoparticle Junction; Danveer Singh, Arindam Dasgupta, Aswathy V.G., **Ravi P.N. Tripathi**, and G. V. Pavan Kumar, *Optics Letters*, 40, 1006-1009 (2015).

- Plasmofluidic Single-Molecule Surface Enhanced Raman Scattering from Dynamic Assembly of Plasmonic Nanoparticles; Partha P. Patra, Rohit Chikkaraddy, **Ravi P.N. Tripathi**, Arindam Dasgupta and G.V. Pavan Kumar, *Nature Communications*, 5, 4357 (2014).

- Remote-Excitation Surface Enhanced Raman Scattering with Counter-Propagating Plasmons: Silver Nanowire-Nanoparticle System; Arindam Dasgupta, Danveer Singh, Shreyash Tandon, **Ravi P.N. Tripathi**,and G. V. Pavan Kumar, *Journal of Nanophotonics*, 8, 083899 (2014)

- Exciton Emission Intensity Modulation of Monolayer MoS_2 via Au Plasmon Coupling; B. Mukherjee, N. Kaushik, **Ravi P. N. Tripathi**, A. M. Joseph, P. K. Mohapatra, S. Dhar, B. P. Singh, G. V. Pavan Kumar, E. Simsek and S. Lodha, *Nature Scientific Report*, In press (2016).

Acknowledgements

Life as a Research Fellow would never be pleasant without continuous assistance and proper direction by many people. Today, when I am on the verge of finishing the journey, I would like to express my gratitude for those people.

First of all, I would like to thank my supervisor *Dr. G. V. Pavan Kumar* for providing me an opportunity to work in his laboratory. His energetic and encouraging approach towards solving a scientific problem is always inspiring. He has been a continuous source of fascinating and innovative ideas. The most enjoyable thing in the lab is independence, both in the terms of lab working hours and choosing the scientific problem. This aspect facilitated me to think independently and originally. Inclusion of all these things made my journey immensely joyful. I would also like to thank to my RAC members *Dr. Souvik Datta* and *Dr. Angsuman Nag*. Their valuable feedbacks and intuitive suggestions in regular RAC meet have helped me in profound understanding of the topic and guiding my thesis in appropriate direction.

Next, I would like to acknowledge all the technical staff especially *Mr. Nilesh Dumbre*, *Mr. Prashant Kale* and *Mr. Anil Shetty* for assisting me in all possible manner. Their exceptional assistance in terms of teaching different techniques (EBL, Photolithography, Sputtering, and thermal evaporation) and giving their valuable inputs have assisted me to work confidently even in unofficial hours.

Successful journey of a PhD student is directly proportional to assistance of lab members. Therefore, I would like to thank my lab seniors *Arindam Dasgupta* and *Partha Pratim Patra* (now I should call them *Dr. Arindam Dasgupta* and *Dr. Partha Pratim Patra*). Their experiences and valuable suggestions have always assisted me not only in research work but also to grow as a modest person.

Rohit Chikkaraddy was an undergraduate student when I joined the lab. However, his knowledge and research experience was never less than a senior. Additionally, I am also thankful to integrated PhD students *Adarsh Vasista*, *Deepak Sharma Shailendra Chaubey*, *Sunny Tiwari* and two BS.MS. students *Harshvardhan Jog*, *Rajat Sawant* to manage some time for discussing on variety of research as well as social topics. I am thanking to them for correct me whenever I would be wrong in any of these topics.

While working and discussing with these people, I didn't realize when they have became my good friends.
I am also grateful to past and present lab colleagues, *Danveer Singh, Aswathy, Jesil, Sreeja, Vandana* and *Dr. Debrina Jana*, for their direct and indirect input in my PhD work.
Success of PhD life can never be concluded without acknowledgement of hostel-friends, *Aditya Mehra, Aditi Nandi, Sneha Banerjee, Kunal Kothekar, Shishir, Nistha, Sanku, Rabindranath, Rohit Kumar, Rejaul, Sunil, Soumendranath, Gunjan* and *Rohit Babar*. Friends are the evergreen source to learn novel things in life. However, some friends leave their enduring impact especially, *Aditya, Aditi, Sneha* and *Kunal*, who are uniquely nice people with down to earth nature. They have always been there for me in every facets of the whole journey.
I acknowledge *Ministry of Human Resource Development (MHRD), India* and *IISER Pune, India*, for providing me the fellowship and other financial support during my research work.
Last but the most vital, I would like to acknowledge those people, who always work in the background. However, their support has always been there for me. In this sequence, first of all, I would like to acknowledge *Ms. Darshika Tomer* and my younger brother *Mr. Shiv P. N. Tripathi* for their love, encouragement and support. Finally, I would like to sincerely acknowledge my parents for motivating me towards research and supporting me in every front of life.

Dedicated to my parents...

Contents

Chapter 1

Introduction

Nanophotonics, bridging the realms of nanotechnology and optics primarily concentrates on the investigation of light-matter interaction at subwavelength scale [1, 2]. In all the nanophotonics' applications, controlling optical field below the diffraction limit, is always an important question to be addressed. The effective answer of this question has relevance in all avenues of science and technology ranging from physics, chemistry and materials science to biological science [1–4]. Till date, the comprehensive understanding of light-matter interaction has revolutionized various scientific domains such as optical communications [5, 6], nanoscale sensor devices[7], molecular spectroscopy[8], imaging methods[9] and quantum optics[10, 11]. Moreover effective manipulation of light at nanoscale has opened up the prospect of exploiting photons as an information carrier in the dense integrated opto-electronic and nanophotonics circuits [5, 6, 12]. Photon, as an information carrier, has the potential to meet the ever increasing demand of transmission speed, high band-width, and information density [12]. Therefore, accomplishing these requirements will proficiently revamp the associated applications in the field of biomedical [13–15], computing [16, 17], information and communication technology [5, 6].

Light manipulation at nanoscale is always a challenging task. To explore this possibility, a variety of scheme have been deployed so far such as photonics crystal fibers [1], optical waveguides [18, 19], micro-resonators [20, 21], metallic and molecular nanoarchitectures[19, 22, 23]. Out of these, only metallic and molecular nanostructures facilitates the confinement and propagation of optical field below the diffraction limits. In view of all these applications, it is found that controlling an optical field principally relies on the collective response of charge particle oscillations created at the surface of nanostructures. In other words, when the light interacts with nanoscale geometry, the free charge present at the surface cloud starts oscillations and result either in the form of multi-fold localized field or propagating field depending on the geometry. These surface waves are converted back to freely propagating photons at the point of discontinuity or defects. Surface wave excitations can be categorised into two parts: plasmons

and excitons. In general terms, plasmons are regarded as collective oscillation of free electron cloud, whereas excitons are considered as collective response of electron-hole pair. Importantly, plasmons play a crucial role in deciding properties of metallic nanostructures, while molecular nanostructure's properties are predominantly determined by excitons. We would sequentially discuss both type of surface excitations and their applications. In the following section, we would be discussing the plasmonics, associated applications and their limitations.

1.1 Plasmonic nano-architectures

Plasmons are the collective oscillation of free electron cloud present at metallic nanostructures' surface. Optical wave can couple to these charge cloud, either in form of propagating field or localized field, depending on their geometry [2, 4]. In the recent years, plasmons have emerged as an important candidate for sub-wavelength light propagation or localization [24]. Moreover, the field manipulation can be achieved at less than classical diffraction limit of electromagnetic field i.e. Abbe's diffraction limit ($< \lambda/2$, where λ is excitation wavelength) [2, 12]. The extraordinary feature of squeezing the light in such a small scale has opened up new prospects of investigating light-matter interaction in a more controlled fashion. To exploit this ability, variety of nanostructures have been synthesized or fabricated using bottom-up (sphere, cubes, triangle and rods) [25, 26] as well as top-down (metamaterials, metasurface, NPs periodic assembly) [25, 27] approaches. The optical properties of these plasmonic structures can be classified in two type of excitations on the basis of their geometry: resonant and non-resonant. The properties of resonant plasmonic structures are mainly directed by localized surface plasmons (LSP) [28, 29], whereas non-resonant plasmonic structures' properties are influenced by surface plasmon polaritons (SPPs)[30, 31].

1.1.1 Localized surface plasmons

Localized surface plasmons are non-propagating excitation of conduction electron in volumetrically confined plasmonic nanostructures coupled to external electromagnetic radiation [28, 29, 31]. These non-propagating plasmons excitation occurs due to confinement of conduction electron within a tiny volume (shown in figure 1.1). Considering the most simple geometry: spherical nanoparticle of diameter d and $d << \lambda$, where λ is wavelength of incident optical field. When the nanoparticle interacts with this optical field, it gets polarized and opposite charges get accumulated at both end of nanoparticle surface, which provide the required restoring force for sustaining coupled oscillation by Columbic interaction. Under this configuration, whenever the resonance condition

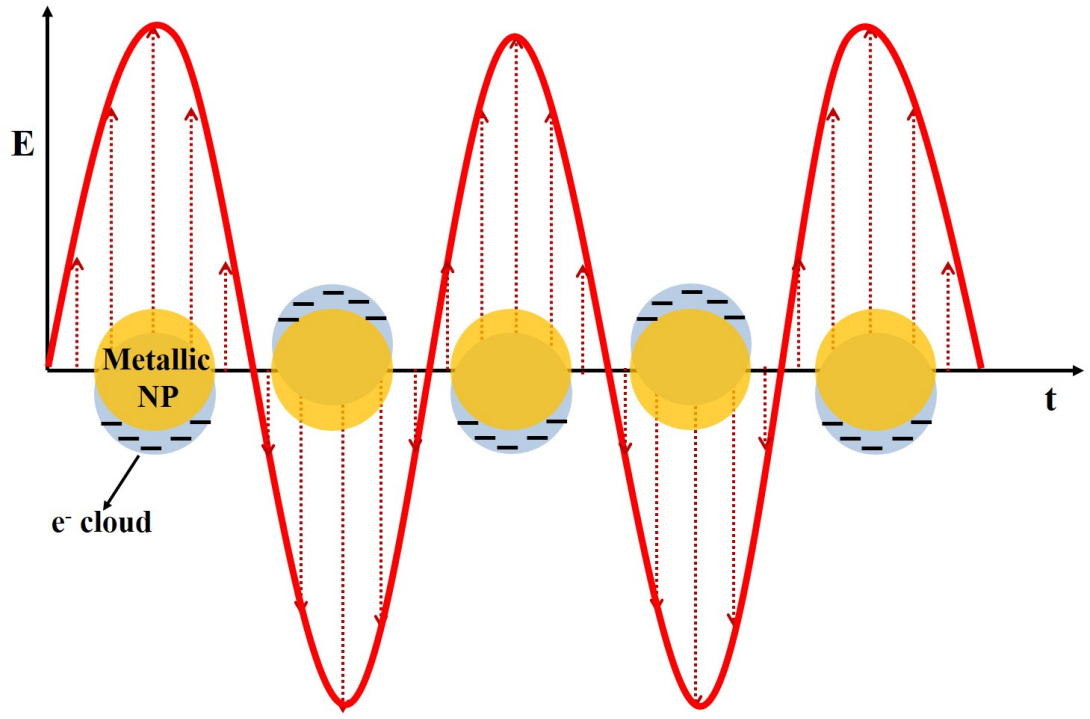

FIGURE 1.1: Schematic representation of localized surface plasmons in spherical nanoparticle

(illumination wavelength is matched with the natural frequency of these coupled oscillation) get satisfied, it causes the LSP resonance modes,which result in strongly enhanced dipolar electric field at the intermediate vicinity of nanoparticles. Such multi-fold near-field enhancement is at the heart of all promising applications of localized plasmonics. Interestingly, these plasmon modes can be further tailored according to their shape and size of nanoparticles [32]. Additionally, the other higher order resonance modes can also be excited with larger particles and particles with different shape [28, 33] such as nano-cube, nano-triangle, NPs dimers etc. Another interesting feature, associated with these nanoparticles is that the plasmon resonance modes can be excited with direct illumination, in contrast to the propagating plasmons modes (discussed in section 1.1.2).

1.1.2 Surface plasmon polaritons

Similar to localized plasmons, the coupled oscillations can also be excited in extended system such as planer metal-dielectric thin-film, metallic nanowires etc. Surface plasmon polaritons (SPPs) are electromagnetic excitation, which can propagate along metal-dielectric interface and evanescently decay in other two perpendicular medium (as shown in figure 1.2). In contrast to LSP, these SPPs modes are not bounded within

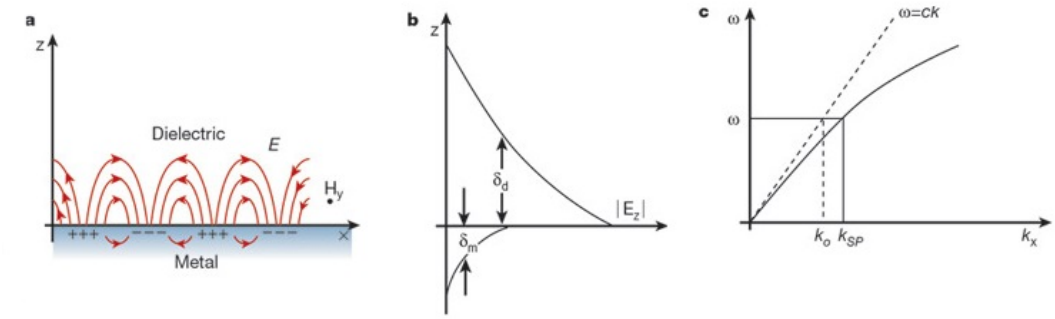

FIGURE 1.2: Schematic representation of Surface plasmon polaritons modes. (a) SPPs propagation at metal-dielectric interface. (b) Electric field distribution along the normal (z-axis) to the extended surface. δ_m and δ_d is the field decay length in two different medium i.e. metal and dielectric. (c)dispersion curve of surface plasmons polaritons and free propagating wave. [Reprinted by permission from Macmillan Publishers Ltd: [Nature]([24]), copyright(2016)]

a small particle volume, therefore it can propagate up to micrometre or centimetre scale and can be further harnessed as an optical waveguide [30]. These propagating waves are hybrid in nature consisting the properties of both photons and coupled oscillatory electrons. Mathematical understanding of such type of excitation has been discussed in various books [4, 34]. Herein, we would be briefly discussing some of the interesting aspects based on those references.

By solving the Maxwell's equation with applying proper boundary conditions, one can obtain the SPPs dispersion relation which shows the frequency dependence of SP wavevectors [4]. The mathematical expressions can be given as equation 1.1, 1.2, 1.3.

$$\frac{c^2 k_{sp}^2}{\omega^2} = \sqrt{\frac{\epsilon_m \epsilon_d}{\epsilon_m + \epsilon_d}} \tag{1.1}$$

$$k_{sp}^2 = \frac{\omega^2}{c^2}\sqrt{\frac{\epsilon_m \epsilon_d}{\epsilon_m + \epsilon_d}} \tag{1.2}$$

$$k_{sp} = k_0\sqrt{\frac{\epsilon_m \epsilon_d}{\epsilon_m + \epsilon_d}} \tag{1.3}$$

where $\frac{\omega}{c} = k_0$ represent the wavevector of photons in vacuum. ϵ_m and ϵ_d are frequency dependent metal and dielectric permittivity. k_{sp} and k_0 denotes wavevector of surface plasmon and free space photons.

Figure 1.2c shows the dispersion curve for SPPs waves. Equation 1.1 highlight that the relation between wavevector of light in matter is significantly different from the

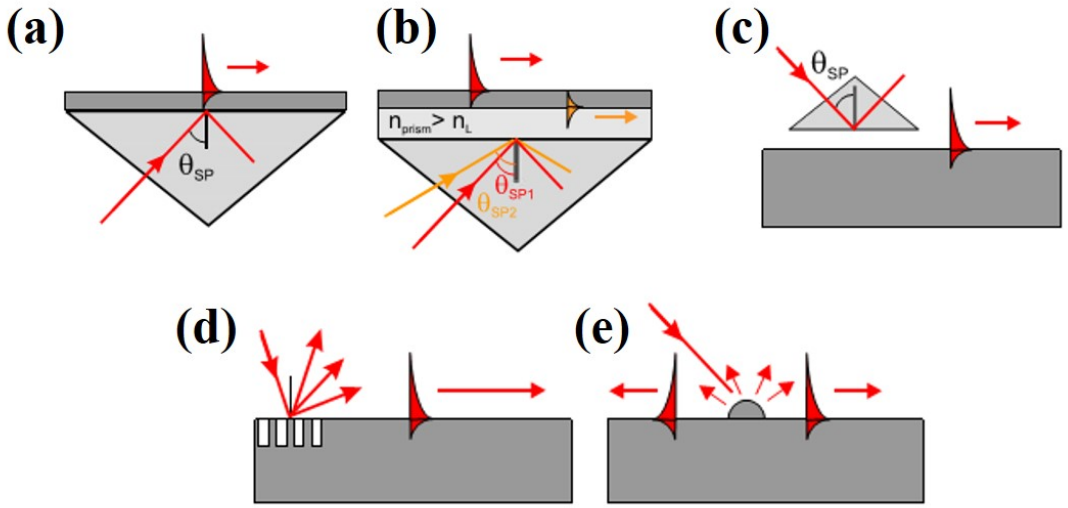

FIGURE 1.3: Schematic representation of different excitation configuration. (a)Kretschman configuration, (b) Two-layer Kretschman configuration, (c) Otto configuration, (d) Carving grating structures and (e) diffraction due to surface defect.[31]

light wavevector in vacuum. Hence, SPPs dispersion curve will never intersect to the free space wavevector and further approaches to maximum value ($\omega_{sp} = \omega_p/\sqrt{1+\epsilon_d}$; where ω_{sp} and ω_p represent surface plasmon frequency and bulk plasmon frequency of metal) for larger wavevectors. Another interesting feature to note is: momentum mismatch between propagating SPPs modes and free space photons and hence, the direct excitation of SPPs wave is impossible. One has to breach this limit of momentum mismatch by providing symmetry breaking. Various experimental schemes have been explored to bridge this momentum mismatch gap[31]. These schemes can be classified into two parts (schematics are shown in figure 1.3):

- Tunnelling of incident electromagnetic field in total internal reflection (TIR) based configuration (Kretschman configuration, Otto configuration)
- Creating an artificial defects (grating coupling, rough surface design).

(i) TIR based excitation scheme: In principle, this method involves the tunnelling of incident electromagnetic field to metal-dielectric interface, resulting in SPPs wave excitation. Two different configuration is possible under this convention.
Kretschmann configuration: Metallic film is directly formed on the glass substrate and placed on the surface of prism with using index matching oil. The metal film is illuminated through dielectric film at a specific angle, greater than critical angle of TIR (schematic shown in figure 1.3a and b). Travelling of light waves in higher

dense medium resulted into increment in wavevector. At a specific angle, the in-plane wavevector satisfies the essential condition of momentum matching and SPPs are generated at metal-dielectric interface. The resonance condition can be defined as equation 1.4

$$k_{sp} = nk_0 \sin\theta_0 \tag{1.4}$$

where k_{sp} and k_0 are corresponding wavevector of surface plasmons and freely propagating waves. θ_0 indicates angle of incident light.
This configuration of SPPs wave excitation has few limitations. Under this configuration, the sample is in direct contact,however the direct contact of the sample is not desirable in some cases. Second limitation is associated with metallic film thickness. The film thickness should be less than skin depth of incident electromagnetic wave. To troubleshoot this issue, another configuration is utilized, termed as Otto configuration.
Otto configuration: Under this configuration, the TIR takes place at the surface close to the metallic surface as shown in figure 1.3 c. The photon tunnelling takes place from the air gap between prism and film surface. The resonance condition remains same under this configuration too and can be given by equation 1.2.
(ii) Creating artificial defects: Alternative way to provide the extra momentum for SPPs excitation is creating defect on the metallic surface [31] such as grating coupling, rough film surface, etc. The addition momentum is provided by diffracted light wavevector component. These diffracted light wavevector coincide with the SPPs wavevectors and result in excitation of SPPs wave on metal-dielectric interface. Considering the simplest case of periodic grating structures of periodicity b, the SPPs wavevector can be expressed as [31] equation 1.5.

$$k_{sp} = k_0 \sin\theta_0 + \frac{2\pi}{b} \tag{1.5}$$

1.1.3 Applications

Plasmonic nanostructures have been explored for various nanophotonic applications ranging from nanoscale light propagation to single molecule detection [35, 36]. All the plasmons assisted applications primarily depend on either field localization or field propagation. When the two plasmonic nanoparticles are brought very close in the presence of external electromagnetic field, this tiny inter-particle gap between these two particles/nanostructures acts as electromagnetic hot-spots. These electromagnetic hot-spots are capable enough to produce multi-fold electric-field enhancement. In addition to nanoparticles assembly, various other approaches have also been explored to obtain high field localization for example nanowire-particle junction [37], tapered

end nanowire [38] and end to end coupled nanowires [39] etc. Such huge enhancements have been harnessed in numerous applications for example surface enhanced Raman spectroscopy (SERS)[40], surface enhanced fluorescence (SEF) [41] and Single molecule detection [36] etc. Importantly, the electric field enhancement can be effectively tailored and tuned by systematically varying various parameters (shape, size etc), which provide an additional degree of freedom to monitor these applications. Another interesting feature of such type of field localization is that it is extremely sensitive to local refractive index. Plasmonic response can be tailored by altering the surrounding dielectric medium [32]. This feature of localized electric field has been harnessed to realize nanoscale chemical- and bio- sensors devices [28, 29] and other microscopy based imaging techniques [9, 42].

Alternatively, plasmonic nanostructures have been employed for manipulating optical field propagation below the diffraction limit [24, 30]. In most of the applications, surface plasmons is generated at one location and is collected at the other location where these waves encounter any defects or discontinuity. At these defect locations, surface plasmons convert back to freely propagating photons and hence, the information is transported at nanoscale. Plasmons waves can travel upto millimetres to centimetres depending on associated loss in nanostructures[1, 24, 30]. Among all the plasmonic nanostructures, one dimensional (1D) geometries especially silver nanowires or thin-films have been most extensively investigated to demonstrate several applications ranging from nanoscale light transportation [39, 42], single and dual channel optical antenna [18, 19], remote excitation SERS [40] to optical alignment/trapping of nanostructures [43, 44] etc. Also, non-linear effects have also been investigated in these structures [45], however use of only metallic nanostructures for nonlinear process is not recommend in photonics community because of associated loss with metals.

In the light of above discussion, it is evident that plasmonic research plays a crucial role in designing the building blocks for various nanoscale devices and applications. However, inspite of these remarkable potentials, there are a few issues associated with these conventional plasmonic nanomaterials especially gold and silver. These limitations are regarded as bottleneck in designing, fabrication and integration of various plamonic and metamaterials devices. In the next section, we would be highlighting few concerns, which have motivated the scientific community to search for alternative nano-photonics materials for compact nanophotonics applications.

1.1.4 Limitations

The applications of conventional plasmonic materials especially silver and gold have been demonstrated as part of nanophotonic applications in optical regime, however

these materials exhibit significant drop in their performance efficiency (propagation loss, hearing loss, low information density etc) within the optical regime due to their interband transition [46, 47]. This interband loss is attributed to electronic transition such as transition of valance electron to fermi surface or an electron near fermi surface to next unoccupied states [47]. Also, these conventional plasmonic materials suffer due to ohmic loss and heating loss. Such type of losses are regarded as detterents while incorporating the plasmonic nanostructures in integrated photonic devices [2, 48]. Additionally, heat decapitation is another important concern to be addressed in exploring these structures for molecular applications or other biological applications [49]. There are few reports availiable to tackle this problem using various methods [48].Furthermore, tuning of plasmonic properties (multicolour tunability, mechanical flexibility, CMOS compatibility) of conventional materials poses challenges in designing and fabrication the nanophotonics devices [46, 47, 50, 51].
Hence, to realize the nanophotonics applications on a larger scale, we have to explore the different approaches, either to boost the performance efficiency of the existing plasmonic materials or an alternative to these plasmonic materials. In the subsequent section, we would be exploring the new class of nanomaterials based on molecular constituents.

1.2 Molecular architectures

To overcome the above mentioned concerns, the molecule based nano-photonic architectures have been extensively explore in the past few years. Molecular nanomaterials can be classified in two parts based on the nature of excitons: inorganic (Wannier-Mott excitons [52, 53]) and organic (Frankel excitons [54, 55]) materials. Both these molecular nanomaterials are not considered as rival for nanophotonic applications. Interestingly, both molecular materials in combination pave the way for conceptualizing variety of radically innovative applications [56–58]. We anticipate that these molecular based nanostructures will revolutionize the field of optical communication and information technology. However, it will be an interesting question to debate who would be playing the major role. The answer of this question relies on how the research on inorganic/organic nanomaterials would proceed in future.

1.2.1 Inorganic nanomaterials

Similar to conventional plasmonic materials, inorganic nanomaterials have registered their importance in modern science and technology ranging from information and telecommunication engineering, photonics devices and biological sciences [59–61]. In recent

years, researchers have explored various nanomaterials e.g. ZnO, CdS, etc, especially in the context of solar cell [59], nanophotonics [60] and opto-electronic applications[62]. Moreover, these inorganic materials have been successfully demonstrated for numerous applications such as field confinement and generation of resonating modes[63], nanoscale optical field propagation [64], nanolasers [65], photovoltaic solar cells [59], live cell imaging [66] and many more. More recently, researchers have come up with another novel approach of using two-dimensional (2D) layered materials for flexible photonics and opto-electronics devices. Layered materials have been demonstrated for several applications such as light emitting diodes [67], photodetectors [67], and optical modulators [68] etc. However, the research is still under way on how to effectively exploit these materials for other opto-electronic and nanophotonics applications.
Nevertheless, there are a few challenges associated with these inorganic materials. The most commonly used inorganic materials is Silicon (Si), however Si has a narrow indirect bandgap so devices using it usually show low luminous efficiency, high power consumption, and limited working frequency[69, 70]. As a solution, this normal Si fibre is replaced by Er^{3+} doped silica for some applications, still it is challenging task to meet the requirement for optical communications [71]. Furthermore, other inorganic nanomaterials such as ZnO, CdS, GaAs, CdTe, PbS, and PbSe, etc have been explored in recent years, however there are still many requirements for which inorganic materials are not ideally matched for example extreme toxicity[72], multicolour broad tunability, mechanical flexibility, low quantum efficiency, photo-responsivity and low-cost process ability[73–76]. Hence, organic nanomaterials have attained significant attention as an alternative for photonics and opto-electronic applications. In the next section, we would be mainly focusing on the properties of organic nanomaterials.

1.2.2 Organic nanomaterials

In the context of photonics applications, researchers have made an extraordinary contribution to achieve unique optical properties with inorganic nanomaterials, however as these materials were thriving, organic nanomaterials have slowly come up as a better choice for nanophotonics and opto-electronics applications [77]. Organic materials are a promising candidate as they combine the materials properties of plastic with high optical cross-sections, broad spectral tunability, large and ultra-fast non-linear responses [74, 75, 78]. These properties strongly contribute for designing and fabricating low-cost photonic devices and integrated circuits for next-generation optical information processing applications [77, 79]. In contrast to inorganic materials, photonic properties of organic molecular materials are dependent on Frenkel exciton-polaritons propagation [54]. Comparing to Wannier-Mott excitons (excitonic binding energy $\sim meV$), Frenkel

excitons (excitonic binding energy $\sim eV$) in organic materials have greater binding energy, and are hence more stable [54]. Adding to this, there are advantages of organic molecular materials, variety in molecular structural engineering, and adaptability to create flexible platforms, which have made organic molecular meso- and nano- structures very attractive candidates for photonics applications [73–78].
Bringing together all these aspects of organic materials, it is evident that organic molecular materials are good choice for designing and fabricating photonic devices and other functional components for integrated circuits. In recent years, organic structures have been explored in various applications such as nano-lasers [80, 81], resonators [20, 82], integrated optical circuits [21], amplifiers [83], photo-detectors [84], optical channels [85], and directional couplers [86]. In the following sub-section, we will discuss few examples on how these type of excitonic nanostructures have been utilized for building useful nanophotonics applications.

1.2.2.1 Recent advances in organic nanophotonics

Despite of being in embryonic stage, organic materials have registered their impression both in terms of designing numerous organic nanostructures as well as realizing nano-optics applications [87]. The comprehensive details on research efforts carried out so far have been tabulated in Table 1.1. Evidently, most of the research revolves around the few aspects such as new organic nanomaterials/nanostructures [12, 20, 21, 75, 78], energy transfer mechanism [73], Raman spectroscopy [88], nanoscale lasers [74], photo-detection [84], photo-electric transducers [12], logic gates [89], optical computing [12], integrated optical circuits [90], field confinement and WGMs generation [20, 82, 91] etc. Notably, there are very few reports on coupling of plasmonic nanostructures with organic nanostructures and other directional couplers [20, 89, 92], however such coupled configuration is at the heart of all nanoscale chip optical circuits. In addition to this, very few reports are available on directional emission analysis of nanostructures. Moreover, the reports are mainly oriented towards plasmonic structures.
Hence, despite of such extraordinary endeavour in its infancy stage, there is a long way to go before realizing organic materials for photonics application at larger scale for example loss reduction in organic lasers [74], control over energy dissipation process [73], directional control over out-coupled optical signals [12] etc. Among all these courses, we have chosen to investigate the directional control over out-coupled optical signal from organic and other hybrid nano-architectures. In recent years, the directional control of optical signal has become imperative to explore in the context of optical channels, directional coupler and other integrated optical circuits. Furthermore, in the context of signal processing applications where the device can perform in both active

and passive domain, it is essential to know the directionality of out-coupled emission for efficiently couple the light to another channel. To address these issues, we probed both individual and hybrid organic nano-architectures for their antenna like behaviour and hence, to put our thesis work in broader prospective, we would start our discussion form basic introduction to optical antenna and its controlling parameters.

TABLE 1.1: Organic nano-/micro- structures and studied applications

Synthesized organic structures	**Studied applications**
Dye doped MOF microcrystal	Wavelength-tunable microlaser [93]
Microspheres	Broadband wavelength tunable microlasers [91]
Microresonators coupled organic nanowire	Organic printed photonics [20, 21]
Waveguide coupled Microdisk	Flexible microdisk WGMs resonators [20, 82]
Silver nanowire coupled with organic waveguide	Logic gates [22, 94]
Microrings	Field confinement [95–98]
Color graded microstructures	Integrated Photonic Heterojunctions [94, 99]
Nanowire, optical waveguide	light transporting, other photonic applications [100–103]
Organic-Metal nanowire hetro junction	Optical modulation [89, 104–106]
Organic photonic heterostructures	Energy Transfer mechanism [107, 108]
Doped organic nanowire	Energy Transfer mechanism [109]
Core-shell organic nanoparticles	Photon up-conversion [110]
Veritcal organic nanowire	Vertical active light source [111, 112]
Microtubes and microrods	Geometry dependent optical loss [113]
Nanoflower	Multicolor Emission [114]
Mulipods, Tube, rod array	Mophology dependent optical properties [115, 116]
Microribbons and Microrods	Vis/NIR Range optical properties [117, 118]
Microsheets	Active waveguide and wavelength filters [119]
Erasable hetrojunction waveguide	Optical delay lines [120]
Hybrid organic/inorganic structures	multicolor luminescence [57, 58, 121]
Nanofiber-resonators coupling	micrometer-scale photonic circuits, Interferometer [122–124]
Veritcal nanowire coupled with graphene	Low loss vertical light source [125]

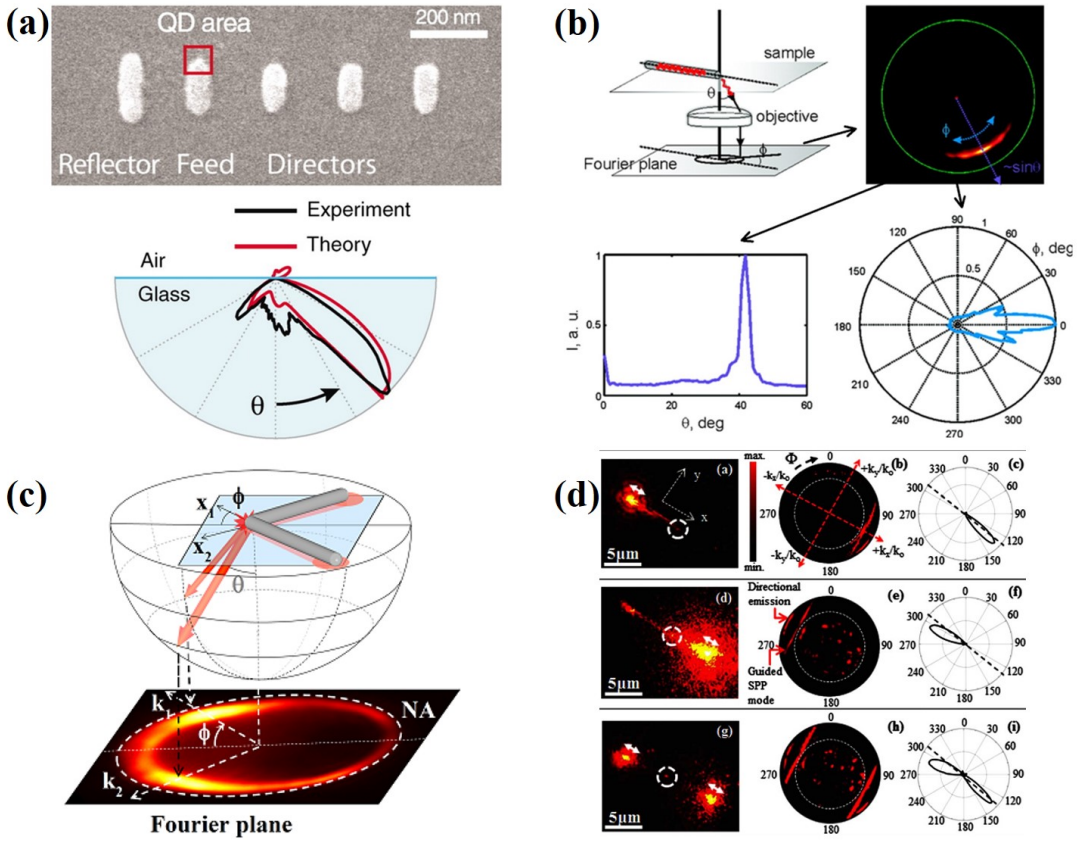

FIGURE 1.4: Directional emission from various plasmonic nanostructures. (a) LSP resonance assisted Yagi-Uda optical antenna [126]. (b) Propagating SPPs based nanowire optical antenna [Reprint (adapted) with permission from [18]. Copyright(2016) American Chemical Society], (c) Serially coupled nanowire antenna [Reprint (adapted) with permission from [19]. Copyright(2016) American Chemical Society], (d) Nanowire-nanoparticle optical antenna [adapted from [23]].

1.3 Optical Antenna

Antenna, as a component is always engaged to direct the localized information to freely propagating waves and vice versa. Electromagnetic antenna especially radiowaves and microwave regime is already in mature stage for example cellular phones, television devices etc. However, optical analogue of such component is still not competently realized. The motivation for designing optical antenna is to direct the free propagating optical field to localized source and vice versa. Similar to conventional antenna, optical field can be manipulated with specific directional control by using the nanoarchitectures such as nanowire [18, 19], nanorods [127] etc. In recent years, the concept of optical antenna has gained significant attention in the context of optical channels [85, 128], directional couplers [86] and integrated circuits [21, 123, 129, 130]. Several study has been reported in this direction, however the efforts are still going on for translating

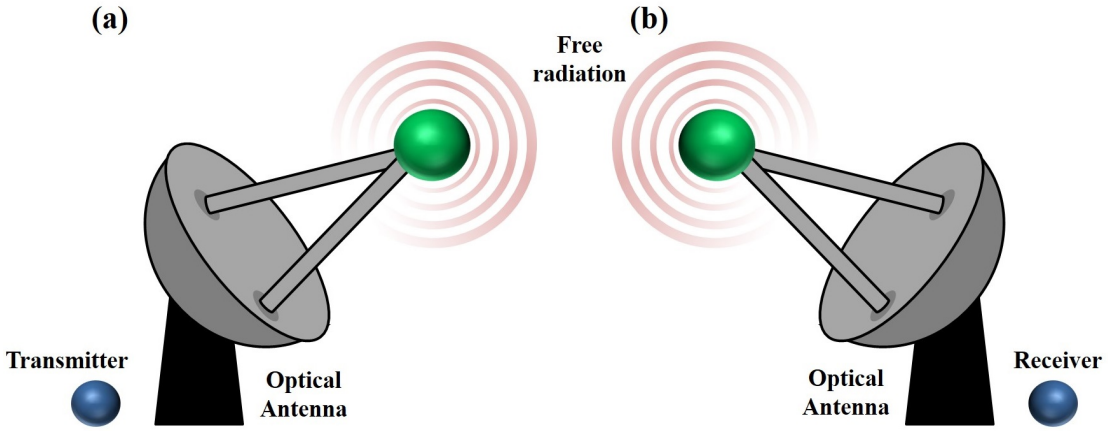

FIGURE 1.5: Schematic representation of working principle of transmitting and receiving optical antenna

the well-stablished antenna theory at optical frequency domain. In figure 1.4, we have discussed some of the ongoing effort to practical realization of an optical antenna. Based on these examples, the importance of an optical antenna can be understood in two folds:

(i) Directing the information from a localized source to far-field domain and vice-versa

(ii) Enhancement in interaction between receiver and transmitter. Furthermore, engagement of an optical antenna can modify the inherent properties of the probed quantum system (atoms, inons and molecules) present in the vicinity of antenna structures.

We schematically represent the working principle of a typical optical antenna in figure 1.5. The performance of an optical antenna device can be arbitrated based on few associated parameters such as antenna efficiency, directivity and gain. These parameters can determine the degree of localization and magnitude of transmitted energy.
Antenna efficiency: Our main objective for engaging optical antenna in nanophotonics applications is to efficiently extract the information from a localized source and transmit to the far-field regime. Quantity, which determine this property of optical antenna is known as antenna efficiency, which further primarily governed by the inherent losses of the antenna. The mathematical express of antenna efficiency is given as equation 1.6.

$$\epsilon_{rad} = \frac{P_{rad}}{P} = \frac{P_{rad}}{P_{rad} + P_{loss}} \tag{1.6}$$

where P indicates the total power collected by the antenna. P_{rad} is the radiated power of antenna and P_{loss} indicate the power dissipated due to metal absorption.

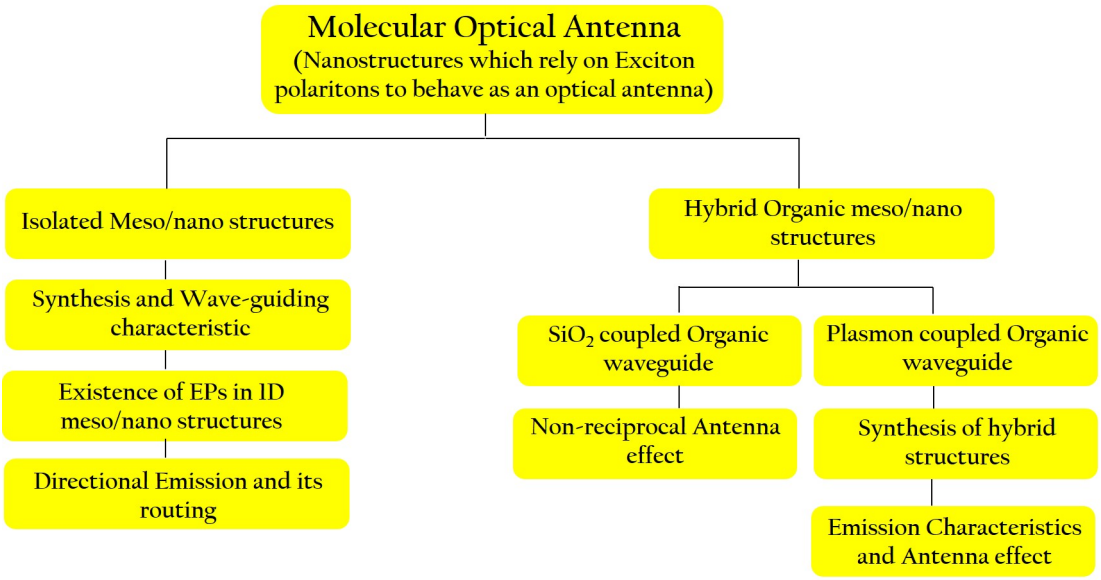

FIGURE 1.6: Schematic representation of the thesis's outline

Directivity: There is an another way to enhance the efficiency of an optical antenna i.e. transmitting majority of information in one specific direction. Directivity is defined as a ratio of intensity in one direction (I_f) to intensity in just opposite direction (I_b). Mathematically it can be express as equation 1.7.

$$D(\theta, \phi) = \frac{4\pi}{P_{rad}} p(\theta, \phi) \tag{1.7}$$

θ and ϕ indicate angular radiation direction and $p(\theta, \phi)$ is angular power density.
Gain: Combining these two individual quantity in one relation and one new quantity can be defined termed as gain. The mathematical expression is given in equation 1.8.

$$G = \epsilon_{rad} D \tag{1.8}$$

Using the reciprocity principle, it is evident that every transmitting antenna can also work as receiving antenna i.e. the information can be transferred to a localized source using such antenna structures as shown in figure 1.5b. In this configuration, efficiency is defined by the amount transfer to the localized source, whereas directivity is defined by the radiation directions which can be collected by antenna structures [131].

1.4 Scope and thesis organization

As we discussed in section 1.2.2.1, efficient control over directionality of the out-coupled light from organic nanostructures, has now become an important issue to explore in the context of optical channels, directional coupler and integrated photonic circuits. Signal processing devices perform in both active and passive operational domain, hence it is important to investigate directional emission of organic molecular nanostructures. Herein, our thesis mainly present the study on probing direction emission from an individual organic nanostructures as well as hybrid nano-architectures. To make a clear understanding of the work presented in the thesis, we show a flow chart of research work shown in figure 1.6.

Chapter2: In this chapter, we discuss about the waveguiding nature of organic waveguide as per excitation wavelength. We also show that the out-coupled light from organic waveguide terminals are directional in nature in both active and passive operational regime. We further extrapolate our study to demonstrate the two interesting applications: i) creating two directional light emitting source with single point illumination; ii) Systematic increment in optical signal transportation with almost similar directionality, in active waveguiding regime by just varying the excitation location along the length of waveguide. In end, by analysing the recorded spectra of guided light, we measure anomalous refractive index as a function of emission energy for demonstrating the presence of exciton-polaritons in organic molecular waveguide light transporting mechanism.

Chapter 3: In the chapter 3, we prepared the hybrid nano-architectures by coupling organic waveguide with silica microsphere. We discuss how the spectroscopic information of the signal can be actively tailored as per excitation location in such hybrid nanostructures. We also show that in active waveguiding regime, the out-coupled light from both the terminus of these structures are directional is nature. Further, we argue the contribution of coupling (microsphere and organic waveguide) in higher angle emission in back focal plane as well as the tailoring of this directional emission from hybrid terminals.

Chapter 4: We investigate the coupling effects in another hybrid geometry i.e. organic nanowire coupled with unstructured plasmonic substrate. To prepare such geometry, we successfully coupled organic nanowire in vertical direction (1D) on a gold thin film (2D). In such unique system, we investigate the coupling effect between single, vertical organic nanowire and plasmonic film. Interestingly, this captured out-coupled emission is found to be directional in nature. Furthermore, using finite element method (FEM) numerical simualtion, we argue on how one can systematically control the directional emission. In the end, we also discuss about the effect on direction light emission due to

variation in coupling angle between organic nanowire and plasmonic film surface.
Chapter 5: Here, we mainly provide the future direction of the presented work in the thesis. One aspect of the future direction is to couple organic nanostructures with plasmonic measurfaces. These meta-surfaces are prepared by combing the top-down and bottom-up approach. We show the preliminary results on preparing these hybrid nano-architectures. These type of hybrid geometry will provide a plateform to investigate the modified radiation patterns, newly arises resonance modes, and life-time of excited states due to strong coupling between organic nanostructures and plasmonic molecules.

Chapter 2

Directional Emission from an Organic Molecular Waveguide

Chapter 2 is an adaptation of the research article, *Journal of Optics (IOP), 2016, 18, 065002*. In this article, we discussed about the directional emission from distal ends of organic waveguide resting on a glass substrate. Further, we demonstrated the presence of exciton-polaritons in such system by measuring anomalous refractive index as a function of emission wavelength. To end, we extended our investigation to demonstrate how one-dimensional organic meso- structures can be utilized as dual channel photolumienscence source with single point excitation.

2.1 Introduction

How to control freely propagating photons using one-dimensional mesoscale materials? [12, 132–136]. This important question has been raised in the context of optoelectronics, micro- and nano-photonics, and an effective answer has relevance not only in fundamental optical physics of one-dimensional materials, but also in applications ranging from quantum technologies to clinical biomedicine. In recent years, controlling the directionality [128, 137] of emitted light from micro- and nanowire waveguides has gained importance in the context of nanophotonics circuits [138–141] and optical antennas [128]. A majority of wire optical antenna that have been studied are made of plasmonic materials such as silver and gold [129, 142–144]. A variety of inorganic semiconductor materials [133, 145] have also been explored in the context of directional light emission. However, there are not many studies on directional emission of light from one-dimensional organic molecular materials, especially those which support exciton-polariton propagation along their length. For the first time, in this work, we experimentally show directional light emission [146–149] characteristics from an organic exciton-polariton mesowire in both active and passive light-transport regimes. Furthermore, by analysing the spectra of the guided light, we measure anomalous behaviour of

real and imaginary parts of the refractive index of the mesowire as a function of emission wavelength. Such measurement can have direct relevance in micro and nanoscale photonic sources based on exciton-polaritons (EPs).

Exciton-polaritons are coupled excitation of excitons and electromagnetic radiation [52, 150–152]. In recent times, EPs have captured attention in the context of both fundamental physical phenomenon such as Bose-Einstein condensation [153–155], and a multiple of applications in optics, photonics and semiconductor optoelectronics [53, 54, 130, 156–160]. There are various inorganic semiconductor such as GaAs, CdTe and ZnO that exhibit Wannier-Mott excitonic states[52, 53, 153, 156, 161], and couple to electromagnetic radiation further facilitating EPs. Alternatively, EPs can also be generated by exciting organic molecular materials with Frenkel excitons [54, 55]. Compared with Wannier-Mott excitons, Frenkel excitons in organic materials have greater exciton-binding energy and longitudinal-transverse exciton splitting energy, and hence more stable [54]. Added to this there are advantages of molecular materials [80, 136, 158, 160, 162] such as greater oscillatory strength of organic molecules, variety in molecular structural engineering, and adaptability to create flexible platforms [163–165], which has made organic molecular meso- and nano-structures very attractive candidates for photonics applications [77, 87, 159, 166–174].

In the context of photonic applications, devices can function in passive or active operational regimes [175, 176]. In the context of optical signal processing, passive operations are those in which the input wavelength is equal to the output wavelength, whereas, in an active regime, the input and output wavelengths are different. One-dimensional organic materials have been shown to operate in both passive [162] and active regimes [136, 160, 177], and hence can be employed for various photonic applications such as laser [20, 80, 81], resonators [55, 178], integrated optical circuits [77] etc. One important application that has not explored is the directional light emission from one-dimensional organic semiconductors. Directional light emission is now an important concept from the point of view of optical antenna [128], interconnects and couplers [12], and there is an imperative to study and quantify directional light emission from such organic molecular mesostructures.

In this paper, we report on the observation and quantification of directional light emission from organic molecular mesowire in the both passive and active regimes. We prepared mesowire structures of diaminoanthraquinone (DAAQ) molecule and specifically

(i) measured directionality of light emission in passive and active optical transport regimes;

(ii) observed anomalous refractive index as a function of wavelength and;

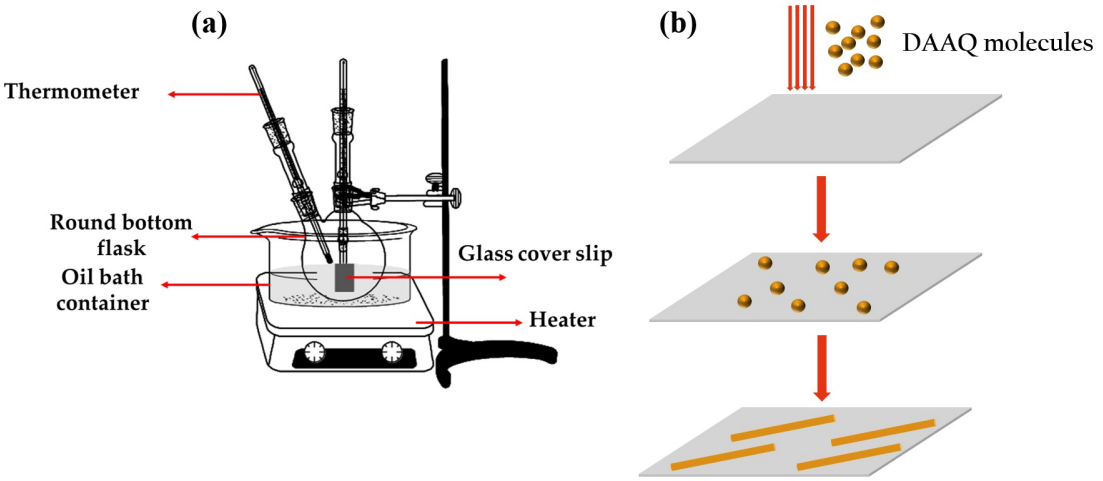

FIGURE 2.1: Schematic representation of synthesis procedure of DAAQ molecular waveguide. (a) Schematic view of constituents arrangement used in synthesizing the DAAQ waveguide on the glass substrate. (idea of the schematic is adopted from [164, 165]) (b) Molecular self-assembly involved in the growth process of DAAQ waveguide is explained in steps by schematic representation.

(iii) showed an interesting application of active light transport in DAAQ mesowire: dual-channel, directional light emission with a single excitation.

All the light-emission studies were performed on a single DAAQ mesowire. The experimental observations were also corroborated by full-wave 3D finite difference time domain (FDTD) simulations.

2.2 Experimental Section

2.2.1 Sample preparation and characterization

1,5 diaminoanthraquinone (DAAQ) waveguides have been synthesized via physical vapor transport method[164, 165]; schematic shown in figure 2.1. The organic compound DAAQ powder (0.5mg, 85% pure, Sigma Aldrich) was dissolved in 50ml ethanol (99.9% pure, MERCK) in double neck round bottom (RB) flask. RB flask was then kept in a rotor cum heat bath at 40^0C to achieve uniform thin film of DAAQ molecules around the wall of round bottom flask. After completion of preparation of thin film around the RB flask, a clean glass coverslip was vertically suspended inside the RB flask through glass bar mounted on the top of RB flask. The whole arrangement was then kept in silicon oil bath and set the temperature of oil-bath at 160^0C - 200^0C as per experimental conditions (shown in figure 2.1a). The length and diameter of the synthesized DAAQ waveguide can be controlled through growth temperature and time

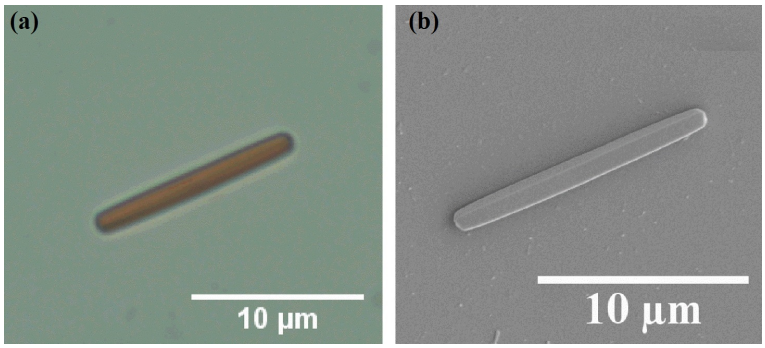

FIGURE 2.2: Conventional optical and SEM images are shown. (a) Optical image of DAAQ waveguide resting on a glass coverslip is shown. Optical image is captured with high numerical aperture (NA) oil-immersion objective lens ($100x$, 1.3NA). (b) SEM image of the same DAAQ waveguide is shown.

duration.

As the temperature of RB flask increases, DAAQ powder is evaporated from the flask's wall and condensed on the surface of glass substrate. The condensed molecules act as a nuclei and get self-assembled. The self-assembly of the molecules result as J-aggregated nano/meso structures (also verified with absorption spectra of molecular solution and nanowires, shown in figure 2.5). The growth process is schematically depicted in figure 2.1b. On the completion of synthesizing process, the glass coverslip was then removed from the RB flask and investigated under optical microscopy and scanning electron microscopy (SEM) (shown in figure 2.2a and 2.2b).

2.2.2 Back focal plane imaging microscopy

2.2.2.1 Basic principles

Directional emission analysis of emitted light is performed using back focal plane (BFP) or Fourier plane (FP) imaging microscopy. BFP imaging microscopy is performed by utilizing the Fourier transform property of a lens. In principle, to perform the Fourier plane imaging, image is positioned at first focal plane of a lens and information is collected at second point. At the second focal point, the collected information is Fourier transformed of the input information. The schematic of the whole process is shown in figure 2.3.

The light emitted from the sample plane can be decomposed into individual plane waves by the lens. Each plane waves having identical k-values would meet at one point at back focal plane of the lens. Hence, at back focal plane, the image is resolved in terms of their directional emission (or k-vector distribution) in contrast to spatially resolved real plane image at first focal. Schematically in figure 2.3a, we show that k-resolved

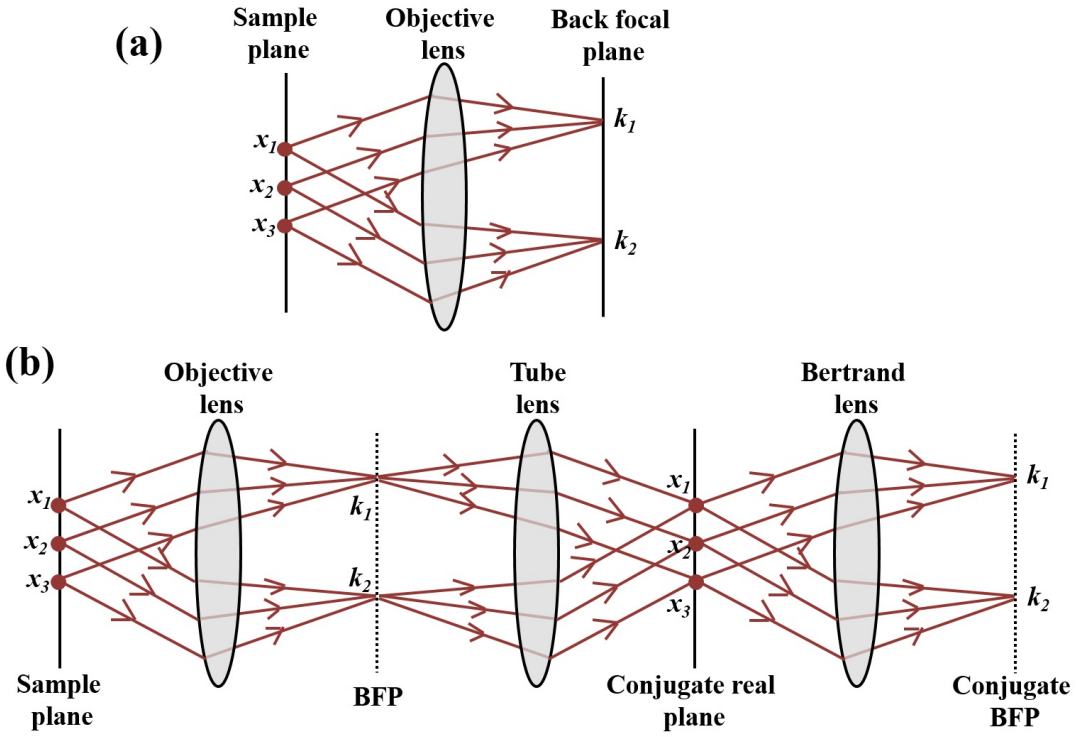

FIGURE 2.3: (a) Schematic representation of image formation at BFP of the objective lens. (b) Schematic demonstration of relaying BFP information from objective lens' BFP to imaging CCD using $4-f$ configuration.

image formation at the Fourier-plane of the lens. The rays emitted from the sample plane in same direction get focused at one point in BFP. Hence, each point in BFP represents different k-vector direction.

Practically, the conventional objective lens formed the BFP image at very short distance, hence extraction of the obtained information exactly from this point is impossible. To overcome this hindrance, we cascade the BFP information by using set of relay lens in 4-f configuration. In figure 2.3b, we show the schematic of BFP imaging incorporating the 4-f configuration. We introduce a tube lens to create a conjugate real image plane (outside the microscope) and then introduce a Bertrand lens to further create a conjugate BFP on the imaging CCD. The comprehensive mathematical explanation about this imaging technique can be also found in Appendix A.

2.2.2.2 Instrumentation

Figure 2.4a shows the schematic of the Fourier microscope setup used to investigate the directional emission of light from individual DAAQ mesowires. This microscope has the following capabilities.

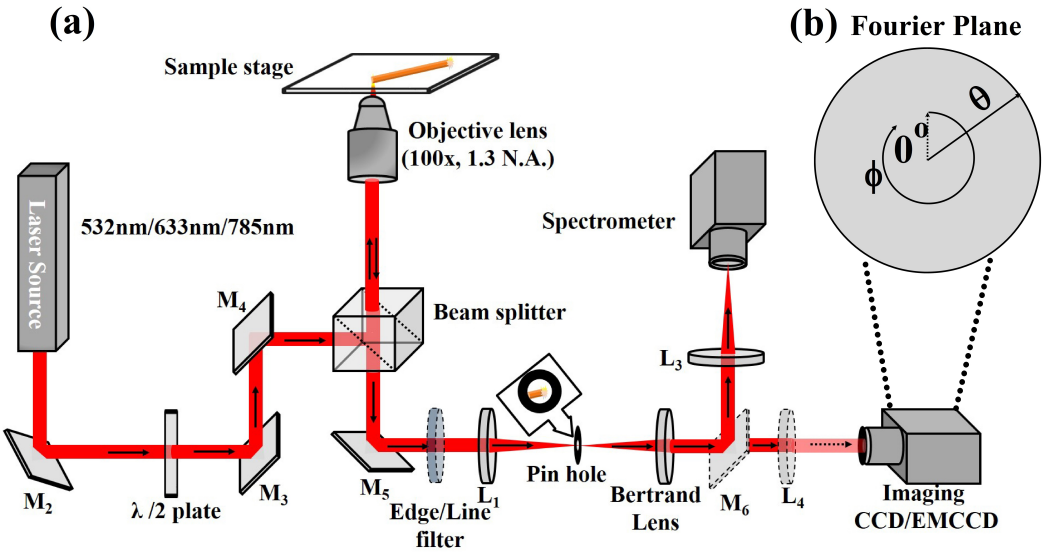

FIGURE 2.4: (a) Schematic of the multi-wavelength Fourier microscope with spatial-filtered collection optics and spectroscopy. The excitation wavelength were 532nm, 633nm and 785nm, which spans a different region of the absorption spectra of the DAAQ mesowire (see figure 2.5a). To determine the directionality of emission from the DAAQ waveguide, an optical Fourier transformation is performed by introducing Bertrand lens in the collection path. For capturing active emission, relevant edge filter is used in the collection optics to reject the excitation wavelength. FP images are captured by EM-CCD camera. For passive emission, corresponding line filter is introduced in optical path and imaging is performed with conventional camera. (b) Description about quantitative analysis of FP image. FP images can be quantified by using two relevant parameters (θ, ϕ). The ϕ is an azimuthal angle $(0^0 < \phi < 2\pi)$ and θ is the radial angle $(0^0 < \theta < 60^0)$, which is restricted by NA of the engaged objective lens to collect the emitted light.

(i) Multiple laser illumination (532nm, 633nm and 785nm) source

(ii) Spatially filtered collection optics

(iii) Spatially resolved photoluminescence (PL) spectroscopy

(iv) Conventional and FP imaging in both passive and active operation regime

The laser beam were individually focused at one end of DAAQ waveguide through higher numerical aperture (NA) oil-immersion objective lens. The emitted light from the other distal end of waveguide was collected by using same objective lens. A spatial filter (in the form of pinhole aperture) introduced at the conjugate image plane can be utilized to collect the emitted light from the other end of DAAQ waveguide. Thus, the collected light was relayed on to a Bertrand lens to form FP image on an imaging

conventional CCD camera or EM-CCD camera. For conventional imaging, another lens (L_4) was introduced between Bertrand lens and imaging CCD. To collect the PL spectra from the distal end of DAAQ waveguide, the spatially filter light was routed using mirror (M_6) and focused on the spectrometer's entrance slit by inserting a lens (L_3). To image passive emission, line filter of relevant wavelengths were introduced in the illumination path and for active emission imaging, edge filter at relevant wavelength were introduced in the path of collection optics to reject the excitation wavelengths.

2.2.2.3 Quantitative analysis

Figure 2.4(b) schematically demonstrate the co-ordinate system in FP, which is relevant to our study. On FP plane, the intensity (I) was measured as a function spherical angles (θ, ϕ) i.e. radial and azimuthal angles. The radial directional signifies the polar angle θ and scales as $nSin\theta$, where n is effective refractive index of the medium (in present case $n = 1.52$). The maximum of radial angle (θ) is also constrained by the numerical aperture of oil-immersion objective lens utilized for imaging (in this case we used $100x$, 1.3NA). Therefore, radial angle (θ) can take value up to $60^0(0^0 < \theta < 60^0)$. The tangential co-ordinate indicates to the azimuthal angle was denoted by $\phi(0^0 < \phi < 2\pi)$.

2.3 Results and discussion

2.3.1 Spectroscopic identification of passive and active transport regime

The absorption spectra of DAAQ molecules in solution (shaded area with red outline), emission spectra of DAAQ molecular solution (dotted red line) and DAAQ waveguide absorption spectra (dotted blue line) resting on glass substrate is shown in figure 2.5. The inset shows the SEM image of one of the waveguide used for our study. Comparing both the absorption spectra, we observe that aggregated phase (shaded area) shows red shift as compared to solution phase (dotted blue line). We can identify two distinct features in the absorption spectra of mesowires. One is red-shift of the absorption maxima and the other is broadening of spectra. The red-shift can be understood as the effect of self-assembly (or J-aggregates) of DAAQ molecules, and the broadening may be due to contribution of molecular conjugation to dielectric substrate (glass in the present case)[179].

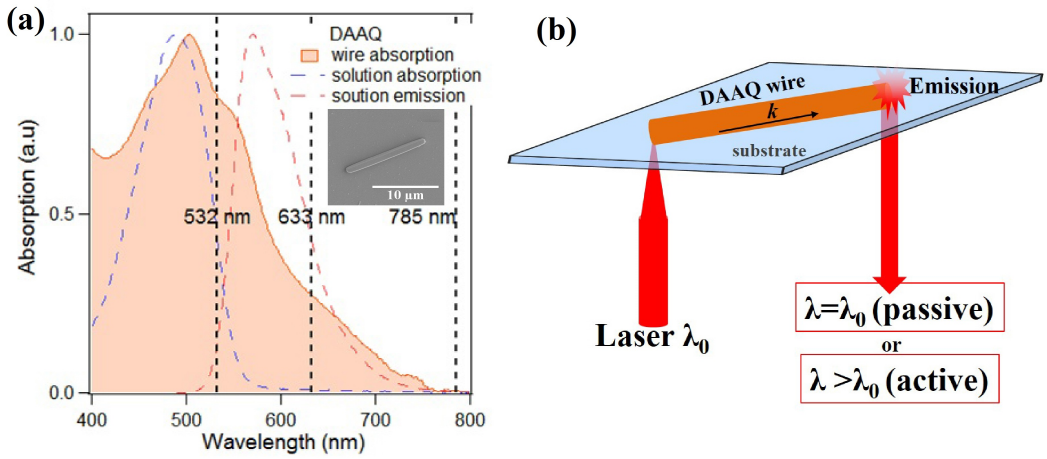

FIGURE 2.5: (a) Absorption spectra of DAAQ solution (dash blue line), DAAQ waveguide (shaded area) and emission spectra (dash red line) of DAAQ solution. Three vertical lines indicate the wavelength of excitation in reference to the absorption band of the DAAQ waveguide. Inset show the SEM image of one of the waveguide used for our study. (b) Schematic of the experimental configuration to probe the directional emission in active and passive waveguiding regime. DAAQ waveguide is resting on the glass coverslip. One of the wire is excited with wavelength (λ_0) and collected the emitted light from other distal end. If the emitted light (λ) is same wavelength as like illuminated wavelength ($\lambda = \lambda_0$), then termed as passive waveguiding. However, if the wavelength of emitted light (λ) is higher than excitation wavelength ($\lambda > \lambda_0$), then termed as active waveguiding. The emitted light was spatially filtered and Fourier-transformed to obtain the directivity of emission in passive and active regimes.

Three vertical lines in the spectra (figure 2.5a) at 532nm, 633nm and 785nm respectively represent the three excitation wavelengths with respect to the waveguide absorption spectra. We chose these three vertical lines at different wavelength according to absorption maxima. One should expect the enhanced absorption at 532nm (closer to absorption maxima of DAAQ waveguide), further results as maximum intensity in active emission. As we move further towards higher order wavelength (i.e. 633nm), the absorption efficiency reduces, and slowly lead to passive emission or in other words, the intensity in active emission will decrease. At 785nm illumination, molecular absorption will be minimal and lead the light emission in passive transport regime. In figure 2.5b, we schematically define passive and active definition. In the schematic, DAAQ waveguide is resting on a glass substrate and we illuminate one end of the DAAQ waveguide with an excitation wavelength (λ_0). At the other distal end of DAAQ waveguide, light emitted either at the same wavelength ($\lambda = \lambda_0$ – passive waveguiding) or higher order wavelength ($\lambda > \lambda_0$ – active waveguiding). Motivation of the above discussed work is

to identify the different light transporting regime. Next, we investigate the waveguiding nature of DAAQ waveguide in these three different operating regime and then, we determine the directionality of these emission.

2.3.2 Waveguiding nature with different excitation laser source

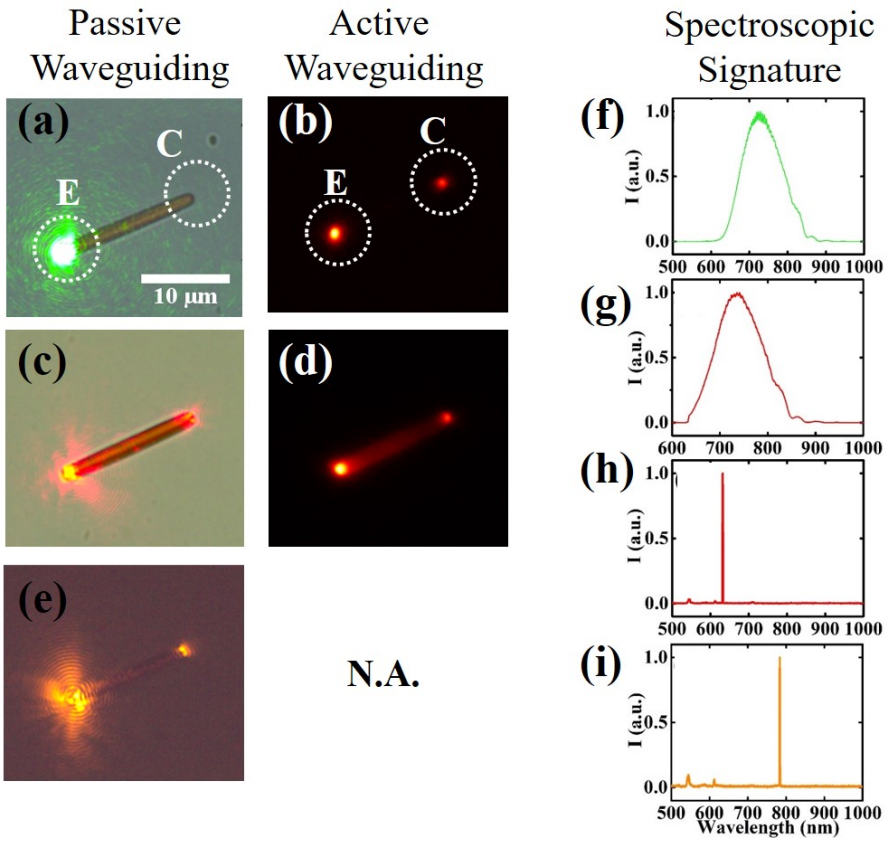

FIGURE 2.6: Conventional optical images with three different laser excitation source. (a) DAAQ waveguide is excited with 532nm at one end. Excitation and collection points are denoted by E and C respectively. We didn't observe any light emitted from other distal end in passive waveguiding regime. (b) PL image is shown with 532nm laser excitation in active waveguiding regime. Here also, the excitation and collection points are indicated with E and C. Similarly, we repeated the experiments with 633nm, (c) passive waveguide (d) active waveguide; and with 785nm (e) passive waveguide. We didn't observe active light emission with 785nm excitation source. To determine the emitted wavelengths, we recorded the emission spectra from waveguide distal end in their respective operation regime. (f) active emission with 532nm, (g) active emission with 633nm, (h) passive emission with 633nm and (i) passive emission with 785nm

Illumination of DAAQ waveguide with 532nm: We illuminated the DAAQ molecular waveguide with 532nm laser source at one end and collected the light from other distal

end. Optical images with laser excitation are shown in figure 2.6. Figure 2.6a represents the passive waveguiding image and figure 2.6b shows the active waveguiding. In figure 2.6a, we illuminated one end of the waveguide (denoted as E) but didn't get any light emitting from other distal end of waveguide (denoted as C). After introducing 532nm edge filter in the collection optics (rejecting the excitation wavelength), we observed active light emission in organic waveguide. In figure 2.6b, we observed PL light at both end i.e. excitation and collection end of waveguide. We further recorded the corresponding spectroscopic signature (shown in figure 2.6f).

Excitation with 633nm laser source: For 633nm excitation, we observed both passive and active waveguiding from waveguide. Optical image are shown in figure 2.6c and figure 2.6d. In figure 2.6c, we illuminated the waveguide at one end and capture the light emitted from the other distal end. Further, we captured the PL image with 633nm laser illumination by introducing relevant edge filter in the collection path. We also recorded the spectroscopic signature in both the operational regime (shown in figure 2.6g and h).

Illumination with 785nm laser source: We focused the laser beam at one end of organic waveguide and collected the emitted light from other distal end (shown in figure 2.6e). However, on introducing the corresponding 785nm edge filter, we didn't observe any PL emission in DAAQ waveguide. We also recorded the corresponding spectroscopic signature (shown in figure 2.6i).

2.3.3 Directional light emission from distal end of waveguide

532nm laser illumination:
Figure 2.7a represents the optical image in active waveguiding regime with 532nm illumination source. The two end of the waveguide show bright signal at higher order wavelength than 532nm. Figure 2.7b represents the FP image of the active emission from distal end of the waveguide. A bright arc at $\theta = 41^0$ indicates the directional light emission. Further, we do the quantitative analysis of captured FP image as a function of ϕ and θ. In figure 2.7c, we plot the light intensity along with ϕ and obtained the spread ($\delta\phi$) to be 78^0. In figure 2.7d, we plot the intensity variation as a function of polar angle (θ) and obtained the spread ($\delta\theta$) to be 11^0.
633nm laser illumination:
Active waveguiding: Figure 2.7e represents the active light emission from waveguide with 633nm laser illumination and associated FP image is shown in figure 2.7f. We further quantitatively analysed captured FP image and plotted the intensity distribution along with azimuthal and polar angle as shown in figure 2.7g ($Ivs\phi$) and 2.7h ($Ivs\theta$), respectively. The spreads in azimuthal angle ($\delta\phi$) and polar angle ($\delta\theta$) are 94^0 and 7.6^0,

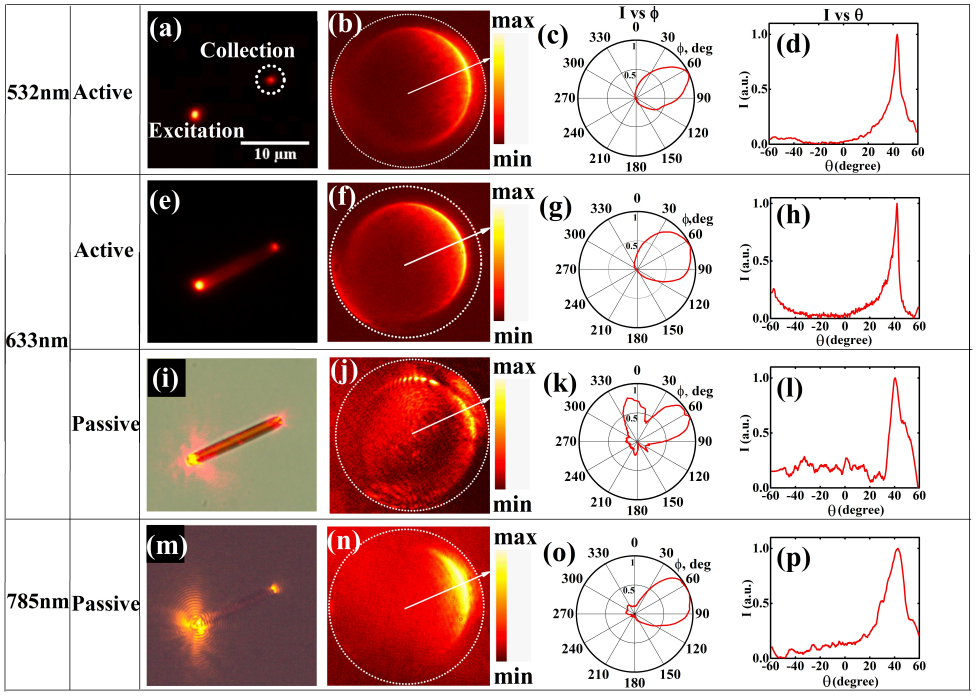

FIGURE 2.7: Conventional and Fourier-plane (FP) imaging and analysis of active and passive directional-light emission at three excitation wavelengths. 532nm lead to active emission shown in (a) PL image. (b) Corresponding FP image is shown from the spatially-filtered region. (c) FP intensity vs ϕ. (d) FP intensity vs θ for 532nm excitation. For 633nm excitation: (e) PL image, (f) corresponding FP image for active emission and corresponding plots (g) FP intensity vs ϕ and (h) FP intensity vs θ. As 633nm leads to passive emission, hence (i) optical image with illumination, (j) corresponding FP image and corresponding plots (k) FP intensity vs ϕ and (l) FP intensity vs θ. For 785nm, only passive emission is observed, therefore (m) optical image with excitation, (n) corresponding FP image and corresponding plots (o) FP intensity vs ϕ and (p) FP intensity vs θ. The edge filter and line filters were engaged in collection-optics for active and passive emission, respectively.

respectively.

Passive waveguiding: We also captured the light from distal of organic waveguide at 633nm. The optical image is shown in figure 2.7i and corresponding FP image is shown in figure 2.7j. Further, we quantitative analysed the captured FP image and corresponding intensity distribution are shown in figure 2.7k ($Ivs\phi$) and in figure 2.7l ($Ivs\theta$). The angular spread in both azimuthal ($\delta\phi$) and polar ($\delta\theta$) angle was calculated 139^0 and 8^0.

785nm laser excitation:

The optical image is shown in figure 2.7m and corresponding FP image is shown in figure 2.7n. The data indicates directional emission from distal end of waveguide. The corresponding quantitative analysis is shown in figure 2.7o (I vs ϕ) and figure 2.7p (I vs θ). The angular spread in both azimuthal ($\delta\phi$) and polar ($\delta\theta$) angle was found 73^0

and 19.7^0.
Based on these results on directional light emission from distal end of DAAQ waveguide, following points can be understood.

(i) For 633nm laser excitation source, both active and passive emission have greater spread (less directional) in azimuthal (ϕ) angle and smaller spread in radial (θ) angles. This indicates that light emitted due to 633nm excitation occupies small set of angles in the numerical aperture (NA) of the lens.

(ii) Compared with all the excitation wavelengths, the active emission intensity (at 532nm laser excitation) has the lowest spread of ϕ and θ values. This indicates that high directionality can be achieved for azimuthal-angular (ϕ) emission for 532nm excitation.

2.3.4 Dual channel directional active emission from waveguide

Next, we explored another interesting aspect of exciton-polariton (explained in section 2.3.7) mediated light propagation. We focused the laser beam arbitrary on the one-dimensional organic waveguide. This lead to the prospect of creating two light emission source with single illumination of a waveguide. Also, we could achieve the two different light emission source with two different directionality. The optical image has been shown in figure 2.8a and corresponding FP images are shown in figure 2.8b and 2.8c. In figure 2.8a, focused laser beam spot is indicated by $excitation$ and two light emitting end by $collection-1$ and $collection-2$. The inset in figure 2.8a shows the magnified SEM images of the two ends of DAAQ waveguide, from where the light was collected. Their respective FP images are shown in figure 2.8b (from $collection-1$) and figure 2.8c (from $collection-2$). In figure 2.8c and 2.8d, we show the emitted light intensity (collected from $collection-1$ end) distribution as a function of ϕ and θ (shown with solid red line). Similarly in figure 2.8c and 2.8d, we show quantitative analysis of the FP image of the light captured from $collection-2$ end (shown with solid blue line). We can observe slight shift in terms of radial angle (figure 2.8d), whereas the spread in emission pattern in figure 2.8c had a single peak in one direction but dual peak feature in other direction. Such distinct feature may be attributed to the end-face morphology of DAAQ waveguide from $collection-1$ to $collection-2$ (see figure 2.8a). Quantification of directional emission is tabulated in Table 2.1.

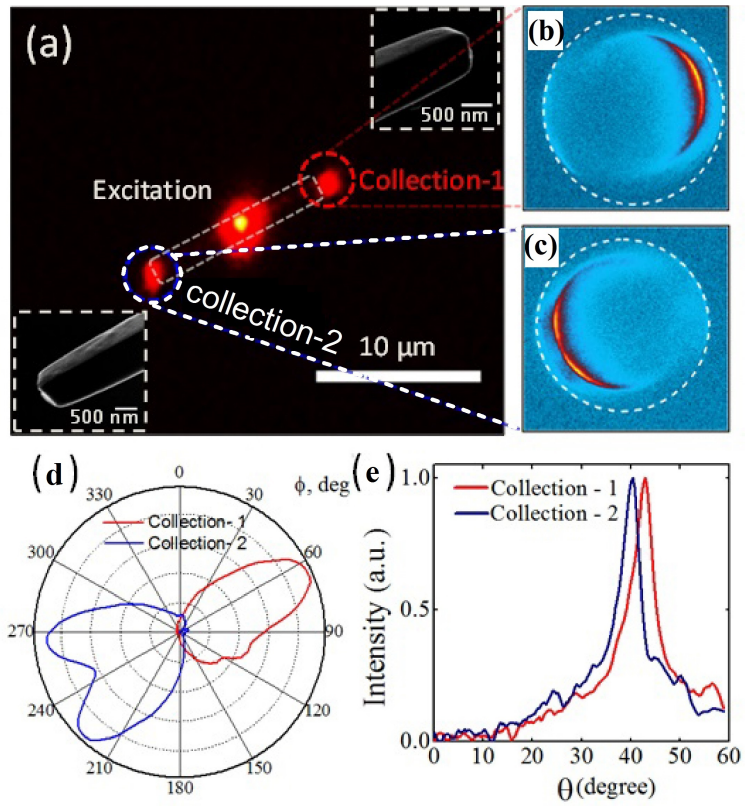

FIGURE 2.8: Single-excitation and dual-collection of active directional emission from the DAAQ waveguide. (a) PL image is shown with laser excitation at the middle of the waveguide and the active emission is observed from the two distal end of waveguide. The insets shows the magnified view of end face morphology of DAAQ waveguide. Corresponding FP images are shown of collected light from two end of organic waveguide i.e. collection-1 (red dash line) and collection-2 (white dash line), respectively. Furthermore, corresponding quantitative analysis is shown in (b) FP intensity vs ϕ and (c) FP intensity vs θ.

TABLE 2.1: Quantification of directional emission from DAAQ mesowire on excitation at the middle

Captured emission end	**FWHM (ϕ)**	**FWHM (θ)**
Collection end-1	68^0	8^0
Collection end-2	116^0	7^0

2.3.5 Dependence of excitation location on active directional emission

Next, we analysed the directionality of emitted light from DAAQ waveguide by varying the excitation location along the waveguide. We didn't observe any drastic change in direction emission of the organic fiber, however we observed significant variation in the emission intensity as the excitation location is brought closer to the collection end. In

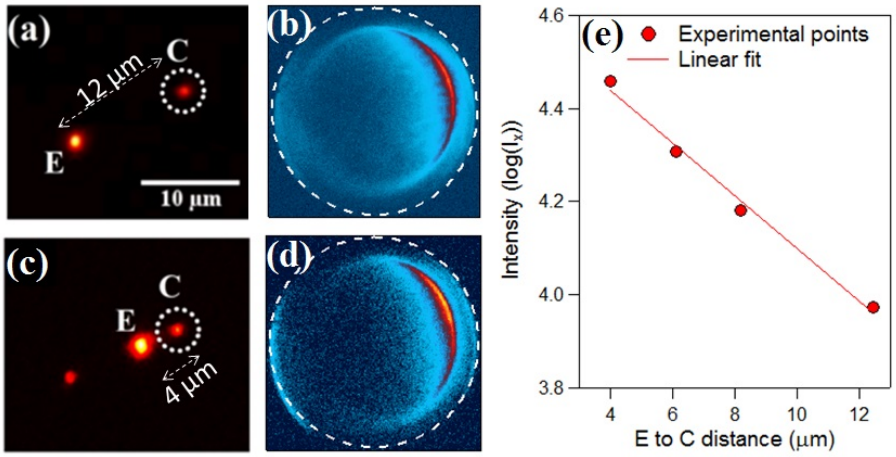

FIGURE 2.9: Dependence of directional light emission in active waveguiding on varying the excitation location. (a) and (c) shows the PL images for two different excitation points on DAAQ waveguide. In case (a), the excitation location is at fixed at one end of organic waveguide, whereas in case (c) excitation location is close to collection end. Letter E and C denote the excitation and collection location respectively and distance is represented by x. (b) and (d) show the corresponding FP images of collected light from point C for two different cases shown in (a) and (c). (e) Variation of emitted light intensity (I_x) in active emission as a function of distance (x) between E and C.

figure 2.9a and 2.9c, we represent the optical images of active light emission by varying the location for two extreme cases (excitation at the end and excitation closet to the collection end). The corresponding FP images and emission intensity distribution are shown in figure 2.9b, 2.9d and 2.9e. We notice the variation in emission intensity as a function of E to C distance, and the plot in figure 2.9e shows an exponential decrement in intensity as the distance from E and C is increased. Furthermore, we quantitatively analysed the captured FP images for four excitation point along the waveguide as a function of ϕ and θ (shown in figure 2.10 and Table 2.2). Emitted light intensity distributions as a function of ϕ are shown in figure 2.10a,c,e and g, whereas figure 2.10b,d,f and h show as a function of θ.

TABLE 2.2: Quantification of directional emission from DAAQ mesowire on varying the excitation along the length

Excitation point end	**FWHM (ϕ)**	**FWHM (θ)**
End point	78^0	10^0
First point along the length	103^0	12^0
Second point along the length	68^0	8^0
Third point along the length	86^0	7^0

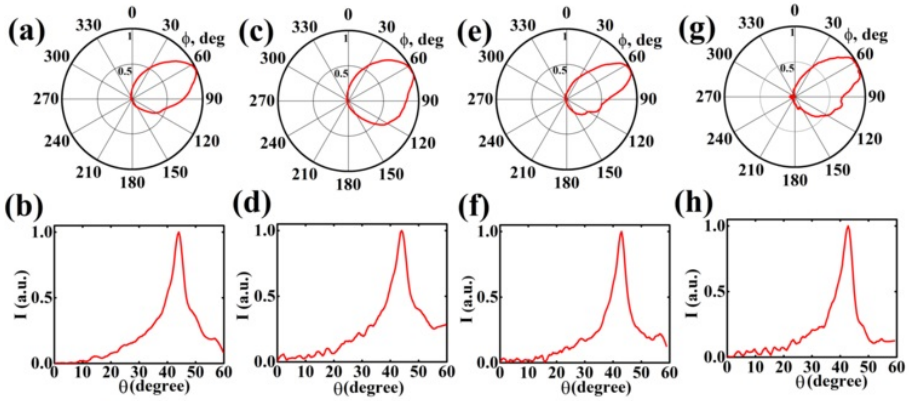

FIGURE 2.10: Quantitative analysis are shown for captured FP images discussed in section 2.3.5. (a), (c), (e) and (f) show the FP intensity vs ϕ, whereas (b), (d), (f) and (h) show FP intensity vs θ for all four cases of varying excitation location along the DAAQ waveguide.

2.3.6 Computational method

In order to further understand our experimental results, especially in the context of mode propagation in passive and active waveguiding regime and its correlation with directional emission, we performed three-dimensional finite difference time domain (3D-FDTD) simulation using lumerical software. We performed the simulation in both far-field and near-field optical regime. To avoid complexity in the simulation, we have restricted our experimental configuration (including glass substrate) to a cylindrical waveguide geometry of length 5μm and diameter 500nm (with smooth side walls). The dielectric function of the waveguide was modelled according to the Lorentz function given as equation 2.1 [180].

$$\epsilon(\omega) = \epsilon_\infty + \frac{f\omega_0^2}{\omega_0^2 - \omega^2 - i\gamma_0\omega} \tag{2.1}$$

where ϵ_∞ is high-frequency component of the organic mesowires dielectric function, f is the reduced oscillator strength, ω_0 is the exciton transition energy and γ_0 is the exciton line width.

To simulate passive waveguiding, 785nm excitation was placed at point E (see figure 2.11a) and the waveguide signal was collected from the location C. The out-couple light was further analysed with respect to directionality (represented as solid red line in figure 2.11c). In the case of active waveguiding, the system was modelled by placing a dipole at point E inside the mesowire geometry. The emission spectra of the fitted dipole was tuned to match with DAAQ molecular emission (shown in figure 2.4). The discussed simulation process was similar to that of Gzera et.al. [148]. We plot the intensity distribution in figure 2.11c. In figure 2.11c, we can compare the angular spread

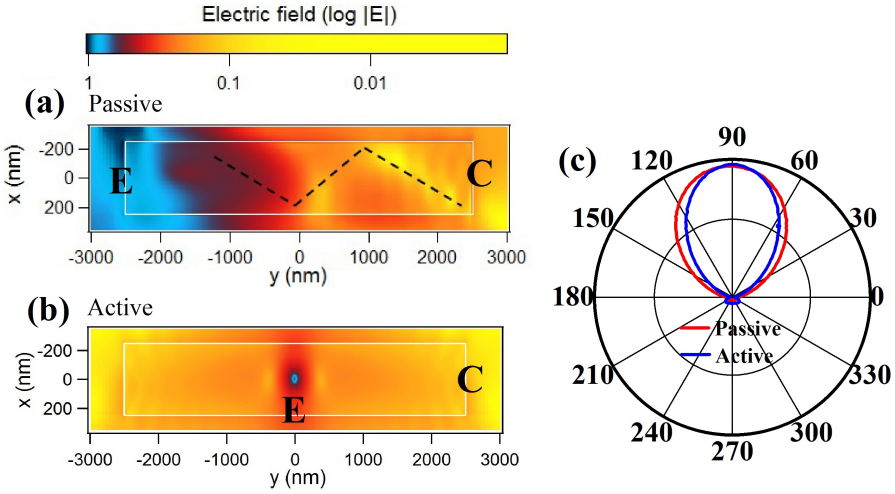

FIGURE 2.11: 3D-FDTD simulation results for (a) passive and (b) active waveguiding of DAAQ waveguide core air-cladding structure resting on glass substrate. Points E and C are the excitation and collection locations. Note that for passive waveguiding, the guided wave travels through total internal reflection (dashed line in (a)). (c) Polar plot comparing the spread in azimuthal angle of the light coming from passive (red) and active (blue) waveguide at point C. The collection was through the glass. It was evident that the passive waveguiding showed greater angular spread (88^0) compared to active waveguiding (68^0).

for both passive (shown as red line) and active emission (shown as blue line). We notice that the angular spread in case of passive is greater than active emission. This trend is in agreement with our experimental observation (discussed in figure 2.7).

2.3.7 Light propagation mechanism in passive and active transportation regime

In the end, we explored the governing mechanism for passive and active waveguiding in DAAQ waveguide. Passive waveguiding mechanism can be understood in terms of total internal reflection (TIR) (discussed in section 2.3.6). Similar to optical fiber, we can notice that guided modes travels through TIR (shown with dotted line in figure 2.11a) [181]. However, we didn't get any information related to active waveguiding mechanism. To explore the mechanism, we measured the anomalous refractive index of a single DAAQ waveguide. The active emission spectra was recorded from the spatially filtered end of DAAQ waveguide with two excitation wavelengths: 532nm and 633nm. The PL maxima for 532nm and 633nm illumination was at 722nm and 727nm respectively. We observed Fabry-Perot (FP) modes in the recorded spectra. However,

for 633nm laser illumination, the PL spectra has superposition of Raman spectral features (higher resolution spectra for both excitation wavelength shown in corresponding insets in figure 2.12a and 2.12 b). Hence, for further exploring the anomalous refractive index in DAAQ waveguide, we excited the organic waveguide with 532nm laser source.
Refractive index (RI) calculation of DAAQ waveguide: We excited one end of organic waveguide and collected the light from other distal end of DAAQ waveguide. Upon excitation one end with photons, they further converted to exciton-polaritons, which propagate along the length of the waveguide. At the distal end of the mesowire, a majority of the exciton-polaritons are converted into photons by radiative recombining the electron-hole pairs. In addition to this emission process at the distal end, a part of the exciton-polaritons were reflected back to other end of waveguide. Thus, these boundary now act as a partially reflecting mirror of a FP cavity. Resultantly, Standing wave pattern was formed inside the cavity and therefore, we observed FP modes in recorded distal end spectra. We used these FP modes to determine the complex refractive index of DAAQ waveguide. The detailed on exciton-polariton propagation mechanism, its connection to FP modes and calculation of RI have been studied in the previous report [54]. Herein, for our measurement, we utilized this knowledge for our study.

Calculation of real part of refractive index via FP modes We have used FP modes to calculate the real part ($n_{||}$) of RI of DAAQ molecules waveguide. We have chosen waveguide of three different length (9μm, 16μm, 21μm). The wires of different lengths were excited with 532nm laser beam source and corresponding spectra was collected from other spatial filtered distal end (see figure 2.12c). We observed FP modes superimposed on the broad PL spectra. The spacing between two consecutive FP peak and real part of refractive index are related by this expression (equation 2.2).

$$\delta\lambda = \frac{\lambda^2}{2n_{||}l} \tag{2.2}$$

where $\delta\lambda$ is spacing between two consecutive peaks. λ is peak wavelength, l is length of mesowire and $n_{||}$ is real part of refractive index.
Utilizing this equation with the observed value of $\delta\lambda$ and waveguide length (l), we calculate the real part of refractive index. The corresponding plot has been shown in figure 2.12d. The best curve is fitted using EP model. More details about EP model is discussed in appendix B
Calculation of imaginary part of refractive index via FP modes To calculate the imaginary part of refractive index ($k_{||}$), we chose the relative longer waveguide (21μm). Herein, we followed the similar procedure discussed in the previous reports [54, 80] for calculating imaginary part of refractive index. We excited the wavguide at different location along the length of waveguide and collect the emission intensity as a function of

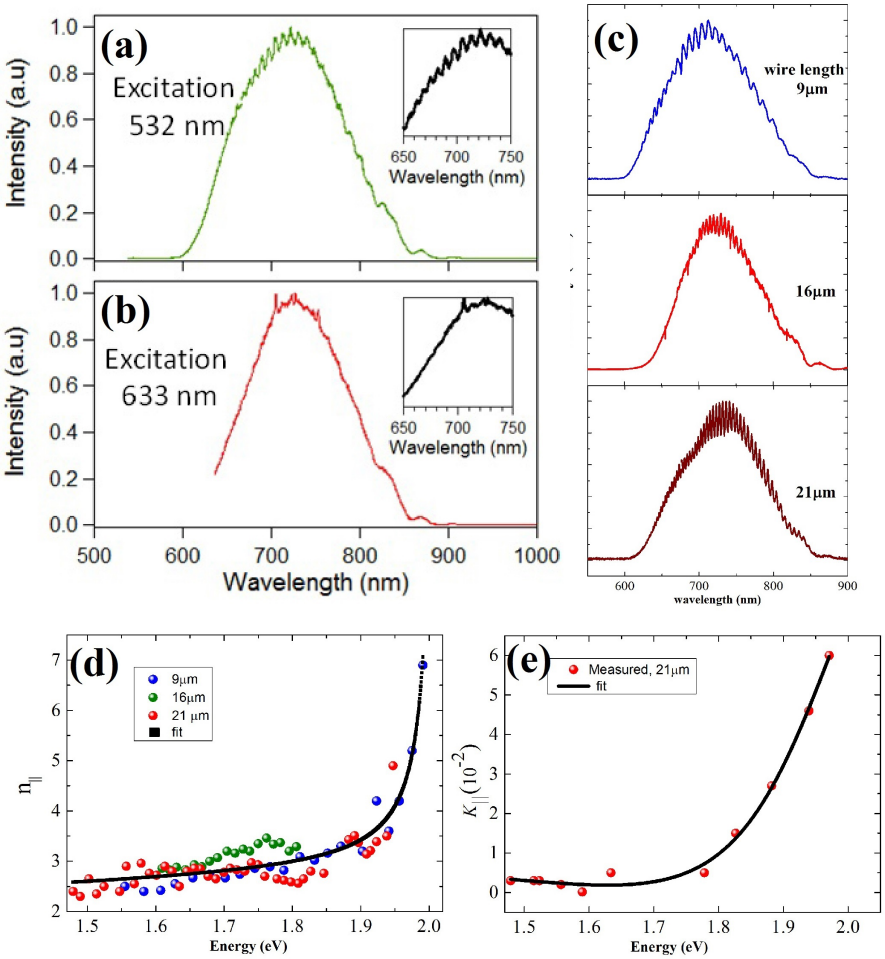

FIGURE 2.12: Spectroscopic signature (PL) obtained from the spatially filtered distal end of a DAAQ waveguide for excitation wavelength (a) 532nm, (b) 633nm. The insets show the magnified view at higher resolution. (c) Active emission collected from waveguide of three different lengths. Variation in (d) real and (e) imaginary part of refractive index as a function of energy. It was evident that the refractive index shows an anomalous increment at higher energies.

distance between excitation point and collection point. Photoluminescence intensity at the excitation location (I_0) and PL intensity at the collection point (I_x) (where x is distance between excitation location and collection location) is related with the following expression (equation 2.3).

$$I_x = I_0 exp(-2\omega k_{||} x/c); \tag{2.3}$$

where I_x is the guided intensity, I_0 is the intensity at excitation location, ω is the frequency of guided light, $k_{||}$ is the imaginary part of refractive index, x is the guided distance and c is the speed of light.

The imaginary part of RI was calculated by measuring the decay in guided fluorescence decay. We recorded the spectra from the distal end in each cases. Intensity at collection point spectra was normalized by excitation location intensity. After computing the imaginary RI value, we plotted the values as a function of energy (shown in figure 2.12e). The best curve is fitted using EP model. More details about EP model is discussed in appendix B

At energies above 1.8eV, we observed an anomalous increment in refractive index values (both for real and imaginary part). This is a characteristic signature of exciton-polariton based light propagation, and has been previously observed for various organic/inorganic meso/nanowire system [54, 80, 182]. The data in figure 2.12d and 2.12e indicates two specific regime. At lower energies values ($1.5eVto1.8eV$), the DAAQ waveguide act as a photonic waveguide, whereas at higher energies ($> 1.8eV$), the optical transport is governed by exciton-polaritons interaction.

2.4 Conclusions

To conclude, in this chapter we have shown directional light emission from an organic molecular waveguide made of DAAQ molecules. The captured light was directional in nature and quantified for both active and passive waveguiding by performing wavelength dependent Fourier-plane optical microscopy and spatially resolved PL spectroscopy. We found that the active emission was more directional as compared to passive emission. In the active light emission regime, organic waveguide showed anomalous refractive index behaviour. Further, we have shown how single organic waveguide can work as dual channel optical router with single point illumination. Moreover, we probed the emitted light directionality by varying the excitation location along the waveguide length.

As a future prospects, such single and dual channel optical router can have direct implications in various applications such as optical interconnects, nano-photonic circuits etc. Furthermore, it would be interesting to explore the directional light emission from the hybrid structures such as organic micro-structures coupled with plasmonic/dielectric substrate. Such findings can not only strengthen our knowledge regarding strong-coupling physics but also in various novel nano-photonics applications.

Chapter 3

Non-reciprocal Directional Emission from a Microsphere coupled Organic Waveguide (MOW)

Chapter 3 is an adaptation of the research article, *Applied Physics Letters, 2016, 108, 031102*. In this article, we discussed about angle-resolved, exciton-polaritons photoluminescence measurements from asymmetric terminals of a microsphere-coupled organic waveguide (MOW). Our results highlight unique directional emission characteristics from a hybrid system and may have direct relevance on single element, exciton-polaritons based nano-photonics device and lasers.

3.1 Introduction

There is a high demand for materials, which can be adapted to realize devices that are inexpensive, flexible and clean. Organic molecular materials cater to this requirement and have been extensively studied in the context of photovoltaics and opto-electronics [77, 159, 162, 167, 183–189]. In the recent years, organic nanomaterials have also been explored in the context of nano-photonics, where optical field has to be manipulated at sub-wavelength scales [54, 55, 77, 189–197]. Specifically, organic semiconductor materials have been explored as they facilitate Frankel exciton-polaritons (EPs), which are essentially quasi-particles of matter and light. The EPs in organic materials arise due to the coupling of Frenkel excitons with electromagnetic radaition [77] and have been extensively studied both in the context of fundamental physics and technological applications [77, 179, 198–200]. Compared to Wannier-Mott excitons in inorganic materials [179, 201], Frenkel EPs have advantage of higher exciton binding energy, larger oscillator strength, high photolumienscence, and greater stability which further helps in guiding photons at subwavelength scale with minimal losses [77, 80, 198, 202–207].

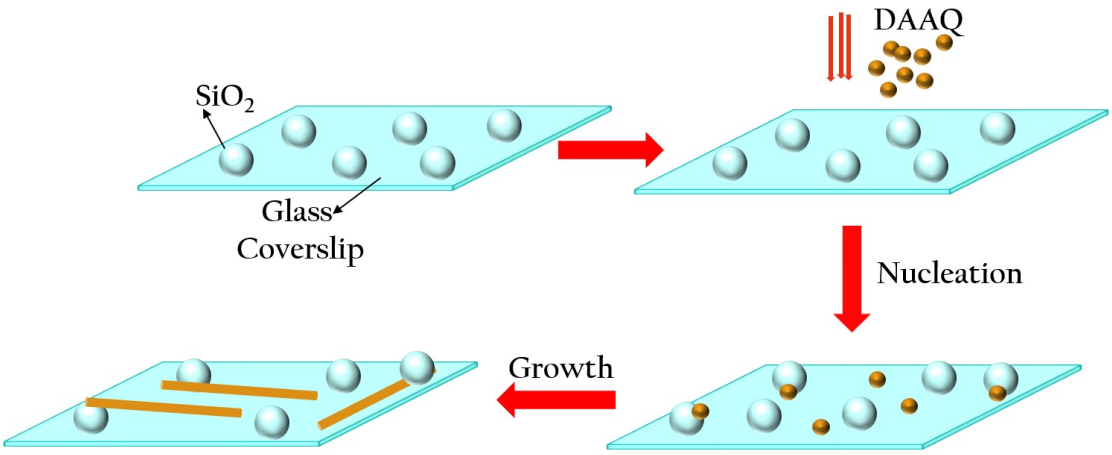

FIGURE 3.1: Schematic of the preparation of microsphere coupled organic waveguide (MOWs). The dielectric microsphere, which we used to prepare these hybrid structures is of SiO_2 (diameter: 3μm) and organic molecular waveguide is made of DAAQ.

Recently, EPs based organic molecular waveguides have been coupled to optical resonator structures such as microspheres and micro-discs [20, 204, 208]. Such coupling is motivated to realize active light sources (lasers and light emitting devices), with large quality factors and minimal coupling loses [20, 208–210]. An unexplored aspect of such coupling is the directionality of light emitted from the terminals of such hybrid architectures. This will be crucial factor to further optimize the active emission devices, and also understand how the out-coupled light can be routed and coupled to other structures on a photonic chip.
Motivated by the above requirement, herein we discussed on characterization of non-reciprocal angular exciton-polaritons emission from the terminals of a hybrid meso-architecture: dielectric microsphere coupled organic mesowire waveguide.

3.2 Experimental section

3.2.1 Sample preparation

A comprehensive synthesis method has been discussed in previous report [20]. We utilized the same knowledge to fabricate such hybrid structures. In a typical preparation method, such hybrid structures were prepared by bottom-up method. The synthesis procedure involved two steps. First, we drop-casted the diluted microsphere (3μm) solution on the clean glass-coverslip and dried it at room temperature in desiccator for 3 to 4 hours. These microsphere drop-casted coverslips were further used to couple DAAQ waveguide. DAAQ waveguide were prepared by physical vapor deposition

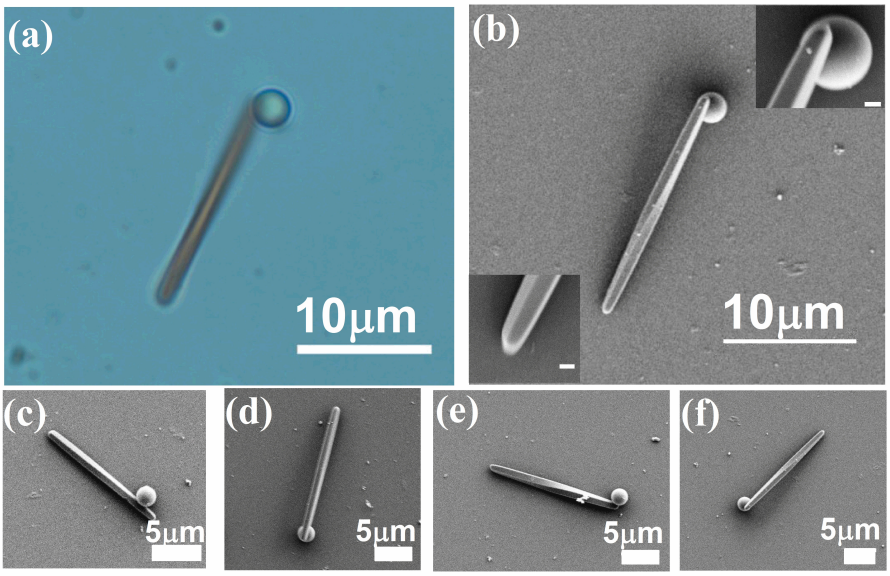

FIGURE 3.2: Microsphere (diameter: 3μm) – coupled organic waveguide (MOW) resting on a glass substrate. (a) Optical and (b) scanning electron microscopy (SEM) image of the same MOW structure. Insets show the higher resolution image of both terminus of the structure. The scale bar is 500nm. (c)-(f) SEM image of a variety of isolated MOW structures.

method [164, 165]. Synthesis process of DAAQ waveguide has already been discussed in chapter 2, section 2.2.1. In brief, 5mg DAAQ powder (85% pure, Sigma Aldrich) was dissolved in 60ml ethanol (99.9% pure, MERCK) in round bottom flask. RB flask was then placed in heating cum rotor bath to make uniform DAAQ molecular thin film around the RB wall. These pre-processed glass-coverslip were suspended inside the RB flask and the whole arrangement were placed in silicon oil bath and increased the temperature up to 170^0C. Since, these pre-processed glass coverslip already had the higher energy sites in the form of microspheres, which acted as a preferential site to couple for new incoming DAAQ molecules (schematically demostrated in figure 3.1) [165]. After 5mins, the glass coverslip was removed from the RB flask and further characterized under optical microscopy and electron microscopy. In figure 3.1, we show the schematic of involved steps to synthesize the microsphere coupled organic waveguide.

3.2.2 Characterization

The prepared samples were investigated under optical microscopy and then electron microscopy. Figure 3.2a shows an optical image of a microsphere coupled organic waveguide (MOW) structure resting on a glass substrate. The scanning electron microscopy image of the same structure is shown in figure 3.2b. The insets in figure 3.2b

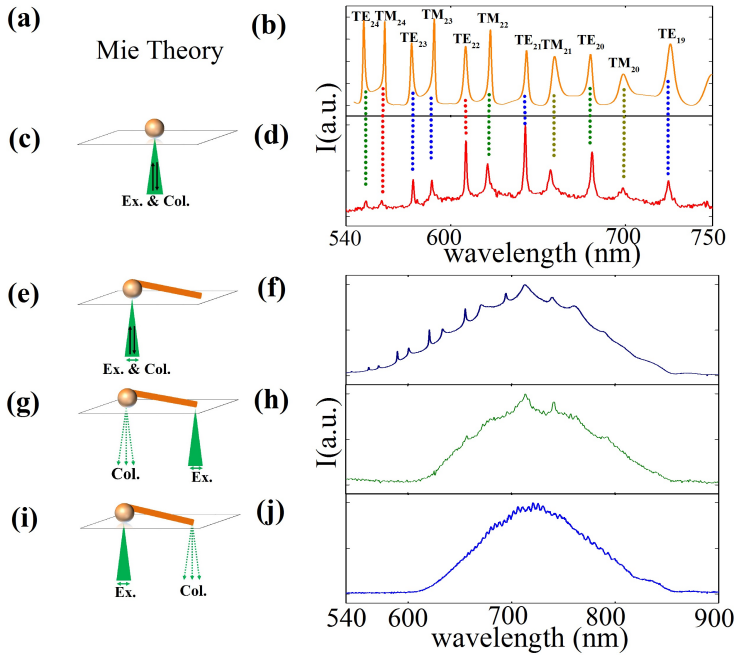

FIGURE 3.3: Spectroscopic signature of isolated DAAQ coated microsphere and MOW structure have been discussed. (a) Whispering gallery modes (WGMs) have been computed by utilizing Mie scattering theory. (b) Computed WGMs have been shown along with cataloguing its modes. Experimental results: (c) DAAQ coated isolated microsphere was illuminated with 532nm laser excitation source and (d) the stokes' shifted spectra was recorded. We see a good agreement in spectra between computed and recorded modes. Next, in MOW structure (e) WGM was captured as we illuminated silica microsphere at the coupled end and PL light was collected from the same terminal. (f) The recorded spectroscopic signature is shown. Thereafter, we remotely excited MOW structure. (g) Free end of MOW structure was illuminated and (h) spectra of out-coupled light from sphere terminal was recorded. (i) Microsphere from coupled end was illuminated and (j) recorded spectra of out-coupled light from free end terminal is shown.

show the high resolution image of the two end terminus of MOW structure. The SEM images in figure 3.2c-f show a variety of MOW structures, indicating repeatability of our preparation method and different way of microsphere- DAAQ waveguide coupling. It is also important to notice that we also observed isolated microspheres coated with DAAQ molecules on the glass coverslip. These isolated microspheres were further used as a control during our directional emission study.

3.3 Results and Discussion

3.3.1 Spectroscopic analysis

We investigated the prepared MOW structures using optical microscopy and spectroscopy. Firstly, we computed whispering gallery modes (WGMs) of a microsphere (3μm) using Mie theory. WGMs can be identified in terms of two polarization states i.e. transverse electric (TE), transverse magnetic (TM) and three other quantum numbers i.e. radial (n), angular (l) and azimuthal (m). The radial quantum number n corresponds to half of the number counted as intensity maxima along the perimeter of the sphere, whereas angular quantum number l implies the number of intensity maxima along the radius of the sphere. The azimuthal quantum number symbolise the degeneracy factor for a given geometry. In figure 3.3a-b show the computed WGMs for 3μm silica microsphere with assigned modes (number in subscript above the associated resonance modes describe radial quantum number n for $l = 1$). The comprehensive mathematical details about WGMs calculation can also be found in appendix- C.

Next, we experimentally probed the spectroscopic feature of isolated DAAQ molecules coated microsphere (schematic shown in figure 3.3c). The microscopy set-up details have been discussed in the previous chapter (see section 2.2 in capture 2), here also we utilized the same microscopy setup. First, we identified isolated DAAQ coated microsphere using 100x, 1.3NA objective lens and illuminated the microsphere with 532nm laser excitation source and recorded the stokes shifted spectra. We engaged 532nm edge filter in the collection path to reject the excitation wavelength. We observed appreciable agreement in both experimentally recorded spectra and theoretically computed spectra (see figure 3.3b and d). The recorded spectra is shown in figure 3.3d. Further, we investigated spectroscopic signature from MOW structure. We remotely illuminated the MOW structures and recorded the spectra. In figure 3.3e, we show schematic of first configuration where we illuminated the microsphere at the coupled end and collected the light from the same terminal. The emitted light was spatially filtered and corresponding spectra is shown in figure 3.3f. We observed pronounced WGMs over the broad photoluminescence (PL) for this configuration. In figure 3.3g, we excited the microsphere at the free end and collected the emitted light from the coupled end of MOW structure. The excitation leads to EPs in the waveguide, which further propagate along its length and out-coupled as PL from sphere-terminus. The light emanating from the collection terminal is spatially filtered using pinhole aperture and recorded the spectra (shown in figure 3.3h). Next, we illuminated sphere-terminus (schematic shown in figure 3.3i) and emitted PL light was collected from free end of MOW structure. The corresponding PL spectra is shown in figure 3.3j. It is evident that the spectroscopic

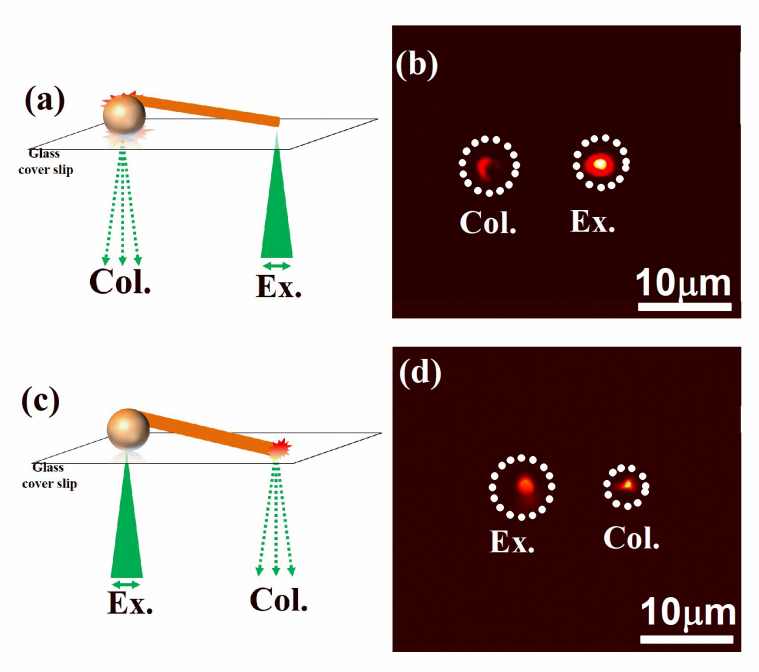

FIGURE 3.4: Two experimental configurations used in directional emission study. (a) Schematic of the first configuration in which free end of MOW structure is excited (indicated as $Ex.$) and the photoluminescence emission was collected (indicated as $Col.$) from the sphere terminus. (b) Photoluminescence image. (c) Schematic of second configuration in which sphere terminus was excited and emission was collected from wire terminus. (d) Photoluminescence image. The excitation source was 532nm laser. For PL imaging, and edge filter was engaged to reject the elastically scattered light.

features can be tuned depending on excitation configuration in a single MOW structure (comparing figure 3.3f, h and j).

3.3.2 Non-reciprocal directional emission from MOWs

The main objective of these experiments was to analyse the directionality of emitted PL signal from the collection points shown in figure 3.4a and b. To probe the directional emission, a home built photoluminescence microscopy with spectroscopic detection and FP imaging capability was utilized [18, 23]. The details for this setup can also be found in section2.3 chapter 2.

For angle-resolved PL measurements, we projected the spatially filtered collected light from MOW terminals on FP plane of the objective lens ($100x$, 1.3NA) and imaged it on EM-CCD (Andor iXon Ultra). The captured FP images was further analysed as a function of two angle, θ and ϕ, where θ is the radial angle defined by numerical aperture of engaged objective lens (in our case, $0^0 < \theta < 60^0$) and ϕ is azimuthal angle

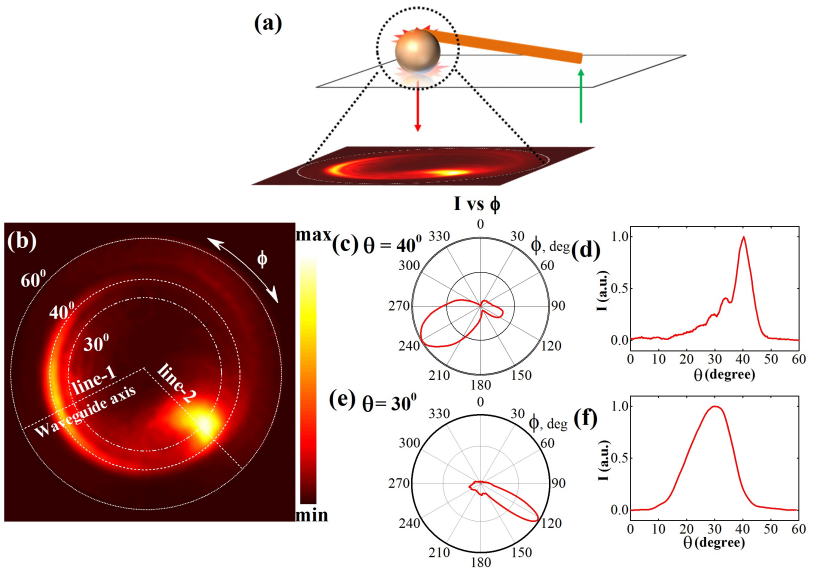

FIGURE 3.5: (a) Schematic of the excitation and emission configuration, and the Fourier-plane (FP) projection of the emitted light. (b) FP image of the intensity of the emitted light from the sphere terminus of MOW structure. The outer-most circle ($\theta = 60^0$) represents the angle of numerical aperture of the objective lens ($100x$, 1.3NA). (c) Intensity distribution as a function of azimuthal angle (ϕ) for $\theta = 40^0$ (close to critical angle of glass-air interface). (d) Intensity distribution as a function of ϕ for $\theta = 30^0$. (f) Intensity distribution as a function of θ for line 2 shown in figure 3.5a.

($0^0 < \phi < 360^0$).

Configuration 1 - Wire illumination, sphere-terminus collection: Figure 3.5a represents the schematic of the experimental configuration with the corresponding projection of emission into Fourier-plane. In figure 3.5b, we show the intensity distribution as function of angles θ and ϕ. The emission was pronounced at two value of polar angles $\theta = 40^0$ and 30^0. Figure 3.5c shows the intensity distribution as a function of ϕ in the direction $\phi = 240^0$, with an azimuthal spread ($\delta\phi$) of around 60^0. Such high forward to backward ratio in the angular emission pattern is similar to the case of plasmonic nanowires [18], an interesting feature to note in our results. In figure 3.5c, we also observed a weak emission around $\phi = 120^0$, with an azimuthal spread of around 30^0. Figure 3.5d shows intensity distribution as a function of θ along the line 1 (as shown in figure 3.5b). The maximum intensity measure was at around 40^0, which is close to the critical angle of glass-air interface (41.5^0) and represents out-coupling of leaky waves [18]. Interestingly, the intensity distribution was oscillatory is nature for θ value less than 40^0. The oscillatory intensity distribution indicates various waveguide modes being channelled at different polar angles. Such oscillatory emission patterns have been

previously reported in complex plasmonic waveguide geometries [211]. Our observation is also unique in the sense that these oscillatory emission patterns has been observed for a hybrid organic waveguide. Furthermore, in order to show the importance of wire-excitation sphere –collection configuration, we compared the angle-resolved emission with sphere-excitation sphere –collection configuration (as shown in figure 3.6). This further highlights the relevance of MOW architecture in the context of directional PL emission.

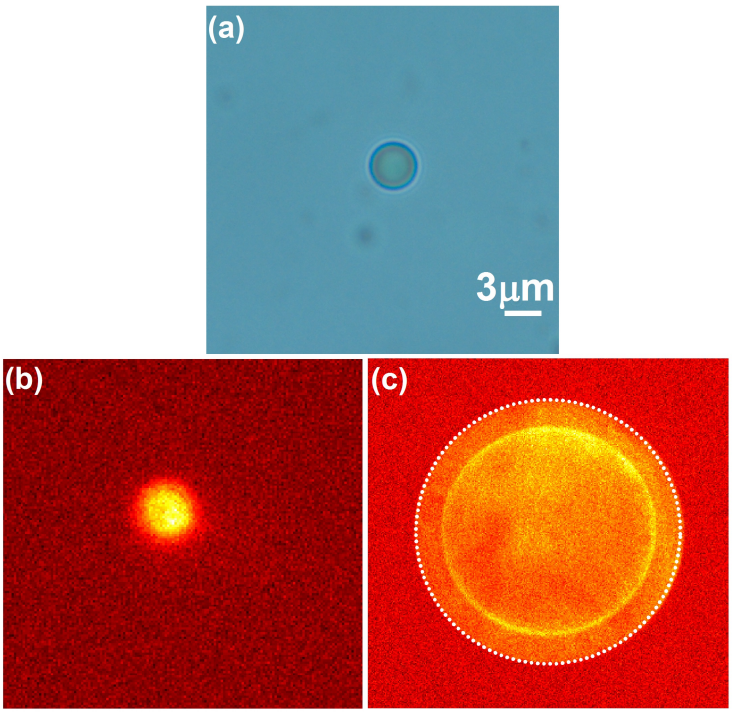

FIGURE 3.6: Angle-resolved PL measurements with isolated DAAQ coated silica microsphere resting on a glass substrate. (a) Optical image of an isolated microsphere (with DAAQ coating); corresponding (b) PL image and its (c) Fourier plane projection. Laser excitation was at 532nm. PL images were obtained after filtering the elastic scattered light with edge filter.

Figure 3.5e shows intensity distribution as a function of ϕ at $\theta = 30^0$. We observed sharp directionality with respect to ϕ with an azimuthal spread as small as 10^0. However, the spread in θ along line 2 (see figure 3.5b) was large as shown in figure 3.5f, with the intensity peaking at $\theta = 30^0$. The origin of this highly directional emission may be due to the direct leakage of exciton-polaritons from the sphere-glass interface. The light emitted from the wire is channelled into the glass. Upon recording the emission through the glass and projecting it into the Fourier plane, we obtained pronounced intensity at two different regions of Fourier plane (as shown in figure 3.5b). The first

region is represented by the arc-like emission. This emission is attributed to directional out-coupling of light from the distal end of waveguide. The second region is represented by bright spot in FP. It is attributed to the focusing effect of the microsphere. Such confined angular distribution suggests a kind of converging-lens effect, probably due to photonic-jet effect [212–214].

The obtained angular emission is sensitive to various parameters such as coupling configuration, coupling distance between microsphere and organic waveguide, size and geometry of microsphere, and waveguide cross-section. Therefore, its angular emission can be precisely tuned by controlling these parameters.

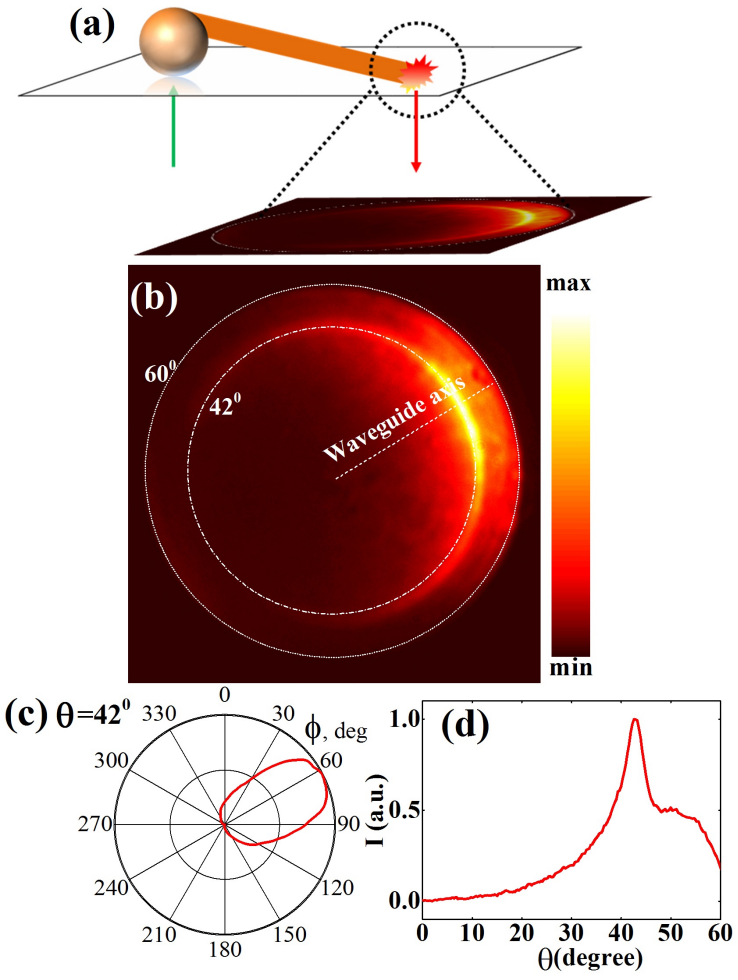

FIGURE 3.7: (a) Schematic of the sphere-excitation and wire-emission configuration, and the Fourier-plane (FP) projection of the emitted light from the distal end of the mesowire. (b) FP image of the intensity of the emitted light from the wire terminus of MOW structure. (c) Intensity distribution as a function of ϕ for $\theta = 42^0$. (d) Intensity distribution as a function of θ for the line shown in figure 3.7b.

Configuration 2- Sphere excitation and wire-terminus collection: Figure 3.7a shows the schematic of the optical configuration, where the microsphere at the coupled end was excited and the optical emission was spatially filtered from the free end of MOW structure (PL image is shown in figure 3.4 c and d). The filtered light was projected onto the Fourier plane. Figure 3.7b shows the intensity distribution of the emitted light as a function of θ and ϕ. The emitted light was directional in nature, with majority of the emission at $\theta = 42^0$. We also observed some emission beyond this angle, upto $\theta = 60^0$. Further, we quantified the captured FP emission by resolving it as a function of ϕ for $\theta = 42^0$, as shown in figure 3.7c. We found the azimuthal angular spread greater than 60^0, which was much greater than the case of sphere terminus emission (shown in figure 3.5c). Figure 3.7d represents the intensity distribution as a function of θ for the dotted line shown in figure 3.7b. We found that the maximum emission occurred at $\theta = 42^0$, which was the critical angle of glass-air interface (41.5^0). Interestingly, we also found some emission beyond the critical angle, which was in contrast to the sphere-terminus emission (shown in figure 3.5d). It is to be noted that the dependence of θ on effective refractive index can be further harnessed as a refractive index sensor [18]. Such emission beyond the critical angle has also been observed in the influence of dye moecules at a dielectric interface and depends on the geometrical factors of the emitter with respect to the substrate [215]. In our case, the wire orientation may also have some connection to the emission beyond the critical angle.

3.4 Conclusion

To summarize, we have studied angle dependent exciton-polariton emission from the two terminus of an MOW structure resting on a glass substrate. Our analysis of the angular emission from the sphere terminus emphasized the two regions of directional emission, of which one of them has an azimuthal spread as small as 10^0. For the wire-terminus emission, the angular spread has a greater azimuthal spread ($> 60^0$), with emission leaking beyond the critical angle of air-glass interface. Our experiments indicates how angular emission varies when the light is collected from two different terminus of a hybrid waveguide: MOW structure. The directionality of light, especially from the sphere terminus can have direct implication on the directional light emitting devices, including one-dimensional exciton-polariton based laser. It would be interesting to further extrapolate our work to observe angle-resolved nonlinear optical emission from two terminus of MOW structure. Such studies can facilitate nano-photonic platform to control and manipulate the optical field at nanoscale regime.

Chapter 4

Radiative Channelling of Nanowire Frenkel Exciton-Polaritons through Surface Plasmons

Chapter 4 is an adaption of a research article *Advanced Optical Materials, in press 2017*. In this article, we discussed about the radiative channelling of nanowire Frenkel exciton-polaritons through surface plasmons. The investigation included the experimental demonstration of near-field coupling between Frenkel exciton-polaritons and surface plasmon polaritons. Moreover, we discussed how to obtain plasmon assisted directional channelling of excitonic emission. Our results highlight the angular channelling of nanowire emission, which have implication in designing efficient single-nanowire photovoltaic devices, and can be harnessed for radiative decay engineering of hybrid nano-photonics sources in coherent and nonlinear optical regimes.

4.1 Introduction

Controlling emission parameters of nanostructures such as intensity and directivity, has emerged as an important task of nanophotonics, and to address this, variety of nanomaterials based on metal, inorganic and organic semiconductors, and dielectrics have been extensively explored [12, 19, 24, 76, 216]. On many of nanostructures studied in the context of subwavelength light propagation, nanowires made of organic semiconductor molecules have drawn significant attention in recent times [20, 54, 167, 171, 217–222].One of the reason is that they facilitate highly stable Frenkel exciton polaritons,[223, 224] which are hybrid states of Frenkel excitons and electromagnetic waves. Since many of the organic semiconducting molecules have large absorption cross-section [12, 76, 77], hyper-polarizability [188, 225], the EPs in such system can be harnessed for active [76], passive [162, 193] and nonlinear wave-guiding [80] of light over millimetre length scale. Such long distance optical transport properties have

been utilized various nanophotonics applications such as optical logic gates [92], resonators [20, 55], nano-lasers [80], and photonic circuits [55, 218] etc.

Interfacing organic molecular platforms with surface plasmons (SPs)[226–228], which are charge density oscillations at metal-dielectric interface, can provide excellent platform to study exciton-plasmon interaction at weak [229] and strong [230, 231] regimes. Interestingly, such coupling can also be harnessed emission for controlling light emission from organic nanostructures[41], down to single photon limit[232]. Various scheme have been explored to interface excitonic systems with surface plasmons such as coupling of quantum dots with plasmonic substrate[233], layered materials with plasmonic lattices [234], core-shell nanoparticles[230], molecular J-aggregates layer with plasmonic nanoparticles [235, 236] and photonic nanowire with gold nanoparticles [232]. These investigations are predominantly confined to probe energy transfer mechanism, recombination processes [237], photoluminescence enhancement [238], Rabi splitting [239], generation of hybrid states [240], bio-sensing applications [194, 241] and low-threshold nonlinear effects [77]. In many of these approaches the dimensionality of the molecular material is either quasi zero-dimensional (0D) or quasi two-dimensional (2D) in nature. So far, there are not many reports in interfacing quasi one-dimensional (1D) organic molecular systems, such as nanowires, with surface plasmons [242, 243]. One such example is vertically oriented organic nanowire on gold thin film [242, 243]. Such as a single, vertical nanowire provides a unique opportiunity to study of 1-D propagating exciton-polaritons with 2D propagating plasmon polaritons at nanoscale. In this coupling scheme, an important issue to be addressed is the out-coupling of EP photoluminescence emission from a single, vertical nanowire into a specific direction through leaky plasmon channels of a gold film. Given that spontaneous emission is isotropic, there is an imperative to channel the nanowire emission, such that a majority of the light is collected and harnessed. Such directional out-coupling of emitted light has consequence on designing photovoltaic devices such as single-nanowire solar cells [237, 244, 245], organic light emitting devices [76, 188], EPs lasers [80] and nano-optical bio-sensors [77, 188].

Hence, herein, we experimentally demonstrate directional, EPs photoluminescence emission channelled from a single, vertical organic nanowire through a plasmonic leaky channel of gold thin film. Figure 4.1 represents the conceptual schematic of the experiment. The tip of a vertical oriented organic semiconducting nanowire made of 1,5diaminoanthraquinone (DAAQ) molecules is excited by a tightly focused laser beam at 532nm wavelength. This excitation is close to absorption band of the molecular nanowire (discussed in chapter 2), which further results in red-shifted EPs generation, and subsequent propagation along the length of the nanowire. The photolumienscence

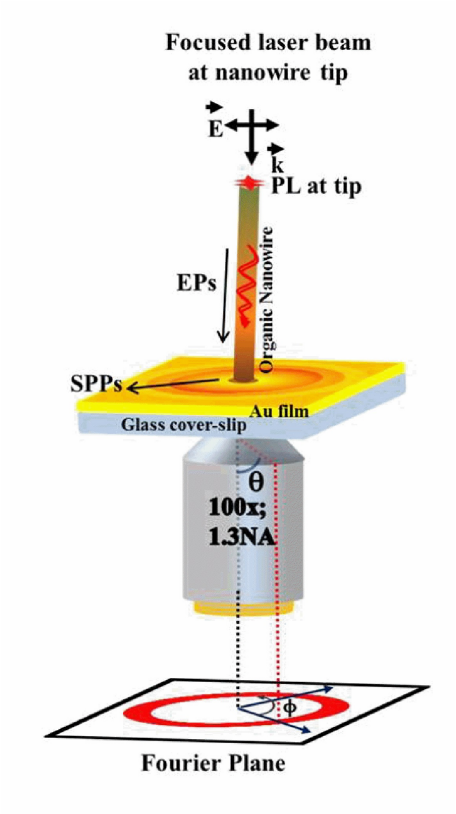

FIGURE 4.1: Conceptual schematic of surface plasmons (SPs) coupled directional emission of Frenkel exciton-polaritons (EPs) from a single, vertical organic nanowire. Tip of nanowire is illuminated with tightly focused laser beam at 532nm wavelength. EPs propagate along the length of nanowire and leak out through plasmonic gold film into the glass substrate. The angular dependence of the leakage photoluminescence radiation is imaged via Fourier-plane imaging technique in the detection channel with a high numerical aperture objective lens. Figure not to scale.

maxima was 722nm (discussed in chapter 2). When the EPs reach the gold film, they leak through the plasmonic channels, and radiatively out-couple at sharp radial angles beyond the critical angle of glass-air interface, which can be captured in the FP of the imaging system [246]. To understand energy transform mechanism under various coupling configurations in our geometry, we have performed finite element method (FEM) based electrodynamics that supports our experimental results. For efficient calculation of leakage radiation pattern in Fourier plane, we have utilized an improved simulation strategy of Yang et al.[247] which is based on Lorentz reciprocity theorem.

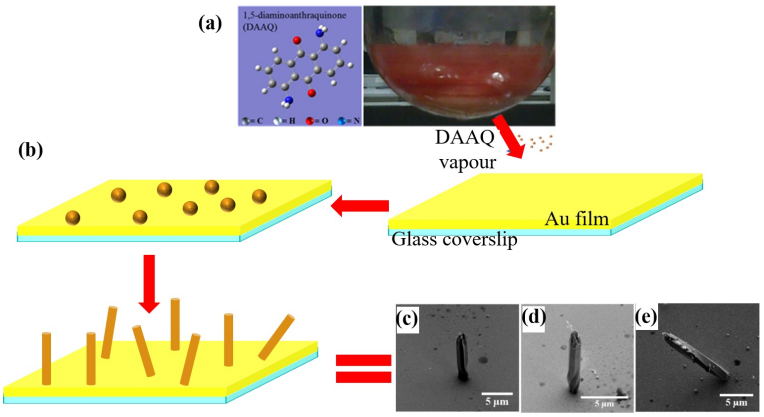

FIGURE 4.2: Growth of vertically oriented organic nanwires on a plasmonic thin film. (a) The chemical structure of the di-aminoanthraqunione (DAAQ) molecule used for the growth of organic nanowires. A photograph image of round bottom flask uniformly coated DAAQ molecular thin film. (b) Schematic of steps involved in growth process of vertical organic nanowire on gold film. (c), (d) and (f) represent the corresponding SEM images captured from the prepared sample.

4.2 Experimental Section

4.2.1 Sample preparation and characterization

The hybrid nanostructures were fabricated using vapour deposition method [112, 164, 165]. An elaborate protocol to prepare such structures has been reported earlier [112, 165]. We have followed the same process to grow these hybrid nano-architectures. In a typical preparation, $10mg$ of DAAQ powder was dissolved with $60ml$ of ethanol in round bottom (RB) flask. A thin film of DAAQ molecules was formed on RB flask by evaporation of ethanol in a heater cum rotor bath at 60^0C. The gold coated ($60nm$) coverslip was then suspended inside the round bottom flask through glass bar mounted on the top, and the whole arrangement was then kept inside the silicon oil-bath (schematic of the whole arrangement has been previously shown in chapter 2, section 2.2.1). The temperature of oil-bath was then increased to $160^0C - 170^0C$, which was monitored by a sensor inserted into the RB flask. The DAAQ molecules were vaporized from the inner wall of the RB flask and condensed on the substrate. After 10 min of deposition at the constant temperature, the glass substrate was removed from the flask (schematic demonstration of the process is shown in figure 4.2a and b). The prepared samples were then characterized under optical microscopy and electron microscopy. Some of the captured SEM images of synthesized nanowire with different orientation are shown in figure 4.2c-e.

We captured large-area field emission scanning electron microscopy (FE-SEM) scans

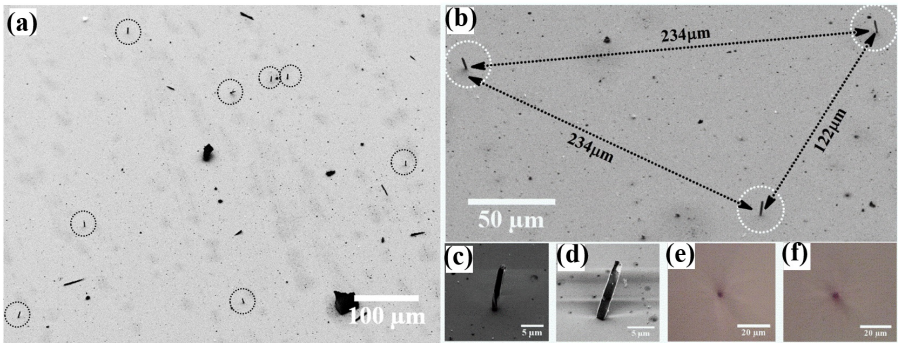

FIGURE 4.3: Field emission scanning electron microscope (FE-SEM) and optical image of individual, vertically oriented DAAQ nanowires on Au-film (60nm). (a) Arial view of Au-film coupled vertical organic nanowire. The black dotted circles indicate vertical organic nanowires. This aerial view also emphasize that the nanowire are well disperse throughout the film surface. (b) Wide-field FEM image of multiple nanowires. Individual vertical organic nanowires are represented by white dotted circles and the distances between two nanowires were sufficiently large for optical microscopy studies. (c) and (d) are higher resolution FE-SEM images of two different individual organic nanowires. (e) and (f) White light reflection image of vertical organic nanowire focused at the tip and at the bottom of nanowire, respectively.

at lower magnification (see figure 4.3a and b), which provides an overview of the prepared sample. The overview image also emphasizes that synthesized vertical organic nanowires are well separated to perform optical measurements from individual nanowire. High resolution FE-SEM images of two individual vertical organic nanowires are shown in figure 4.3c and d. Further, the optical images if an individual vertical organic nanowire are shown in figure 4.3e (focused at the tip) and figure 4.3f (focused at the base).

4.2.2 Instrumentation

We investigated the prepared hybrid structures through our home-built microscope setup shown in figure 4.4. This microscope consisted the following capabilities:

(i) focused laser beam illumination from the top;

(ii) dual channel microscopy and single channel PL spectroscopy;

(iii) real plane and Fourier plane (FP) imaging from lower channel

In the upper channel, 532nm laser excitation source (continuous-wave laser) was used to illuminate the nanowire. A 532nm line filter (Semrock Max line, LL01-532) and

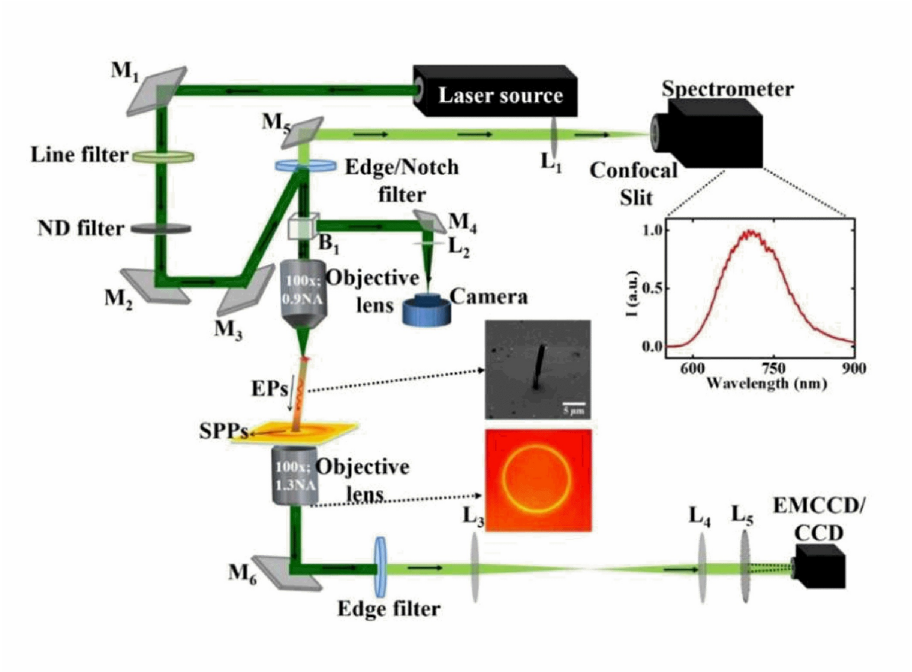

FIGURE 4.4: Schematic of optical set-up employed for conventional and Fourier plane PL imaging. Individual organic nanowire was illuminated by a 532nm laser source using $100x$, 0.9NA objective lens. The PL spectrum was recorded from the tip of organic nanowire (shown on right side). The leakage radiation was captured through $100x$, 1.3NA oil-immersion objective lens. Fourier and real plane imaging were performed with combination of lens (L_3, L_4 and L_5). The excitation wavelength was rejected by introducing edge filter in collection path and FP image was captured by an EM-CCD camera. Inset shows FE-SEM image and corresponding FP image of one of the nanowires. Optical schematic diagram not to scale.

a neutral density (ND) filter were engaged in the illumination path to ensure monochromatic, low power excitation. The tip of vertical organic nanowire was carefully focused upon and illuminated with an objective lens ($100x$, 0.9NA, spot-size 1-2μm). Backscattered light was collected from the same objective lens and optical images as well as photoluminescence (PL) spectra of the nanowire were captured by routing light to camera (for conventional imaging) or spectrometer (LabRam HR, 789mm focal length, pinhole size = 200μm, 600 grooves/mm grating) in the upper channel of microscope.

In the lower channel, the leakage radiation (LR) was collected through the glass substrate with high numerical aperture ($100x$, 1.3NA) oil-immersion objective lens. To reject the excitation wavelength, we introduce 532nm edge filter (Semrock Razoredge, LP03-532RU) in collection optics. The real plane and FP imaging were performed with the combination of tube lens (L_3), Bertrand lens (L_4) and L_5. The resulting image was captured with EM-CCD/CCD. For single nanowire studies, we correlated the FE-SEM

image of a single nanowire with its optical image in real and Fourier space. Inset in figure 4.4 shows one such correlated image of a single nanowire and its PL image in Fourier space captured FP image was quantified using two parameters (θ and ϕ). The radial angle, θ is restricted by numerical aperture (NA) of imaging oil-immersion objective lens ($0^0 < \theta < 60^0$) and the azimuthal angle ϕ, can vary from 0^0 to 360^0.

4.3 Results and Discussion

4.3.1 Directional emission from Au-film coupled organic nanowire

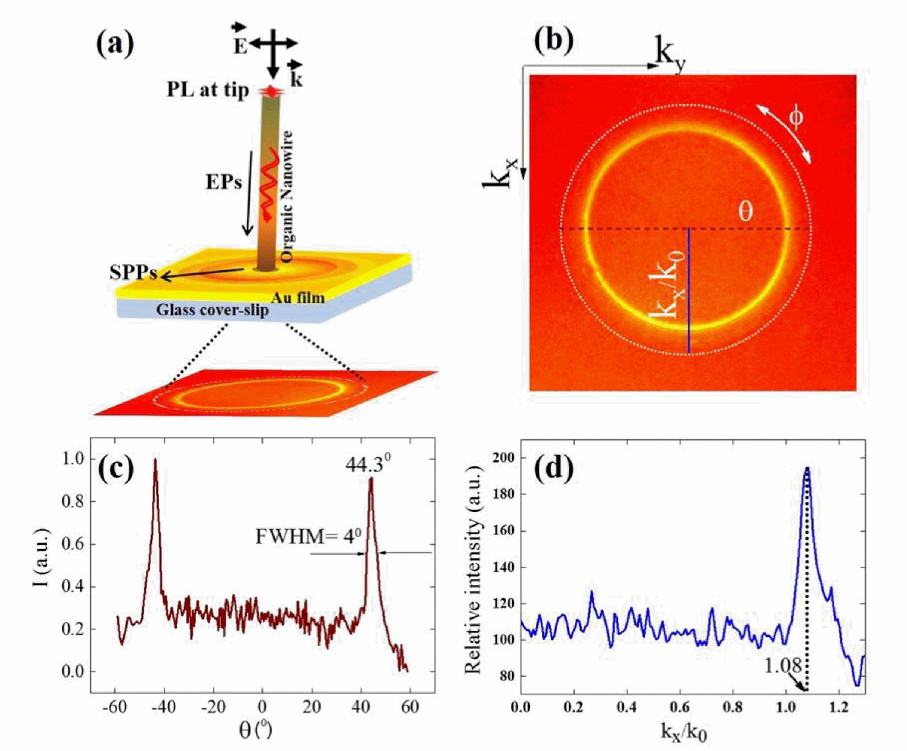

FIGURE 4.5: (a) Schematic of the excitation configuration and the Fourier-plane (FP) projection of leakage radiation through the substrate. (b) Captured FP image of plasmon coupled EP photoluminescence from a single vertical organic nanowire. The outer circle corresponds to numerical aperture of oil-immersion objective lens. (c) Intensity distribution as a function of radial angle (θ) along the dotted (brown) line in figure 4.5(b). (d) Intensity distribution as a function of k_x/k_0 along the solid line (blue) in figure 4(b).

Our main objective was to probe out-coupled directional emission of EPs from a single, vertical organic nanowire. Figure 4.5a shows the schematic of the experiment with corresponding projection of emission onto the Fourier plane. The intensity distribution as a function of co-ordinate angles θ and ϕ is shown in figure 4.5b. The outer

circle represents the numerical aperture (NA) of the imaging objective lens ($\theta = 60^0$). We observed that the emitted light was directional in nature, and majority of emission occurred at a defined radial angle. We plotted the intensity distribution (shown in figure 4.5c) as a function of θ along the horizontal line (dashed brown line in figure 4.5b). We found the maximum emission occurred at $\theta = 44.3^0$, which is beyond the critical angle of air-glass interface (41.1^0), and can be termed as evanescently out-coupled forbidden light [248]. Such emission is observed because of near-field optical coupling, and is attributed to interaction of evanescent field components of molecular emission dipole with plasmonic thin film [248, 249]. We also found that forbidden light emission was sensitive to dipole position above the plasmonic substrate (discussed in section 4.3.3 and 4.3.4). We emphasize that the captured forbidden light has significant implications in designing high numerical aperture imaging systems to interrogate semiconductor nanowire [250] using sub-diffraction spatial resolution microscopy [249], and complements the imaging using conventionally allowed light.

4.3.2 Effective refractive index of hybrid leaky mode

We further analysed the wave-vector of leaky modes and calculated the effective refractive index (n_{eff}) by FP image. Procedure of such as calculation can be found in chapter 2. Figure 4.5d shows the intensity distribution as a function of k_x/k_0 along the vertical line (as shown with solid blue line in figure 4.5b). We found the maximum intensity at $k_x/k_0 = 1.08$, which indicates effective refractive index value of leaky modes. The reduction in effective refractive index highlights that the leaky modes are distinct from the bound EPs modes of an isolated organic waveguide, which has greater effective index (discussed in chapter 2). Importantly, the leaky modes in such hybrid system have combined physical characteristic of plasmons and excitons [251]. Mixture of these physical characteristic have numerous advantages over isolated organic or plasmonic nanostructures and can potentially facilitate test-beds for strong and weak-coupling physics, low propagation loss waveguides [252], high speed data transmittance [12], mode conversion [253] and efficiency enhancement in energy harvesting devices [254].

4.3.3 Numerical analysis

To corroborate our experimental observation from a vertically oriented nanowire, we performed finite element method (FEM) based, full-wave numerical simulation using COMSOL software (version 5.1). Our geometry to simulate vertical nanowire emission was similar to previous literature [255]. The schematic of the simulated geometry is shown in figure 4.6a. It consisted of a DAAQ cylinder of refractive index (discussed in

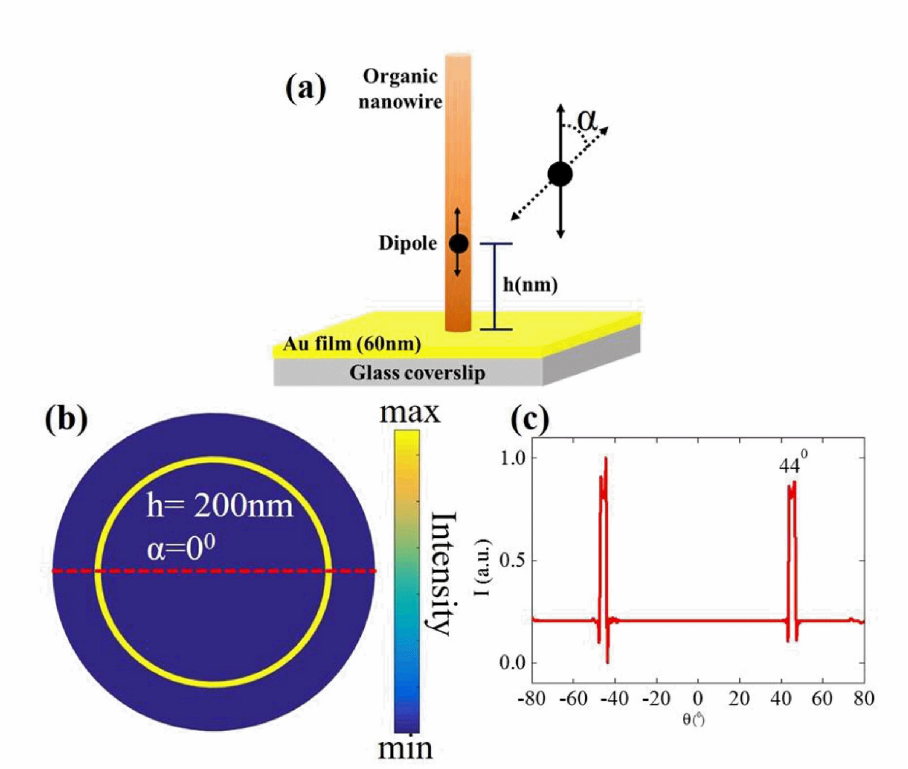

FIGURE 4.6: (a) Schematic view of 3D simulated geometry from a vertical nanowire. The emission dipole radiates at $\lambda = 700nm$. Dipole distance above the film is shown by h and orientation angle is indicated by α with respect to its vertical orientation. (b) Simulated far-field intensity projection of captured leaky emission through the glass substrate. (c) Intensity distribution as a function of radial angle (θ) along the dashed (red) line shown in figure 5(b).

chapter 2), in which vertical emission dipole was embedded at a distance h from a gold thin film (60nm) on top of a glass substrate. The angle α represents the angle between the ling axis of the nanowire and the dipole orientation (shown in figure 4.6a). The wavelength of dipole emission is fixed at $700nm$ (discussed in chapter 2, section 2.3.7). For the analysis of far-field radiation emission from stratified simulation geometry, as in our case, an accurate method to transform near-field to far-field intensity is necessary. For this purpose, we have adapted the recently developed simulation strategies of Yang et.al [247].

Figure 4.6b represents the simulated far-field intensity projection of leaky emission for dipole placed at $h = 200nm$ and $\alpha = 0$. The emission was confined to a narrow range of angle in the far-field. Figure 4.6c shows the intensity distribution as a function of polar angle θ at $\theta = 44^0$. This is in excellent agreement with our experimentally observed value (44.3^0) as discussed in data related to figure 4.5b and c. The fact that the

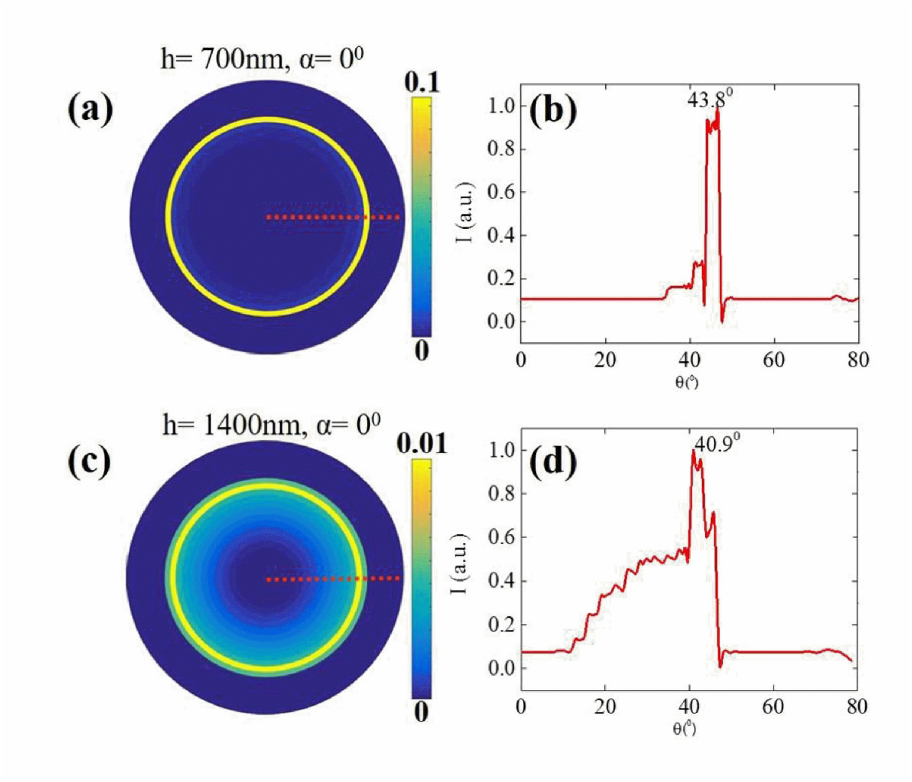

FIGURE 4.7: Far-field leakage radiation pattern from a nanowire as a function of distance between the vertical dipole and the plasmonic thin film. (a) Far-field radiation pattern for dipole placed at $h = 700nm$; (b) corresponding intensity distribution for the dashed line shown in a. (c) Far-field radiation pattern for dipole placed at $h = 1400nm$; (d) corresponding intensity distribution for the dashed line shown in c. Note that the intensity changes for the two cases discussed.

emission occurs at angle beyond critical angle of glass-air interface clearly indicates near-field coupling between the emission dipole of the nanowire and plasmonic thin film.

With this insight, we can understand the observed emission as a three step process. (i) EPs are excited at free end of the nanowire via focused laser beam illumination, which propagates towards the other end of the nanowire. (ii) At the nanowire-metal junction, EPs couple to SPPs via near-field interaction, and thereby excite the propagating SPPs along the gold-air interface. (iii) This propagating SPP field diverges from the interaction point, and the transferred energy radiatively leaks through the dielectric medium with higher refractive index, which is glass substrate in our case.

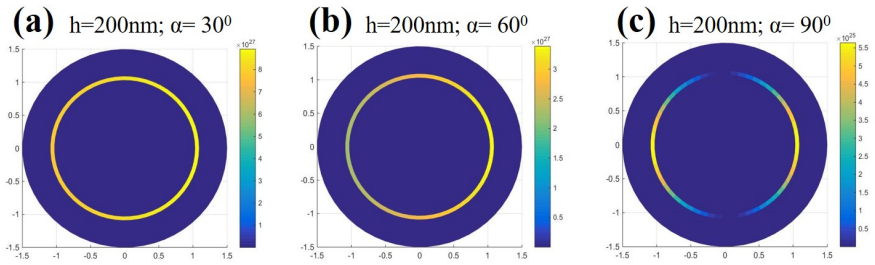

FIGURE 4.8: Numerical simulated leaky far-field patterns for varying dipole orientation above the gold film. (a) , (b) and (c) Simulated far field projections have been shown for different orientation $30^0, 60^0 and 90^0$ respectively.

4.3.4 Angular emission tunability in film coupled organic nanowire

In the context of the discussed geometry, it would be interesting to ask whether one can vary the parameters of emission, such as its angle and intensity as a function of geometrical variables. To address this, first we numerically explored emission dependence on dipole position, h, above the plasmonic film. A vertical dipole was placed at $h = 700nm$ ($h = \lambda$, emission wavelength) above the gold surface and far-field emission was calculated as shown in figure 4.7a. We found that the emission occurred at angles on either side of critical angle of glass-air interface (shown in figure 4.7b). However, when the dipole was placed at $h = 1400nm$, which indicates a far-field coupling regime, we observed majority of the light emitted at or below the critical angles (shown in figure 4.7c and d). Furthermore, the intensity of the emitted light changes by an order magnitude when the dipole is displaced further away from the surface. Such angular and intensity dependence of emitted light on the position of dipole is well known in the literature [248, 249], and in the context of our work, it indicates that by changing the gap between the nanowire emission dipole and plasmonic surface, one can potentially switch the coupling between the near-field and far-field.

In addition to the dependence of h, we explored the dependence of angle α (at constant h) on the emission parameters (shown in figure 4.8). The leakage intensity was found to be maximum in the case of vertical dipole ($\alpha = 0^0$) and minimum in case of horizontal dipole ($\alpha = 90^0$). This result could be understood in the context of method of images,[248] which suggested that vertical dipole ($\alpha = 0^0$) efficiently coupled with plasmons compared to the horizontal dipoles ($\alpha = 90^0$). In the context of our geometry, these data indicated that by systematically varying the angle between the nanowire growth and the surface normal of the plasmonic film, the dipole orientation, and hence the outcoupled quantum efficiency of the emitted light could be potentially tuned.

4.4 Conclusion

To summarize, we have demonstrated, for the first time, plasmon-coupled directional channelling of Frenkel EPs from an individually, vertically oriented, organic nanowire. The observed leakage of the directional emission through plasmonic channels predominantly occurred at directions beyond the critical angle of glass-air interface indicating near-field coupling between EPs and surface plasmons, which was supported by numerical simulations. Furthermore, the simulations revealed the relevance of the two parameters: distance and orientation between the emission dipole of nanowire and the plasmonic surface, which could be further harnessed to engineer the angle and intensity of the exciton-polaritons emission from a single organic nanowire device. We envisage that the results presented herein can be utilized for various applications, such as: to improve light collection efficiency on organic photovoltaic devices; single nanowire based coherent sources, where the directionality of the stimulated emission can be precisely controlled through the plasmonic leakage channels. Since the nanowires that we use are large hyper-polarizability values, our studies can be extrapolated to nonlinear optical effects from a hybrid Frenkel exciton-surface plasmon system.

Chapter 5

Future outlook and conclusion

The work presented in the thesis is mainly focused on investigating the ability of directing light from variety of organic semiconductor nano-architectures. A small comparison between plasmonic nanowire and organic molecular waveguide is demonstrated in Table 5.1. In chapter 2, we presented the work on spatially directing the emitted light (both in active and passive operational regime) to specific direction by utilizing DAAQ molecular waveguide. All the photonic properties of organic nanomaterials are mainly directed by exciton-polaritons (EPs) propagation. These EPs assisted organic materials are ideal to fabricate micro-resonators spanning their emission over the whole visible spectrum. However, tailoring their resonant modes with defined directional emission is still a challenge. To address this issue, we have explored another facet of molecular coupling i.e. coupling of organic waveguide/nanowire with dielectric microstructure and plasmonic structures. In chapter 3, we explored optical microcavity (SiO_2 micropshere) coupled organic waveguide. In such hybrid configuration, the WGMs of microsphere was utilized for signal modulation (active element) and organic waveguide was used for signal transportation in defined direction. Additionally, directional emission from such coupling architectures would be crucial to further optimize the active emission devices and also to understand how out-coupled light can be routed and coupled to other structures on a nanophotonic chip. In capture 4, we interfaced organic molecular platform with plasmonic substrate and characterize it in near-field coupling regime. We presented the evidence of directional, EPs assisted PL emission channelled from a single vertical organic nanowire through a plasmonic leaky channel of gold film.

As a future direction, we are interested in exploring the exciton-plasmon coupling effect in two dimensional (2D) plasmonic lattice coupled to one dimensional (1D) organic nanowire. Plasmonic lattices, which exhibit collective plasmon oscillations, can efficiently tailor the behaviour of quantum emitters (quantum dots, molecules, nitrogen vacancy) placed in their vicinity. Moreover plasmonic properties can be further tuned by tailoring various parameters such as varying the individual constituent size, geometry, inter-particle distance and their arrangement [25] etc. We anticipate that efficient

TABLE 5.1: Comparison between plasmonic nanowire and Organic nanowire

Plasmonic nanowire	**Molecular nanowire**
Merits	
subwavelength propagation	
field confinement and localization	
geometry and polarization dependent signal modulation	
Active tuning of resonances	
Difference	
SPPs based propagation	TIR/EPs based propagation
Easily get oxidized	highly stable
Passive transportation	Passive and Active transportation
Huge propagation and heat loss	low loss propagation
Single channel emission	single and dual channel emission
—-	Modulation of out-coupled intensity in active waveguiding
External gain medium is required	molecules itself work as active medium

exciton-plasmons coupling in such type of hybrid configurations may facilitate deeper insight in various fundamental quantum phenomena such as coherent energy exchange [11, 256], photon entanglement [11, 257], and cavity assisted electrodynamics [258]. Along these lines, we have made some advancement in terms of fabrication of such hybrid nano-architectures. In this technique, it is relatively easier to control the positon of nano-particle with various shape and size by simply varying the template constituents' parameters. In the following section, we discuss about preparation of plasmonic lattices/ cavities by using template assisted nano-particle self-assembly process.

5.1 Experimental Section

5.1.1 Preparation of hybrid nano-architectures

The preparation of hybrid nanostructures is two-step process. First step involves both top-down and bottom-up approach to fabricate the plasmonic lattices [25]. In the second step, the organic structures were coupled via physical vapour deposition method [112, 164, 165]. In a typical preparation method, the templates were patterned using electron beam lithography (EBL) method. Figure 5.1a represent the schematic of template preparation procedure. Comprehesive detail of the procedure can be found in previous reports [259–261]

We used Silicon (Si) wafer to prepare the template. First, the Si wafer (1cm $\times$ 1cm)

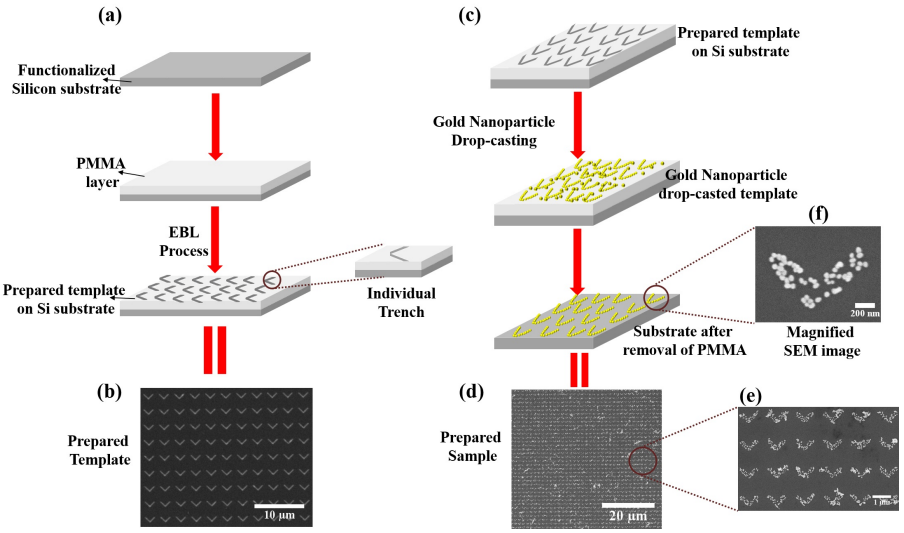

FIGURE 5.1: Preparation of plasmonic lattices using template assisted nanoparticles assembly. (a) Schematic representation of template fabrication. (b) SEM image of the prepared template. (c) Schematic demonstration of nanoparticles self-assembly in fabricated template. (d) Aerial view of the prepared plasmonic lattice. (e) Plasmonic lattice at higher magnification and (f) Higher magnification view of an isolated constituent of prepared lattice. [Manuscript under preparation]

was cleaned using isopropanol, HF acid, DI-water and ultra-sonication method. This treated Si−wafer was used for surface functionalization with Aminopropyltriethoxy silane and then kept for pre-baking at temperature 150^0C for 10 mins. Further, this Si-wafer was used for spin-coating of EBL resist (polymethyl methacrylate (PMMA), Molecular weight: 950K) at 8000rpm and then kept for post-baking at temperature 150^0C for 30 mins. The processed Si-wafer was subsequently used for EBL patterning. The longer arm of the trench was 700nm and width was 200nm. Figure 5.1b represents the SEM image of one of the prepared templates. This prepared template was further used for self-assembly of desired nanoparticle (shown in figure 5.1c). We used gold nanoparticle (diameter: 60nm) to get self-assembled on prepared template. The prepared template was dipped in gold nanoparticles solution. Since, these nanoparticles were opposite charged compared to the functionalized Si-surface, these NPs got attached at the surfaces. Si-wafer was then kept in N-Methylpyrrolidine for 30mins and taken out from the solution. The prepared sample was then investigated under scanning electron microscopy (SEM) to observe the quality of the prepared. Figure 5.1d shows the SEM image of the fabricated sample. The magnified view are also shown in figure 5.1e and f. It is evident that the self-assembly of gold nanoparticles were consistent over a large Si-surface area.

Moreover, we prepared various templates on functionalize Si-wafer with scale down

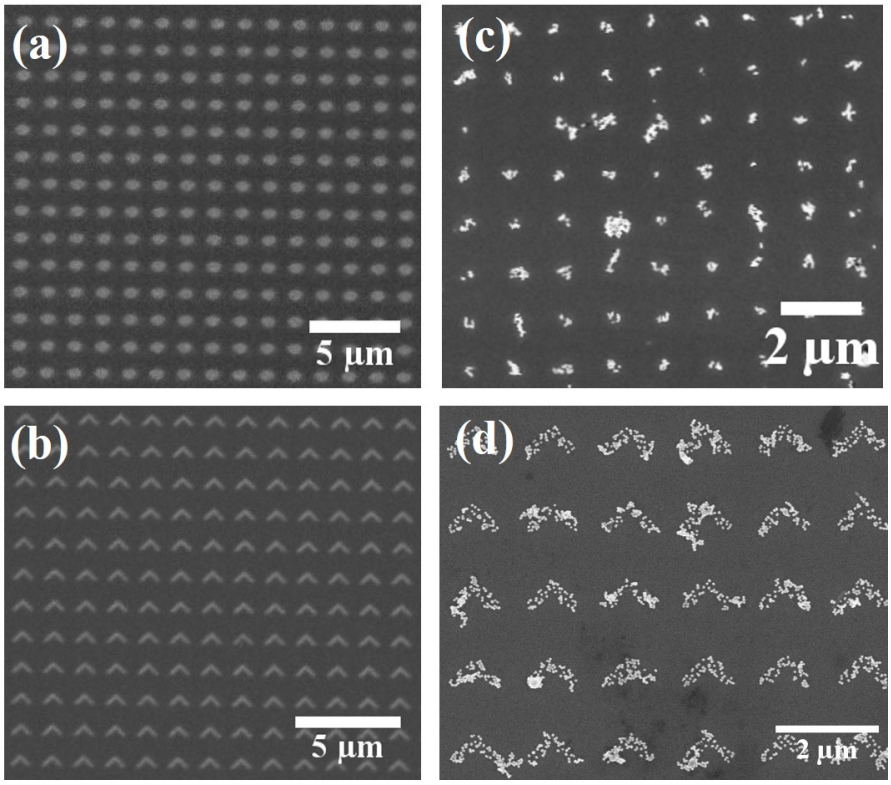

FIGURE 5.2: Different plasmonic lattices prepared using template assisted assembly method. SEM image of prepared template (a) circular shape trench (b) Triangular trench. (c) and (d) Nanoparticles assembled plasmonic lattice. [Manuscript under preparation]

to 150nm for repeating the consistency of this method. Figure 5.2 show SEM images of two different types of prepared templates and corresponding fabricated samples with gold nanoparticles on the Si-wafer. Figure 5.2a and c represent conventional SEM image of prepared templates, whereas figure 5.2b and d show the SEM image of a small section of finally prepared sample. However, the process of optimizing of this technique is still underway in our laboratory.

5.2 Future plans

With the prepared samples, our first aim is to explore directional emission of such hybrid nano-architectures. In future, it would be interesting to explore such hybrid structures for probing radiation pattern modification in secondary emission such as Raman spectrum, fluorescence etc., fluorescence life-time and energy-momentum spectroscopy. Moreover, it would also be interesting to investigate the new resonant modes because of coupling of organic nanomaterials with plasmonic cavities/lattices. These

type of measurements are important for building various compact nano-photonic devices, spectroscopic techniques and directional nanoscale optical sources with high quality factors. Furthermore, such investigations can facilitate new dimension to understand the prevailing quantum phenomena in optical physics.

5.3 Summary of the thesis

Effective control over optical field at nanoscale is an important aspect of nanophotonics applications. This question has been raised in the context of opto-electronics and micro-/nano- photonics, and the answer has relevance not only in fundamental optical physics of one dimensional materials but also in various applications ranging from quantum technologies to clinical biomedicine. In recent times, controlling directionality of emitted light from micro-/nano- wires has drawn significant attention. Precisely controlling and tailoring the radiation properties in a nanowire antenna is imperative for efficiently routing the out-coupled emission, which will be further crucial to achieve more advanced functions as well as coupling-efficiency enhancement in various applications such as solar cells, photo-detectors etc. Therefore, it is essential to develop a simple and robust method to tailor the radiation properties as per requirements on nanophotonical chip. In this context, a variety of nanowire optical antenna that have been made of conventional plasmonic materials (i.e. gold and silver) and various inorganic nanomaterials have been explored. However, there are still many applications and requirements for which these nanomaterials are not ideally suitable, such as multicolour broadband tunability, mechanical flexibility and low-cost processing. As a solution, the meso/nano- structures made of organic molecular materials are a promising candidate for these photonic applications.

Organic nanomaterials exhibit greater exciton-binding energy, large oscillator strength, wide spectral tunability, molecular flexibility and stability. Various applications have been explored however, one important application that has not been explored is the directional light emission from one-dimensional organic semiconductors. Moreover, it would also be important to understand the influence on directionality due to coupling with other dielectric or plasmonic geometry. In this thesis, we made an attempt to address some of the above mentioned nano-photonic facets.

In chapter 2, we discussed light guiding properties of organic waveguide in both passive and active operational regime. In the context of optical signal processing, passive operation are defined as: input wavelength is equal to output wavelength, whereas in an active regime: the input and output wavelength are different. The passive and active operational regimes were correlated with excitation energy, which was further assured

with measured anomalous refractive index as a function of energy. It was evident with this measurement that organic waveguide showed two distinct features as far as illumination wavelength is concerned i.e. excitation energy (<1.8eV) performs as photonic fibre and act as passive waveguide, whereas excitation energy (>1.8eV), the waveguiding properties were mainly governed with exciton-polaritons propagation.
Further, we probed directionality of light emission in both active and passive regime. Comparing the spread in azimuthal angle and radial angles, we understood that higher directionality can be achieved with 532nm excitation. Moreover, in case of 633nm illumination, the waveguide shows its dual nature i.e. waveguide exhibit both active and passive transport of light, whereas at 785nm, only passive waveguiding is observed. In the end, we extrapolated our study to show an interesting application of active light transport in organic waveguide: i) dual-channel directional light emission with a single illumination; ii) Enhanced optical signal with possession of identical directionality. These measurements will be crucial in designing the photonic signal processing and optical communication devices.
Another interesting aspect of these organic nanomaterials is their resonating modes attributed to exciton-polaritons propagation inside the cavity. Therefore, organic materials would be ideal to fabricate micro-/nano-resonators spanning their emission over the whole visible spectrum. However, tailoring their resonance modes in a controlled manner with defined directionality is still a challenge. Hence, in chapter 3, we addressed this issue by coupling organic waveguide with silica microsphere. We demonstrated how these coupled configuration can be simultaneously used as directional light emitter and signal modulator. In these hybrid configurations, the WGMs of microsphere can be exploited for signal modulation (active element) and organic waveguide can be utilized for signal transportation. Moreover, the light can be efficiently directed by remotely exciting its two different terminals. We observed non-reciprocal directional active light emission with significant variation in radial angle in captured Fourier-plane image.
In the last part of this work, we extended our investigation in the direction of plasmon coupled organic nanomaterials. Such coupled nano-architectures comprising of excitonic and plasmonic constituents have emerged as important platforms to explore polariton coupling and light emitting devices at nanoscale. Interfacing organic molecular platforms with surface plasmons provide excellent test bed not only to study exciton-plasmon interaction but also can be exploited for manipulating optical field down to single photon limit. A majority of scheme regarding to exciton-plasmons coupling is limited to either quasi-zero dimensional or quasi two dimensional in nature. Moreover, the investigations are predominantly restricted to energy transfer, recombination process,

or photoluminescence enhancement. However, not many reports have discussed controlling the directionality of emitted light in single, vertical organic nanowire (1D) with plasmonic gold film (2D). Therefore, in chapter 4, we addressed this issue and showed directional, exciton-polariton photoluminescence emission channelled from vertical organic nanowire through plasmonic leaky channel of gold film. Further, we also discussed how the directional emission can be tailored with systematically varying coupling angle of organic nanowire and coupling distance above the plasmonic film.
In conclusion, we believe that the work discussed in this thesis can be further utilized for various nano-photonic and photovoltaic applications, single nanowire based coherent sources, and improving the light collection efficiency in existing technologies. These developments would have significance in all branch of science and technology ranging from physics, material science to biological science.

Appendix A

Principle of Back Focal Plane imaging

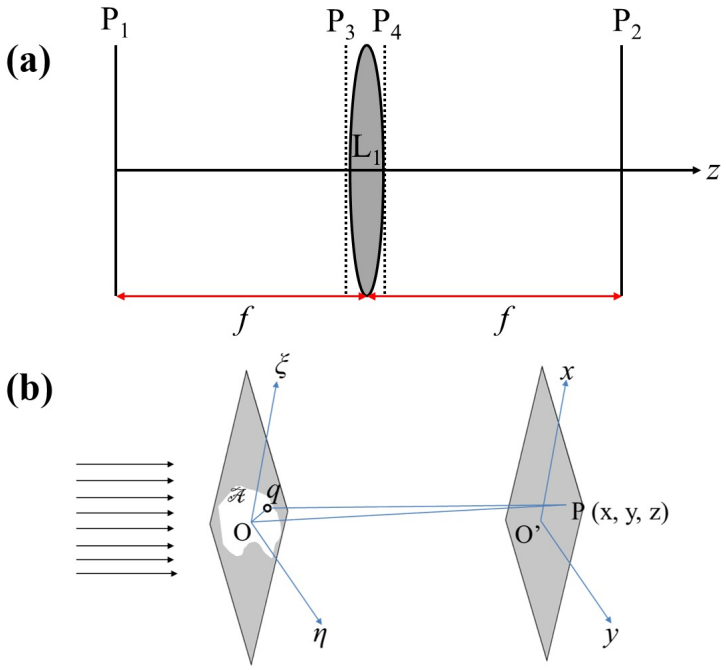

FIGURE A.1: Schematic represent of the working principle of back focal plane imaging using spherical lens. [181]

Back focal plane imaging or Fourier plane imaging works on the basic concept spherical lenses' phase transformation property. Phase transformed information can be obtained at second focal plane lens/objective lens. Mathematical treatment of such kind of transformation has been discussed undergraduate optics textbook [181, 262, 263]. We have adopted the same formulation to discuss the principle of FP imaging by objective lens.

We assume that $h(x, y)$ represents the field distribution on the front focal plane of lens (shown as P_1 in the figure A.1 a) and $g(x, y)$ show the field distribution second focal point of the lens (shown as P_2 in figure A.1a). To calculate the field distribution at plane P_2, we first write the field distribution at plane (indicated by P_3) close to the lens (L_1). Evidently, the field will undergo Fresnel diffraction (as demonstrated in figure A.1 b)

[181] and hence, the field distribution at plane P_3 can be written as equation A.1.

$$u|_{P_3} = \frac{i}{\lambda f}\exp(-ikf)\int\int h(\xi,\eta)\exp(\frac{ik}{2f}[(x-\xi)^2+(y-\eta)^2])d\xi d\eta \qquad (A.1)$$

where ξ and η indicate any arbitrary points in local coordinate system.
The field represented by equation A.1 will pass through the lens. Therefore, the effect of lens has to be taken into account by multiplying the incident field with the transmittivity factor p_L. Transmittivity factor can be expressed as equation A.2.

$$p_L = \exp(\frac{ik}{2f}(x^2+y^2)^2) \qquad (A.2)$$

After introducing transmittivity factor attributed to lens, the field distribution at plane P_4 can be written as equation A.3.

$$u|_{P_4} = \frac{i}{\lambda f}\exp(i\alpha(x^2+y^2))\int\int h(\xi,\eta)\exp(-i\alpha[(x-\xi)^2+(y-\eta)^2])d\xi d\eta \qquad (A.3)$$

where $\alpha = \frac{k}{2f} = \frac{\pi}{\lambda f}$
The field distribution will again undergo to Fresnel diffraction and the resultant field distribution at plane P_2 can be written as equation A.4.

$$u|_{P_2} = (\frac{i}{\lambda f}\exp(-ikf))^2[\sqrt{\frac{\lambda f}{2}}(1-i)]^2\int\int \exp(2\pi i(u\xi+v\eta))h(\xi,\eta)d\xi d\eta \qquad (A.4)$$

where $u = \frac{x}{\lambda f}$ and $v = \frac{y}{\lambda f}$
Equation A.4 provide the information on second focal or back focal plane of the lens, which is effectively Fourier transformation of the lens. It is important to note that the integral limits are taken to $-\infty$ to $+\infty$ i.e. the lens is extended to infinite. Also, we would like to emphasize the fact that the field is distributed in two dimensions, therefore, the light emitted from the sample can be fractionalized into individual plane waves. Each plane wave directing in one direction have identical k-values, which will meet at one point after transformation. Hence, the image is resolved according to their k-vector distribution at back focal plane.
However, the practical situation for obtaining Fourier transformed information is a bit tedious job. Practically, the conventional objective lens formed the back focal plane image at very short distance, hence the information extraction is impossible. To troubleshoot this issue, we cascade the obtained information from objective lens' BFP to imaging CCD by using $4-f$ configuration (discussed in chapter 2 and section 2.2.2). Schematic of the $4-f$ configuration has been shown in chapter 2, figure 2.3.

Appendix B

Brief discussion on EP model

Conventional way to understand the light propagation mechanism in nanoscale optical fibres, Maxwell's equations are solved after inclusion of material dispersion properties with appropriate boundary conditions [182]. However, this approach provide the satisfactory solutions only for the cases of low excitation energy. As the excitation wavelength is chosen closer to the absorption band, this conventional way of defining light propagation is no more valid and start showing deviation particularly if the excitons are present [54, 182]. Furthermore, these excitonic materials' dielectric function also show strong dependence on various other factors such as incident wave-vector, spatial dispersion and interaction of excitons resonances. Therefore, it is essential to consider all these aspects while discussing active light transportation in molecular nanofibers for contemplating the polaritonic effect. These treatment has been previously explored in various inorganic/organic molecular waveguide context [54, 80, 182, 264]. We have utilized the same knowledge in our investigation to probe exciton-poalriton mediated active light.

B.1 EP model fitting

In our case, we investigate nano/micro- fiber made of organic molecules. These organic molecules facilitates Frankel's excitons, strongly interact with incident photons and results as the formation of exciton-polaritons. This polariton coupling mechanism, large oscillator strength and size effect ($\sim$ optical wavelength) can results the significant difference in dielectric constant as compared to their macroscopic crystal. The dielectric function in such EPs medium can be given by equation B.1.

$$\epsilon(\omega, k_{||}) = \epsilon_b[1 + \frac{\omega_L^2 - \omega_T^2}{\omega_T^2 - \omega^2 + -\iota\omega\gamma}] \tag{B.1}$$

where ϵ_b is the background dielectric constant. γ is the damping constant. ω_L, ω_T are the longitudinal and transverse exciton frequency, respectively.
We extract the function corresponding to real and imaginary part of refractive index

using expansion method and complex analysis. Based on the obtained functions, the best fitted curve were obtained using MATLAB.

B.2 Dielectric function of excitonic materials

The above mentioned equation is taken from the landmark work reported by Hopfield on theory of interacting excitonic resonance [265, 266] and further followed by Lagois [267] using the coupled oscillator model. Hopfield predicated that the light-matter interaction should be distinguished. Herein, we would be briefly discussing some interesting aspects of coupled oscillator model, which was used to demonstrate the anomalous refractive index behaviour. For simplicity, we consider an assembly of identical uncoupled oscillators [268]. In figure B.1 a, we show the schematic of coupled oscillator model for spring-mass system. We further assume that the lattice arrangement in light propagation direction. Under these assumption, the equation of motion of coupled oscillations can be given as equation B.2.

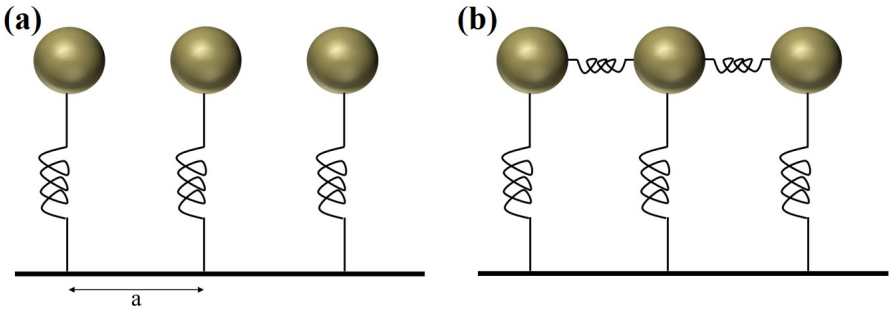

FIGURE B.1: Schematic demonstration of oscillations in dielectric by simple mechanical model (a) Uncoupled (b) Coupled

$$m\frac{d^2x}{dt^2} + \gamma m\frac{dx}{dt} + \beta x = eE_0e^{-i\omega t} \tag{B.2}$$

where γ is damping constant and β is force constant. The general solution of this equation can be given as equation B.3

$$x(t) = x_0\exp(-i\sqrt{(\omega_0^2 - \frac{\gamma^2}{4})}t)\exp(\frac{-\gamma t}{2}) + x_p\exp(-i\omega t) \tag{B.3}$$

where ω_0 is eigenfrequency of harmonic oscillations. Inserting the equation B.3 in equation B.2, we can extract the usual resonance given as equation B.4

$$x_p = \frac{eE_0}{m}(\omega_0^2 - \omega^2 - \iota\omega\gamma)^{-1} \tag{B.4}$$

As we are all familiar that these oscillations are connected with dipole moments possessed by every oscillations and a polarizibility. Including all these factors, we get the polarization density P (given by the equation B.5) and further, we can obtain the dielectric function given as equation B.6, B.7

$$P = \frac{Ne^2}{m}(\omega_0^2 - \omega^2 - \iota\omega\gamma)^{-1}E_0 \tag{B.5}$$

$$D = \epsilon_0 E + P \tag{B.6}$$

$$\epsilon(\omega) = 1 + \frac{Ne^2}{\epsilon_0 m}(\omega_0^2 - \omega^2 - \iota\omega\gamma)^{-1} \tag{B.7}$$

where $\frac{Ne^2}{\epsilon_0 m}$ can be defined as oscillator strength (denoted as f) which can be further related to experimental measurable quantity i.e. $\omega_L^2 - \omega_T^2$; where ω_L and ω_T are longitudinal and transverse oscillations frequency, can be measured through reflection spectra [54, 182].

$$n(\omega) = \sqrt[\frac{1}{2}]{\frac{1}{2}\sqrt[\frac{1}{2}]{(\epsilon_1(\omega) + [\epsilon_1^2(\omega) + \epsilon_2^2(\omega)])}} \tag{B.8}$$

$$k(\omega) = \sqrt[\frac{1}{2}]{\frac{1}{2}\sqrt[\frac{1}{2}]{(-\epsilon_1(\omega) + [\epsilon_1^2(\omega) + \epsilon_2^2(\omega)])}} \tag{B.9}$$

where ϵ_1 and ϵ_2 can be given by following equations

$$\epsilon_1(\omega) = \epsilon_0(1 + \frac{f(\omega_0^2 - \omega^2)}{(\omega_0^2 - \omega^2)^2 + \omega^2\gamma^2}) \tag{B.10}$$

$$\epsilon_2(\omega) = \epsilon_0(\frac{\omega\gamma f}{(\omega_0^2 - \omega^2)^2 + \omega^2\gamma^2}) \tag{B.11}$$

Next, we try to understand the behaviour of refractive index. To get the infomration, first we get the expression for real and imaginary part of dielectric constant. We all are familiar with the relation between n and $\epsilon(\omega)$. Using some elementary complex analysis methods, we were able to obtain the expression for real and imaginary part of refractive index. From the obtained equation B.8 and B.9, we closely observe the behaviour of refractive index. We found that refractive index increases drastically as one approach towards the resonance from low energy side. Importantly, we have not accounted the mutual interaction between excitonic resonances in the above discussed calculations. On considering this aspect, the resultant frequency may vary due to mutual coupling (shown in figure B.1 b), however the anomalous behaviour in RI remain same [268].

This trend is similar to our experimental observation and we obtained best curve fitting of the experimental point using MATLAB.

Appendix C

Optical Microcavity

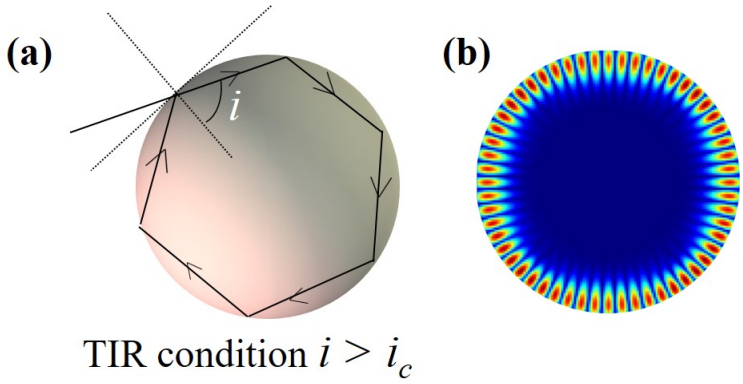

FIGURE C.1: schematic ray diagram of light confinement inside the optical microcavity by TIR mechanism. (b) FDTD simulation of WGMs in a typical silica microsphere (RI= 1.5)

Optical microcavity is an optical setup which facilitates unconventional squeezing of light in a tiny volume [269]. Such extraordinary confinement of photons can afford high quality optical resonator modes and large optical power with minimal losses [269, 270]. These resonating modes can be generated by exploiting various direct and indirect optical excitation methods based on prisms coupling, integrated fibre, tapered fibre, waveguide coupling etc [20]. Interestingly, these resonance modes as well as large optical power can be transferred by triggering the cavities with small perturbations [271]. In the recent years, microcavity especially of micrometre dimension have drawn significant attention in the context of probing non-linear optics [272, 273], sensors [274], super-resolution microscopy [275], photonic jets [276, 277], optical filters [278], integrated photonics circuits [279], optical communication devices [280], cavity assisted electrodynamics [281] etc.

As a principle, the concept of resonant cavity was previously known, however the optical analogue of such cavities have been recently explored. Acoustic resonator cavity was first discovered in St. Paul cathedral church and associated explanation was provided by Lord Rayleigh [282, 283]. As per given explanation, these acoustic waves

closely travel along with the surface of the curved cavity and consequently undergo to multiple reflections. These reflection resultants in standing wave patterns and causes the resonating modes inside the cavity structures [282–284]. Similar to acoustic resonance modes, optical microcavity can attribute resonance modes named as Whispering gallery modes (WGMs) in optical regime. The quality of resonance modes are determined by quality factor (Q), which is defined by the ration between energy stored and dissipated power inside the cavity [269, 270]. In principle, an ideal microcavity can support squeezing the light for infinite time (i.e. with any losses) and would show very sharp resonance peak (FWHM = 0). However, such micro-cavities don't exist in practice due to their inherent loss associated with tunnelling of the resonating modes. The deviation of these resonating modes from the ideal condition is described by quality factor. Higher the quality factor, light will be efficiently trapped inside the cavity for longer time.

C.1 Basic Theory

Strict analytical solution for WGMs generation in optical microcavities have been discussed in various text books [270, 284]. We have adapted the similar mathematical treatment to discuss the optical phenomena in microsphere [284]. To discuss the basic theory, we consider the most simple geometry *Spherical microcavity* of diameter d. The incidence angle of light is i and critical angle of light is i_c. In principle, optical microcavity works on total internal reflection (TIR) of incident electromagnetic radiation shown in figure C.1. TIR condition is satisfied by the equation C.1.

$$i > i_c = Sin^{-1}(\frac{1}{N}) \tag{C.1}$$

where N represents the refractive index of dielectric sphere.

When the incident light wave strikes the surface of microcavity at an angle $i > i_c$, the rays get trapped inside the cavity. These rays circulate close to the surface of the geometry and undergo multiple reflection. Multiple reflection resultants in formation of standing wave patterns and further origin of WGMs modes. Additionally, TIR reflection also causes intensity loss due to tunnelling of these modes. The resonance condition of these modes can be described by equation C.2.

$$\frac{2\pi d}{\lambda} = \frac{L}{N} \tag{C.2}$$

Where L is defined as angular momentum of the modes inside the cavity.
The complete analytical solution can be obtained by exact solving the Maxwell's equation for any specified geometry using proper boundary condition, known as Lorentz-Mie theory [285]. The corresponding solution are obtained with spherical harmonics l, and m. l indicates order of spherical harmonic and m azimuthal mode number. Also, the resonance modes can be further identified based on their polarization vector P i.e. Transverse electric (TE) modes: $\vec{r}.\vec{E} = 0$, Transverse magnetic (TM) modes: $\vec{r}.\vec{B} = 0$. Considering all these classification, the resultant field can be expresses as equation C.3, C.4, C.5 and C.6.

$$\vec{E}_{lm}^{TE}(\vec{r}) = E_0 \frac{f_l(r)}{K_0(r)} \vec{X}_l^m(\theta, \phi) \tag{C.3}$$

$$\vec{B}_{lm}^{TE}(\vec{r}) = \frac{E_0}{ic}\left(\frac{f_l^{'}(\vec{r})}{K_0^2 \vec{r}} \vec{Y}_l^m(\theta, \phi) + \sqrt{l(l+1)} \frac{f_l(r)}{K_0^2 r^2} \vec{Z}_l^m(\theta, \phi)\right) \tag{C.4}$$

$$\vec{E}_{lm}^{TM}(\vec{r}) = \frac{E_0}{N^2}\left(\frac{f_l^{'}(\vec{r})}{K_0^2 \vec{r}} \vec{Y}_l^m(\theta, \phi) + \sqrt{l(l+1)} \frac{f_l(r)}{K_0^2 r^2} \vec{Z}_l^m(\theta, \phi)\right) \tag{C.5}$$

$$\vec{B}_{lm}^{TM}(\vec{r}) = -\frac{iE_0}{c} \frac{f_l(r)}{K_0(r)} \vec{X}_l^m(\theta, \phi) \tag{C.6}$$

where

$$\vec{X}_l^m = \vec{\bigtriangledown} \times \frac{\vec{r}}{\sqrt{l(l+1)}} \tag{C.7}$$

$$\vec{Y}_l^m = r\vec{\bigtriangledown} \times \frac{Y_l^m}{\sqrt{l(l+1)}} \tag{C.8}$$

$$\vec{Z}_l^m = Y_l^m \hat{r} \tag{C.9}$$

where N is refractive index of dielectric sphere. These equations can be further simplified as follows

$$f_l(r) = \psi_l(NK_0 r); r < d \tag{C.10}$$

$$f_l(r) = A\psi_l(K_0 r) + B\psi_l(K_0 r); r > d \tag{C.11}$$

These equations are the solution of Riccuti-Bessel radial equation, where $\psi_l(\rho) = \rho j_l(\rho)$ and $X_l(\rho) = \rho n_l(\rho)$ where j_l and n_l are spherical Bessel and Neumann function.

Bibliography

[1]A. F. Koenderink, A. Alù, and A. Polman, "Nanophotonics: shrinking light-based technology", Science **348**, 516–521 (2015).

[2]J. A. Schuller, E. S. Barnard, W. Cai, Y. C. Jun, J. S. White, and M. L. Brongersma, "Plasmonics for extreme light concentration and manipulation", Nature materials **9**, 193–204 (2010).

[3]D. K. Gramotnev and S. I. Bozhevolnyi, "Plasmonics beyond the diffraction limit", Nature photonics **4**, 83–91 (2010).

[4]S. A. Maier, *Plasmonics: fundamentals and applications* (Springer Science & Business Media, 2007).

[5]S. A. Maier, M. L. Brongersma, P. G. Kik, S. Meltzer, A. A. Requicha, and H. A. Atwater, "Plasmonics—a route to nanoscale optical devices", Advanced Materials **13**, 1501–1505 (2001).

[6]E. Ozbay, "Plasmonics: merging photonics and electronics at nanoscale dimensions", science **311**, 189–193 (2006).

[7]J. N. Anker, W. P. Hall, O. Lyandres, N. C. Shah, J. Zhao, and R. P. Van Duyne, "Biosensing with plasmonic nanosensors", Nature materials **7**, 442–453 (2008).

[8]E. Le Ru and P. Etchegoin, *Principles of surface-enhanced raman spectroscopy: and related plasmonic effects* (Elsevier, 2008).

[9]P. Nordlander, "Plasmonics: subwavelength imaging in colour", Nature Photonics **2**, 387–388 (2008).

[10]Z. Jacob and V. M. Shalaev, "Plasmonics goes quantum", Science **334**, 463–464 (2011).

[11]M. S. Tame, K. McEnery, Ş. Özdemir, J Lee, S. Maier, and M. Kim, "Quantum plasmonics", Nature Physics **9**, 329–340 (2013).

[12]J. Clark and G. Lanzani, "Organic photonics for communications", Nature photonics **4**, 438–446 (2010).

[13]M. Hu, J. Chen, Z.-Y. Li, L. Au, G. V. Hartland, X. Li, M. Marquez, and Y. Xia, "Gold nanostructures: engineering their plasmonic properties for biomedical applications", Chemical Society Reviews **35**, 1084–1094 (2006).

[14]X. Huang, S. Neretina, and M. A. El-Sayed, "Gold nanorods: from synthesis and properties to biological and biomedical applications", Advanced Materials **21**, 4880–4910 (2009).

[15]S. Abalde-Cela, P. Aldeanueva-Potel, C. Mateo-Mateo, L. Rodríguez-Lorenzo, R. A. Alvarez-Puebla, and L. M. Liz-Marzán, "Surface-enhanced raman scattering biomedical applications of plasmonic colloidal particles", Journal of the Royal Society Interface **7**, S435–S450 (2010).

[16]H. A. Atwater, "The promise of plasmonics", Scientific American **296**, 56–62 (2007).

[17]R. Zia, J. A. Schuller, A. Chandran, and M. L. Brongersma, "Plasmonics: the next chip-scale technology", Materials today **9**, 20–27 (2006).

[18]T. Shegai, V. D. Miljkovic, K. Bao, H. Xu, P. Nordlander, P. Johansson, and M. Kall, "Unidirectional broadband light emission from supported plasmonic nanowires", Nano letters **11**, 706–711 (2011).

[19]A. Dasgupta, D. Singh, R. P. N. Tripathi, and G. V. P. Kumar, "Directional fluorescence emission mediated by chemically-prepared plasmonic nanowire junctions", The Journal of Physical Chemistry C **120**, 17692–17698 (2016).

[20]R. Chikkaraddy, A. Dasgupta, S. D. Gupta, and G. V. P. Kumar, "Microsphere-coupled organic waveguides: preparation, remote excitation of whispering gallery modes and waveguiding property", Applied Physics Letters **103**, 031112 (2013).

[21]C. Zhang, C.-L. Zou, Y. Zhao, C.-H. Dong, C. Wei, H. Wang, Y. Liu, G.-C. Guo, J. Yao, and Y. S. Zhao, "Organic printed photonics: from microring lasers to integrated circuits", Science advances **1**, e1500257 (2015).

[22]Y. J. Li, Y. Yan, C. Zhang, Y. S. Zhao, and J. Yao, "Embedded branch-like organic/metal nanowire heterostructures: liquid-phase synthesis, efficient photon-plasmon coupling, and optical signal manipulation", Advanced Materials **25**, 2784–2788 (2013).

[23]D. Singh, A. Dasgupta, V. G. Aswathy, R. P. N. Tripathi, and G. V. P. Kumar, "Directional out coupling of light from a plasmonic nanowire nanoparticle junction", Optics letters **40**, 1006–1009 (2015).

[24]W. L. Barnes, A. Dereux, and T. W. Ebbesen, "Surface plasmon subwavelength optics", Nature **424**, 824–830 (2003).

[25]G. Cao, *Synthesis, properties and applications* (World Scientific, 2004).

[26]H. Wang, D. W. Brandl, P. Nordlander, and N. J. Halas, "Plasmonic nanostructures: artificial molecules", Accounts of chemical research **40**, 53–62 (2007).

[27]J. Henzie, J. Lee, M. H. Lee, W. Hasan, and T. W. Odom, "Nanofabrication of plasmonic structures*", Annual review of physical chemistry **60**, 147–165 (2009).

[28]K. A. Willets and R. P. Van Duyne, "Localized surface plasmon resonance spectroscopy and sensing", Annu. Rev. Phys. Chem. **58**, 267–297 (2007).

[29]E. Hutter and J. H. Fendler, "Exploitation of localized surface plasmon resonance", Advanced Materials **16**, 1685–1706 (2004).

[30]G. V. P. Kumar, D. Singh, P. P. Patra, and A. Dasgupta, "Subwavelength propagation and localization of light using surface plasmons: a brief perspective", Pramana **82**, 59–70 (2014).

[31]A. V. Zayats and I. I. Smolyaninov, "Near-field photonics: surface plasmon polaritons and localized surface plasmons", Journal of Optics A: Pure and Applied Optics **5**, S16 (2003).

[32]S. Oldenburg, R. Averitt, S. Westcott, and N. Halas, "Nanoengineering of optical resonances", Chemical Physics Letters **288**, 243–247 (1998).

[33]P. Nordlander, C Oubre, E Prodan, K Li, and M. Stockman, "Plasmon hybridization in nanoparticle dimers", Nano letters **4**, 899–903 (2004).

[34]A. V. Zayats and S. A. Maier, *Active plasmonics and tuneable plasmonic metamaterials* (Wiley Online Library, 2013).

[35]K. Kneipp, Y. Wang, H. Kneipp, L. T. Perelman, I. Itzkan, R. R. Dasari, and M. S. Feld, "Single molecule detection using surface-enhanced raman scattering (sers)", Physical review letters **78**, 1667 (1997).

[36]P. P. Patra and G. V. P. Kumar, "Single-molecule surface-enhanced raman scattering sensitivity of ag-core au-shell nanoparticles: revealed by bi-analyte method", The journal of physical chemistry letters **4**, 1167–1171 (2013).

[37]A. Dasgupta, D. Singh, S. Tandon, R. P. N. Tripathi, and G. V. P. Kumar, "Remote-excitation surface-enhanced raman scattering with counter-propagating plasmons: silver nanowire-nanoparticle system", Journal of Nanophotonics **8**, 083899–083899 (2014).

[38]M. I. Stockman, "Nanofocusing of optical energy in tapered plasmonic waveguides", Physical review letters **93**, 137404 (2004).

[39]R. Chikkaraddy, D. Singh, and G. V. P. Kumar, "Plasmon assisted light propagation and raman scattering hot-spot in end-to-end coupled silver nanowire pairs", Applied Physics Letters **100**, 043108 (2012).

[40]A. Dasgupta, D. Singh, and G. V. P. Kumar, "Dual-path remote-excitation surface enhanced raman microscopy with plasmonic nanowire dimer", Applied Physics Letters **103**, 151114 (2013).

[41]S.-H. Cao, W.-P. Cai, Q. Liu, and Y.-Q. Li, "Surface plasmon-coupled emission: what can directional fluorescence bring to the analytical sciences?", Annual Review of Analytical Chemistry **5**, 317–336 (2012).

[42]D. Singh, M. Raghuwanshi, and G. V. P. Kumar, "Propagation of light in serially coupled plasmonic nanowire dimer: geometry dependence and polarization control", Applied Physics Letters **101**, 111111 (2012).

[43]P. P. Patra, R. Chikkaraddy, S. Thampi, R. P. N. Tripathi, and G. V. P. Kumar, "Large-scale dynamic assembly of metal nanostructures in plasmofluidic field", Faraday discussions **186**, 95–106 (2016).

[44]P. P. Patra, R. Chikkaraddy, R. P. N. Tripathi, A. Dasgupta, and G. V. P. Kumar, "Plasmofluidic single-molecule surface-enhanced raman scattering from dynamic assembly of plasmonic nanoparticles", Nature communications **5** (2014).

[45]M. Kauranen and A. V. Zayats, "Nonlinear plasmonics", Nature Photonics **6**, 737–748 (2012).

[46]G. V. Naik, J. Kim, and A. Boltasseva, "Oxides and nitrides as alternative plasmonic materials in the optical range [invited]", Optical Materials Express **1**, 1090–1099 (2011).

[47]G. V. Naik, V. M. Shalaev, and A. Boltasseva, "Alternative plasmonic materials: beyond gold and silver", Advanced Materials **25**, 3264–3294 (2013).

[48]P. K. Jain, X. Huang, I. H. El-Sayed, and M. A. El-Sayed, "Review of some interesting surface plasmon resonance-enhanced properties of noble metal nanoparticles and their applications to biosystems", Plasmonics **2**, 107–118 (2007).

[49]G Baffou, R Quidant, and C Girard, "Heat generation in plasmonic nanostructures: influence of morphology", Applied Physics Letters **94**, 153109 (2009).

[50]P. R. West, S. Ishii, G. V. Naik, N. K. Emani, V. M. Shalaev, and A. Boltasseva, "Searching for better plasmonic materials", Laser & Photonics Reviews **4**, 795–808 (2010).

[51]V. E. Babicheva, N. Kinsey, G. V. Naik, M. Ferrera, A. V. Lavrinenko, V. M. Shalaev, and A. Boltasseva, "Towards cmos-compatible nanophotonics: ultra-compact modulators using alternative plasmonic materials", Optics express **21**, 27326–27337 (2013).

[52]L. K. van Vugt, S. Rühle, P. Ravindran, H. C. Gerritsen, L. Kuipers, and D. Vanmaekelbergh, "Exciton polaritons confined in a zno nanowire cavity", Physical review letters **97**, 147401 (2006).

[53]G. Malpuech, A. Di Carlo, A. Kavokin, J. J. Baumberg, M. Zamfirescu, and P. Lugli, "Room temperature polariton lasers based on gan microcavities", Applied physics letters **81**, 412–414 (2002).

[54]K. Takazawa, J.-i. Inoue, K. Mitsuishi, and T. Takamasu, "Fraction of a millimeter propagation of exciton polaritons in photoexcited nanofibers of organic dye", Physical review letters **105**, 067401 (2010).

[55]K. Takazawa, J.-i. Inoue, K. Mitsuishi, and T. Takamasu, "Micrometer-scale photonic circuit components based on propagation of exciton polaritons in organic dye nanofibers", Advanced Materials **23**, 3659–3663 (2011).

[56]J Serbin, A Egbert, A Ostendorf, B. Chichkov, R Houbertz, G Domann, J Schulz, C Cronauer, L Fröhlich, and M Popall, "Femtosecond laser-induced two-photon polymerization of inorganic–organic hybrid materials for applications in photonics", Optics letters **28**, 301–303 (2003).

[57]S. Basak and R. Chandrasekar, "Multiluminescent hybrid organic/inorganic nanotubular structures: one-pot fabrication of tricolor (blue–red–purple) luminescent parallepipedic organic superstructure grafted with europium complexes", Advanced Functional Materials **21**, 667–673 (2011).

[58]P. Escribano, B. Julián-López, J. Planelles-Aragó, E. Cordoncillo, B. Viana, and C. Sanchez, "Photonic and nanobiophotonic properties of luminescent lanthanide-doped hybrid organic–inorganic materials", Journal of Materials Chemistry **18**, 23–40 (2008).

[59]J. M. Ball, M. M. Lee, A. Hey, and H. J. Snaith, "Low-temperature processed meso-superstructured to thin-film perovskite solar cells", Energy & Environmental Science **6**, 1739–1743 (2013).

[60]D. Bimberg, "Quantum dot based nanophotonics and nanoelectronics", Electronics Letters **44**, 1 (2008).

[61]R. Dastjerdi and M. Montazer, "A review on the application of inorganic nano-structured materials in the modification of textiles: focus on anti-microbial properties", Colloids and Surfaces B: Biointerfaces **79**, 5–18 (2010).

[62]D. Liang, G. Roelkens, R. Baets, and J. E. Bowers, "Hybrid integrated platforms for silicon photonics", Materials **3**, 1782–1802 (2010).

[63]T. Nobis, E. M. Kaidashev, A. Rahm, M. Lorenz, and M. Grundmann, "Whispering gallery modes in nanosized dielectric resonators with hexagonal cross section", Physical review letters **93**, 103903 (2004).

[64]B. Jalali and S. Fathpour, "Silicon photonics", Journal of lightwave technology **24**, 4600–4615 (2006).

[65]C. Zhang, F. Zhang, T. Xia, N. Kumar, J.-i. Hahm, J. Liu, Z. L. Wang, and J. Xu, "Low-threshold two-photon pumped zno nanowire lasers", Optics express **17**, 7893–7900 (2009).

[66]A. V. Kachynski, A. N. Kuzmin, M. Nyk, I. Roy, and P. N. Prasad, "Zinc oxide nanocrystals for nonresonant nonlinear optical microscopy in biology and medicine", The Journal of Physical Chemistry C **112**, 10721–10724 (2008).

[67]F. Xia, H. Wang, D. Xiao, M. Dubey, and A. Ramasubramaniam, "Two-dimensional material nanophotonics", Nature Photonics **8**, 899–907 (2014).

[68]M. Liu, X. Yin, E. Ulin-Avila, B. Geng, T. Zentgraf, L. Ju, F. Wang, and X. Zhang, "A graphene-based broadband optical modulator", Nature **474**, 64–67 (2011).

[69]S. S. Iyer and Y.-H. Xie, "Light emission from silicon", Science **260**, 40–46 (1993).

[70]D. J. Lockwood, "Light emission in silicon", Semiconductors and Semimetals **49**, 1–35 (1997).

[71]Y.-M. Hua, Q. Li, Y.-L. Chen, and Y.-X. Chen, "Frequency upconversion in er 3+-and yb3+ er3+-doped silica fibers", Optics communications **88**, 441–445 (1992).

[72]J. Li, X. Chang, X. Chen, Z. Gu, F. Zhao, Z. Chai, and Y. Zhao, "Toxicity of inorganic nanomaterials in biomedical imaging", Biotechnology advances **32**, 727–743 (2014).

[73]W. Zhang and Y. S. Zhao, "Organic nanophotonic materials: the relationship between excited-state processes and photonic performances", Chemical Communications (2016).

[74]W. Zhang, J. Yao, and Y. S. Zhao, "Organic micro/nanoscale lasers", Accounts of Chemical Research **49**, 1691–1700 (2016).

[75]C. Zhang, Y. Yan, Y. S. Zhao, and J. Yao, "From molecular design and materials construction to organic nanophotonic devices", Accounts of chemical research **47**, 3448–3458 (2014).

[76]Y. Yan and Y. S. Zhao, "Organic nanophotonics: from controllable assembly of functional molecules to low-dimensional materials with desired photonic properties", Chemical Society Reviews **43**, 4325–4340 (2014).

[77]Y. S. Zhao, *Organic nanophotonics* (Springer, 2015).

[78]R. Chandrasekar, "Organic photonics: prospective nano/micro scale passive organic optical waveguides obtained from π-conjugated ligand molecules", Physical Chemistry Chemical Physics **16**, 7173–7183 (2014).

[79]S. Wang, "Principles and characteristics of integratable active and passive optical devices", Semiconductors and Semimetals **22**, 1–202 (1985).

[80]C. Zhang, C.-L. Zou, Y. Yan, R. Hao, F.-W. Sun, Z.-F. Han, Y. S. Zhao, and J. Yao, "Two-photon pumped lasing in single-crystal organic nanowire exciton polariton resonators", Journal of the American Chemical Society **133**, 7276–7279 (2011).

[81]Q. H. Cui, Y. S. Zhao, and J. Yao, "Photonic applications of one-dimensional organic single-crystalline nanostructures: optical waveguides and optically pumped lasers", Journal of Materials Chemistry **22**, 4136–4140 (2012).

[82]C. Wei, S.-Y. Liu, C.-L. Zou, Y. Liu, J. Yao, and Y. S. Zhao, "Controlled self-assembly of organic composite microdisks for efficient output coupling of whispering-gallery-mode lasers", Journal of the American Chemical Society **137**, 62–65 (2014).

[83]B. Crone, A Dodabalapur, R Sarpeshkar, A Gelperin, H. Katz, and Z Bao, "Organic oscillator and adaptive amplifier circuits for chemical vapor sensing", Journal of applied physics **91**, 10140–10146 (2002).

[84]P. Peumans, V Bulović, and S. R. Forrest, "Efficient, high-bandwidth organic multilayer photodetectors", Applied Physics Letters **76**, 3855–3857 (2000).

[85]S. Tomaru, M. Kawachi, and M. Kobayashi, "Organic crystals growth for optical channel waveguides", Optics communications **50**, 154–156 (1984).

[86]D. Zang and S. Forrest, "Crystalline organic semiconductor optical directional couplers and switches using an index-matching layer", IEEE photonics technology letters **4**, 365–368 (1992).

[87]L. Gu, J Livenere, G Zhu, E. E. Narimanov, and M. Noginov, "Quest for organic plasmonics", Applied Physics Letters **103**, 021104 (2013).

[88]E RamanjaneyaáReddy et al., "Passive optical waveguiding tubular pharmaceutical solids and raman spectroscopy/mapping of nano-/micro-scale defects", CrystEngComm **16**, 4696–4700 (2014).

[89]Y. Yan, C. Zhang, J. Y. Zheng, J. Yao, and Y. S. Zhao, "Optical modulation based on direct photon-plasmon coupling in organic/metal nanowire heterojunctions", Advanced Materials **24**, 5681–5686 (2012).

[90]R. T. Chen, "Polymer-based photonic integrated circuits", Optics & Laser Technology **25**, 347–365 (1993).

[91]C. Wei, M. Gao, F. Hu, J. Yao, and Y. S. Zhao, "Excimer emission in self-assembled organic spherical microstructures: an effective approach to wavelength switchable microlasers", Advanced Optical Materials (2016).

[92]Y. Yan, C. Zhang, J. Y. Zheng, J. Yao, and Y. S. Zhao, "Optical modulation based on direct photon-plasmon coupling in organic/metal nanowire heterojunctions", Advanced Materials **24**, 5681–5686 (2012).

[93]Y. Wei, H. Dong, C. Wei, W. Zhang, Y. Yan, and Y. S. Zhao, "Wavelength-tunable microlasers based on the encapsulation of organic dye in metal–organic frameworks", Advanced Materials **28**, 7424–7429 (2016).

[94]A. L. Pyayt, B. Wiley, Y. Xia, A. Chen, and L. Dalton, "Integration of photonic and silver nanowire plasmonic waveguides", Nature nanotechnology **3**, 660–665 (2008).

[95]C. Zhang, C.-L. Zou, Y. Yan, C. Wei, J.-M. Cui, F.-W. Sun, J. Yao, and Y. S. Zhao, "Self-assembled organic crystalline microrings as active whispering-gallery-mode optical resonators", Advanced Optical Materials **1**, 357–361 (2013).

[96]H. Dong, C. Zhang, X. Lin, Z. Zhou, J. Yao, and Y. S. Zhao, "Dual-wavelength switchable vibronic lasing in single-crystal organic microdisks", Nano Letters (2016).

[97]S. Kushida, D. Braam, C. Pan, T. D. Dao, K. Tabata, K. Sugiyasu, M. Takeuchi, S. Ishii, T. Nagao, A. Lorke, et al., "Whispering gallery resonance from self-assembled microspheres of highly fluorescent isolated conjugated polymers", Macromolecules **48**, 3928–3933 (2015).

[98]D. Okada, T. Nakamura, D. Braam, T. D. Dao, S. Ishii, T. Nagao, A. Lorke, T. Nabeshima, and Y. Yamamoto, "Color-tunable resonant photoluminescence and cavity-mediated multistep energy transfer cascade", ACS nano **10**, 7058–7063 (2016).

[99]C. Zhang, Y. Yan, J. Yao, and Y. S. Zhao, "Manipulation of light flows in organic color-graded microstructures towards integrated photonic heterojunction devices", Advanced Materials **25**, 2854–2859 (2013).

[100]J. Wang, G. Zhang, Z. Liu, X. Gu, Y. Yan, C. Zhang, Z. Xu, Y. Zhao, H. Fu, and D. Zhang, "New emissive organic molecule based on pyrido [3, 4-g] isoquinoline framework: synthesis and fluorescence tuning as well as optical waveguide behavior", Tetrahedron **69**, 2687–2692 (2013).

[101]T. L. Penner, H. R. Motschmann, N. J. Armstrong, M. C. Ezenyilimba, and D. J. Williams, "Efficient phase-matched second-harmonic generation of blue light in an organic waveguide", (1994).

[102]G. Hewig and K Jain, "Frequency doubling in an organic waveguide", Optics Communications **47**, 347–350 (1983).

[103]V. Kozlov, V Bulović, P. Burrows, and S. Forrest, "Laser action in organic semiconductor waveguide and double-heterostructure devices", Nature **389**, 362–364 (1997).

[104]C. Zhang, Y. Yan, Y. S. Zhao, and J. Yao, "Synthesis and applications of organic nanorods, nanowires and nanotubes", Annual Reports Section" C"(Physical Chemistry) **109**, 211–239 (2013).

[105]J. Li, W. Zhang, Q. Li, and B. Li, "Excitation of surface plasmons from silver nanowires embedded in polymer nanofibers", Nanoscale **7**, 2889–2893 (2015).

[106]Y. J. Li, X. Xiong, C.-L. Zou, X. F. Ren, and Y. S. Zhao, "One-dimensional dielectric/metallic hybrid materials for photonic applications", Small **11**, 3728–3743 (2015).

[107]C. Zhang, Y. Yan, Y.-Y. Jing, Q. Shi, Y. S. Zhao, and J. Yao, "One-dimensional organic photonic heterostructures: rational construction and spatial engineering of excitonic emission", Advanced Materials **24**, 1703–1708 (2012).

[108]J. Y. Zheng, Y. Yan, X. Wang, Y. S. Zhao, J. Huang, and J. Yao, "Wire-on-wire growth of fluorescent organic heterojunctions", Journal of the American Chemical Society **134**, 2880–2883 (2012).

[109]C. Zhang, J. Y. Zheng, Y. S. Zhao, and J. Yao, "Self-modulated white light outcoupling in doped organic nanowire waveguides via the fluctuations of singlet and triplet excitons during propagation", Advanced Materials **23**, 1380–1384 (2011).

[110]C. Zhang, J. Y. Zheng, Y. S. Zhao, and J. Yao, "Organic core–shell nanostructures: microemulsion synthesis and upconverted emission", Chemical Communications **46**, 4959–4961 (2010).

[111]Y. S. Zhao, J. Wu, and J. Huang, "Vertical organic nanowire arrays: controlled synthesis and chemical sensors", Journal of the American Chemical Society **131**, 3158–3159 (2009).

[112]R. Chikkaraddy, P. P. Patra, R. P. N. Tripathi, A. Dasgupta, and G. V. P. Kumar, "Plasmon-controlled excitonic emission from vertically-tapered organic nanowires", Nanoscale **8**, 14803–14808 (2016).

[113]Y. S. Zhao, J. Xu, A. Peng, H. Fu, Y. Ma, L. Jiang, and J. Yao, "Optical waveguide based on crystalline organic microtubes and microrods", Angewandte Chemie **120**, 7411–7415 (2008).

[114]Y. S. Zhao, W. Yang, and J. Yao, "Organic nanocrystals with tunable morphologies and optical properties prepared through a sonication technique", Physical Chemistry Chemical Physics **8**, 3300–3303 (2006).

[115]R. Vattikunta, D. Venkatakrishnarao, M. A. Mohiddon, and R. Chandrasekar, "Self-assembly of "chalcone" type push-pull dye molecules into organic single crystalline microribbons and rigid microrods for vis/nir range photonic cavity applications", ChemPhysChem **17**, 3435–3441 (2016).

[116]N. Chandrasekhar and R. Chandrasekar, "Reversibly shape-shifting organic optical waveguides: formation of organic nanorings, nanotubes, and nanosheets", Angewandte Chemie International Edition **51**, 3556–3561 (2012).

[117]Y. S. Narayana, D. Venkatakrishnarao, A. Biswas, M. A. Mohiddon, N. Viswanathan, and R. Chandrasekar, "Visible–near-infrared range whispering gallery resonance from photonic μ-sphere cavities self-assembled from a blend of polystyrene and poly [4, 7-bis (3-octylthiophene-2-yl) benzothiadiazole-co-2, 6-bis (pyrazolyl) pyridine] coordinated to tb (acac) 3", ACS applied materials & interfaces **8**, 952–958 (2015).

[118]D. Venkatakrishnarao and R. Chandrasekar, "Engineering the self-assembly of dcm dyes into whispering-gallery-mode μ-hemispheres and fabry–pèrot-type μ-rods for visible–nir (600–875 nm) range optical microcavities", Advanced Optical Materials **4**, 112–119 (2016).

[119]N. Chandrasekhar, S. Basak, M. A. Mohiddon, and R. Chandrasekar, "Planar active organic waveguide and wavelength filter: self-assembled meso-tetratolylporphyrin hexagonal nanosheet", ACS applied materials & interfaces **6**, 1488–1494 (2014).

[120]D. Venkatakrishnarao, M. A. Mohiddon, N. Chandrasekhar, and R. Chandrasekar, "Photonic microrods composed of photoswitchable molecules: erasable heterostructure waveguides for tunable optical modulation", Advanced Optical Materials **3**, 1035–1040 (2015).

[121]O. Benson, "Assembly of hybrid photonic architectures from nanophotonic constituents", Nature **480**, 193–199 (2011).

[122]K. Takazawa, J.-i. Inoue, K. Mitsuishi, and T. Takamasu, "Micrometer-scale photonic circuit components based on propagation of exciton polaritons in organic dye nanofibers", Advanced Materials **23**, 3659–3663 (2011).

[123]D. Ammermann, C. Rompf, and W. Kowalsky, "Photonic devices based on crystalline organic semiconductors for optoelectronic integrated circuits", Japanese journal of applied physics **34**, 1293 (1995).

[124]K. Takazawa, J.-i. Inoue, K. Mitsuishi, and T. Kuroda, "Ultracompact asymmetric mach–zehnder interferometers with high visibility constructed from exciton polariton waveguides of organic dye nanofibers", Advanced Functional Materials **23**, 839–845 (2013).

[125]J.-Y. Zheng, H. Xu, J. J. Wang, S. Winters, C. Motta, E. Karademir, W. Zhu, E. Varrla, G. S. Duesberg, S. Sanvito, et al., "Vertical single-crystalline organic nanowires on graphene: solution-phase epitaxy and optical microcavities", Nano Letters **16**, 4754–4762 (2016).

[126]A. G. Curto, G. Volpe, T. H. Taminiau, M. P. Kreuzer, R. Quidant, and N. F. van Hulst, "Unidirectional emission of a quantum dot coupled to a nanoantenna", Science **329**, 930–933 (2010).

[127]V. Aswathy, P. P. Patra, and G. V. P. Kumar, "Geometry-dependent anti-stokes sers radiation patterns from gold nanorod dimers", Journal of Optics **17**, 114011 (2015).

[128]L. Novotny and N. Van Hulst, "Antennas for light", Nature Photonics **5**, 83–90 (2011).

[129]H. Wei and H. Xu, "Nanowire based plasmonic waveguides and devices for integrated nanophotonic circuits", Nanophotonics **1**, 155–169 (2012).

[130]T. Liew, A. Kavokin, T Ostatnick $\acute{y}$, M Kaliteevski, I. Shelykh, and R. Abram, "Exciton polariton integrated circuits", Physical review B **82**, 033302 (2010).

[131]P. Bharadwaj, B. Deutsch, and L. Novotny, "Optical antennas", Advances in Optics and Photonics **1**, 438–483 (2009).

[132]V. Kozlov, V Bulović, P. Burrows, and S. Forrest, "Laser action in organic semiconductor waveguide and double-heterostructure devices", Nature **389**, 362–364 (1997).

[133]R. Yan, D. Gargas, and P. Yang, "Nanowire photonics", Nature Photonics **3**, 569–576 (2009).

[134]T. Liu, Y. Li, Y. Yan, Y. Li, Y. Yu, N. Chen, S. Chen, C. Liu, Y. Zhao, and H. Liu, "Tuning growth of low-dimensional organic nanostructures for efficient optical waveguide applications", The Journal of Physical Chemistry C **116**, 14134–14138 (2012).

[135]F. Quan, "Green photonics", Journal of Optics **14**, 024001 (2012).

[136]Y. Yan, C. Zhang, J. Yao, and Y. S. Zhao, "Recent advances in organic one-dimensional composite materials", Advanced Materials **25**, 3627–3638 (2013).

[137]P. Biagioni, J.-S. Huang, and B. Hecht, "Nanoantennas for visible and infrared radiation", Reports on Progress in Physics **75**, 024402 (2012).

[138]A. Akimov, A Mukherjee, C. Yu, D. Chang, A. Zibrov, P. Hemmer, H Park, and M. Lukin, "Generation of single optical plasmons in metallic nanowires coupled to quantum dots", Nature **450**, 402–406 (2007).

[139]M. L. Brongersma and P. G. Kik, *Surface plasmon nanophotonics* (Springer, 2007).

[140]S. Bozhevolnyi, *Plasmonic nanoguides and circuits* (Pan Stanford, 2009).

[141]T. W. Ebbesen, C. Genet, and S. I. Bozhevolnyi, "Surface plasmon circuitry", Physics Today **61**, 44 (2008).

[142]X. Guo, Y. Ma, Y. Wang, and L. Tong, "Nanowire plasmonic waveguides, circuits and devices", Laser & Photonics Reviews **7**, 855–881 (2013).

[143]X. Xiong, C.-L. Zou, X.-F. Ren, A.-P. Liu, Y.-X. Ye, F.-W. Sun, and G. C. Guo, "Silver nanowires for photonics applications", Laser & Photonics Reviews **7**, 901–919 (2013).

[144]Y. Huang, Y. Fang, Z. Zhang, L. Zhu, and M. Sun, "Nanowire supported plasmonic waveguide for remote excitation of surface enhanced raman scattering", Light: Science & Applications **3**, e199 (2014).

[145]O. L. Muskens, J. G. Rivas, R. E. Algra, E. P. Bakkers, and A. Lagendijk, "Design of light scattering in nanowire materials for photovoltaic applications", Nano letters **8**, 2638–2642 (2008).

[146]Y. Fontana, G. Grzela, E. P. Bakkers, and J. G. Rivas, "Mapping the directional emission of quasi-two-dimensional photonic crystals of semiconductor nanowires using fourier microscopy", Physical Review B **86**, 245303 (2012).

[147]J Brewer, C. Maibohm, L Jozefowski, L. Bagatolli, and H.-G. Rubahn, "A 3d view on free-floating, space-fixed and surface-bound para-phenylene nanofibres", Nanotechnology **16**, 2396 (2005).

[148]G. Grzela, R. Paniagua-Dominguez, T. Barten, Y. Fontana, J. A. Sanchez-Gil, and J. Gomez Rivas, "Nanowire antenna emission", Nano letters **12**, 5481–5486 (2012).

[149]R Paniagua-Dominguez, G Grzela, J. G. Rivas, and J. Sanchez-Gil, "Enhanced and directional emission of semiconductor nanowires tailored through leaky/guided modes", Nanoscale **5**, 10582–10590 (2013).

[150]J Lagois and B Fischer, "Experimental observation of surface exciton polaritons", Physical Review Letters **36**, 680 (1976).

[151]F. Yang, J. Sambles, and G. Bradberry, "Long-range coupled surface exciton polaritons", Physical review letters **64**, 559 (1990).

[152]A. Kavokin, J. J. Baumberg, G. Malpuech, and F. P. Laussy, *Microcavities*, Vol. 16 (OUP Oxford, 2011).

[153]H. Deng, H. Haug, and Y. Yamamoto, "Exciton polariton bose-einstein condensation", Reviews of modern physics **82**, 1489 (2010).

[154]T. Byrnes, N. Y. Kim, and Y. Yamamoto, "Exciton polariton condensates", Nature Physics **10**, 803–813 (2014).

[155]J. D. Plumhof, T. Stöferle, L. Mai, U. Scherf, and R. F. Mahrt, "Room temperature bose einstein condensation of cavity exciton polaritons in a polymer", Nature materials **13** (2014).

[156]P. Savvidis, J. Baumberg, R. Stevenson, M. Skolnick, D. Whittaker, and J. Roberts, "Asymmetric angular emission in semiconductor microcavities", Physical Review B **62**, R13278 (2000).

[157]S Christopoulos, G. B. H. Von Högersthal, A. Grundy, P. Lagoudakis, A. Kavokin, J. Baumberg, G Christmann, R Butté, E Feltin, J.-F. Carlin, et al., "Room temperature polariton lasing in semiconductor microcavities", Physical review letters **98**, 126405 (2007).

[158]Y. S. Zhao, A. Peng, H. Fu, Y. Ma, and J. Yao, "Nanowire waveguides and ultraviolet lasers based on small organic molecules", Advanced Materials **20**, 1661–1665 (2008).

[159]S. K. Saikin, A. Eisfeld, S. Valleau, and A. Aspuru-Guzik, "Photonics meets excitonics: natural and artificial molecular aggregates", Nanophotonics **2**, 21–38 (2013).

[160]W. Yao and Y. S. Zhao, "Tailoring the self-assembled structures and photonic properties of organic nanomaterials", Nanoscale **6**, 3467–3473 (2014).

[161]H. Deng, G. Weihs, C. Santori, J. Bloch, and Y. Yamamoto, "Condensation of semiconductor microcavity exciton polaritons", Science **298**, 199–202 (2002).

[162]R. Chandrasekar, "Organic photonics: prospective nano/micro scale passive organic optical waveguides obtained from π-conjugated ligand molecules", Physical Chemistry Chemical Physics **16**, 7173–7183 (2014).

[163]J. Kasprzak, M Richard, S Kundermann, A Baas, P Jeambrun, J. Keeling, F. Marchetti, M. Szymańska, R Andre, J. Staehli, et al., "Bose–einstein condensation of exciton polaritons", Nature **443**, 409–414 (2006).

[164]Y. S. Zhao, J. Wu, and J. Huang, "Vertical organic nanowire arrays: controlled synthesis and chemical sensors", Journal of the American Chemical Society **131**, 3158–3159 (2009).

[165]Y. S. Zhao, P. Zhan, J. Kim, C. Sun, and J. Huang, "Patterned growth of vertically aligned organic nanowire waveguide arrays", ACS nano **4**, 1630–1636 (2010).

[166]P. B. W. Jensen, J. Kjelstrup-Hansen, and H.-G. Rubahn, "Multicolor nanofiber based organic light emitting transistors", Organic Electronics **14**, 3324–3330 (2013).

[167]J. Kjelstrup-Hansen, C. Simbrunner, and H.-G. Rubahn, "Organic surface-grown nanowires for functional devices", Reports on Progress in Physics **76**, 126502 (2013).

[168]T. Leißner, C. Lemke, J. Fiutowski, J. W. Radke, A. Klick, L. Tavares, J. Kjelstrup-Hansen, H.-G. Rubahn, and M. Bauer, "Morphological tuning of the plasmon dispersion relation in dielectric-loaded nanofiber waveguides", Physical review letters **111**, 046802 (2013).

[169]C. Maibohm, M. Rastedt, F. Kutscher, O. Frey, R. Beckhaus, H. G. Rubahn, and K. Al Shamery, "Optical waveguiding and temperature dependent photoluminescence of nanotubulars grown from molecular building blocks", Chemical Physics Letters **590**, 87–91 (2013).

[170]X. Wang, Q. Liao, Z. Xu, Y. Wu, L. Wei, X. Lu, and H. Fu, "Exciton polaritons with size tunable coupling strengths in self-assembled organic microresonators", ACS Photonics **1**, 413–420 (2014).

[171]D. Venkatakrishnarao and R. Chandrasekar, "Engineering the self assembly of dcm dyes into whispering-gallery-mode μ-hemispheres and fabry–perot-type μ-rods for visible–nir (600–875 nm) range optical microcavities", Advanced Optical Materials **4**, 112–119 (2016).

[172]M. J. Gentile, S Núñez-Sánchez, and W. L. Barnes, "Optical field enhancement and subwavelength field confinement using excitonic nanostructures", Nano letters **14**, 2339–2344 (2014).

[173]A. Cacciola, C. Triolo, O. Di Stefano, A. Genco, M. Mazzeo, R. Saija, S. Patane, and S. Savasta, "Subdiffraction light concentration by j aggregate nanostructures", ACS Photonics **2**, 971–979 (2015).

[174]M. Philpott, A Brillante, I. Pockrand, and J. Swalen, "A new optical phenomenon: exciton surface polaritons at room temperature", Molecular Crystals and Liquid Crystals **50**, 139–162 (1979).

[175]S. Wang, "Principles and characteristics of integratable active and passive optical devices", Semiconductors and Semimetals **22**, 1–202 (1985).

[176]S Mias and H Camon, "A review of active optical devices: i. amplitude modulation", Journal of micromechanics and microengineering **18**, 083001 (2008).

[177]S. M. Yoon, J. Lee, J. H. Je, H. C. Choi, and M. Yoon, "Optical waveguiding and lasing action in porphyrin rectangular microtube with subwavelength wall thicknesses", ACS nano **5**, 2923–2929 (2011).

[178]K. Takazawa, Y. Kitahama, Y. Kimura, and G. Kido, "Optical waveguide self-assembled from organic dye molecules in solution", Nano letters **5**, 1293–1296 (2005).

[179]C. J. Bardeen, "The structure and dynamics of molecular excitons", Annual review of physical chemistry **65**, 127–148 (2014).

[180]A. E. Schlather, N. Large, A. S. Urban, P. Nordlander, and N. J. Halas, "Near field mediated plexcitonic coupling and giant rabi splitting in individual metallic dimers", Nano letters **13**, 3281–3286 (2013).

[181]A. K. Ghatak and K Thyagarajan, *Optical electronics* (Cambridge University Press, 1989).

[182]L. K. Van Vugt, B. Piccione, and R. Agarwal, "Incorporating polaritonic effects in semiconductor nanowire waveguide dispersion", Applied Physics Letters **97**, 061115 (2010).

[183]Z. R. Li, *Organic light-emitting materials and devices* (CRC press, 2015).

[184]D. Konios, C. Petridis, G. Kakavelakis, M. Sygletou, K. Savva, E. Stratakis, and E. Kymakis, "Photovoltaics: reduced graphene oxide micromesh electrodes for large area, flexible, organic photovoltaic devices", Advanced Functional Materials **25**, 2206–2206 (2015).

[185]Y. S. Zhao, H. Fu, A. Peng, Y. Ma, Q. Liao, and J. Yao, "Construction and optoelectronic properties of organic one-dimensional nanostructures", Accounts of chemical research **43**, 409–418 (2009).

[186]F. S. Kim, G. Ren, and S. A. Jenekhe, "One-dimensional nanostructures of π conjugated molecular systems: assembly, properties, and applications from photovoltaics, sensors, and nanophotonics to nanoelectronics", Chemistry of Materials **23**, 682–732 (2010).

[187]T. Kim, L. Zhu, R. O. Al-Kaysi, and C. J. Bardeen, "Organic photomechanical materials", ChemPhysChem **15**, 400–414 (2014).

[188]M. Schiek, F. Balzer, K. Al-Shamery, J. R. Brewer, A. Lützen, and H.-G. Rubahn, "Organic molecular nanotechnology", Small **4**, 176–181 (2008).

[189]F. Quochi, "Random lasers based on organic epitaxial nanofibers", Journal of Optics **12**, 024003 (2010).

[190]J. Xu, S. Semin, T. Rasing, and A. E. Rowan, "Organized chromophoric assemblies for nonlinear optical materials: towards (sub) wavelength scale architectures", Small **11**, 1113–1129 (2015).

[191]W. Yao, G. Han, F. Huang, M. Chu, Q. Peng, F. Hu, Y. Yi, H. Jiang, J. Yao, and Y. S. Zhao, "H-like organic nanowire heterojunctions constructed from cooperative molecular assembly for photonic applications", Advanced Science **2** (2015).

[192]F. Balzer, V. G. Bordo, A. C. Simonsen, and H. G. Rubahn, "Optical waveguiding in individual nanometer scale organic fibers", Physical Review B **67**, 115408 (2003).

[193]S. Basak and R. Chandrasekar, "Passive optical waveguiding organic rectangular tubes: tube cutting, controlling light propagation distance and multiple optical outputs", Journal of Materials Chemistry C **2**, 1404–1408 (2014).

[194]N. Chandrasekhar, M. A. Mohiddon, and R. Chandrasekar, "Organic submicro tubular optical waveguides: self-assembly, diverse geometries, efficiency, and remote sensing properties", Advanced Optical Materials **1**, 305–311 (2013).

[195]F. Balzer, V. Bordo, A. C. Simonsen, and H. G. Rubahn, "Isolated hexaphenyl nanofibers as optical waveguides", Applied physics letters **82**, 10–12 (2003).

[196]F. Balzer and H. G. Rubahn, "Dipole-assisted selfassembly of light-emitting pnp needles on mica", Applied Physics Letters **79** (2001).

[197]F. Balzer and H. G. Rubahn, "Growth control and optics of organic nanoaggregates", Advanced Functional Materials **15**, 17–24 (2005).

[198]X. Chen and H. Fuchs, *Soft matter nanotechnology: from structure to function* (John Wiley & Sons, 2015).

[199]S.-Y. Min, T. S. Kim, Y. Lee, H. Cho, W. Xu, and T. W. Lee, "Organic nanowire fabrication and device applications", Small **11**, 45–62 (2015).

[200]J. Yang, D. Yan, and T. S. Jones, "Molecular template growth and its applications in organic electronics and optoelectronics", Chemical reviews **115**, 5570–5603 (2015).

[201]J. J. Piet, P. N. Taylor, B. R. Wegewijs, H. L. Anderson, A. Osuka, and J. M. Warman, "Photoexcitations of covalently bridged zinc porphyrin oligomers: frenkel versus wannier-mott type excitons", The Journal of Physical Chemistry B **105**, 97–104 (2001).

[202]M. Zamfirescu, A. Kavokin, B. Gil, G. Malpuech, and M. Kaliteevski, "Zno as a material mostly adapted for the realization of room-temperature polariton lasers", Physical Review B **65**, 161205 (2002).

[203]Y. S. Zhao, J. Xu, A. Peng, H. Fu, Y. Ma, L. Jiang, and J. Yao, "Optical waveguide based on crystalline organic microtubes and microrods", Angewandte Chemie **120**, 7411–7415 (2008).

[204]C. Zhang, Y. S. Zhao, and J. Yao, "Optical waveguides at micro/nanoscale based on functional small organic molecules", Physical Chemistry Chemical Physics **13**, 9060–9073 (2011).

[205]K. Takazawa, "Flexibility and bending loss of waveguiding molecular fibers self-assembled from thiacyanine dye", Chemical Physics Letters **452**, 168–172 (2008).

[206]H. Yanagi and T. Morikawa, "Self-waveguided blue light emission in p-sexiphenyl crystals epitaxially grown by mask-shadowing vapor deposition", Applied physics letters **75**, 187–189 (1999).

[207]T. Yokoyama, "Self assembled templating for the growth of molecular nanodots", Applied Physics Letters **96**, 3101 (2010).

[208]C. Wei, S.-Y. Liu, C. L. Zou, Y. Liu, J. Yao, and Y. S. Zhao, "Controlled self assembly of organic composite microdisks for efficient output coupling of whispering gallery mode lasers", Journal of the American Chemical Society **137**, 62–65 (2014).

[209]Y. Dong, K. Wang, and X. Jin, "Package of a dual tapered fiber coupled microsphere resonator with high q factor", Optics Communications **350**, 230–234 (2015).

[210]Y. Dong, K. Wang, and X. Jin, "Packaged microsphere taper coupling system with a high q factor", Applied optics **54**, 277–284 (2015).

[211]L. Zhu, D. Zhang, R. Wang, P. Wang, H. Ming, R. Badugu, L. Du, X. Yuan, and J. R. Lakowicz, "Metal dielectric waveguides for high efficiency fluorescence imaging", The Journal of Physical Chemistry C **119**, 24081–24085 (2015).

[212]Z. Wang, "Microsphere super resolution imagingy", Nanoscience Volume 3 **3**, 193 (2016).

[213]A. Darafsheh, N. I. Limberopoulos, J. S. Derov, D. E. Walker Jr, and V. N. Astratov, "Advantages of microsphere assisted super resolution imaging technique over solid immersion lens and confocal microscopies", Applied Physics Letters **104**, 061117 (2014).

[214]A. Darafsheh, C. Guardiola, A. Palovcak, J. C. Finlay, and A. Cárabe, "Optical super resolution imaging by high-index microspheres embedded in elastomers", Optics letters **40**, 5–8 (2015).

[215]H. H. Choi, H. J. Kim, J. Noh, C.-W. Lee, and W. Jhe, "Measurement of angular distribution of radiation from dye molecules coupled to evanescent wave", Physical Review A **66**, 053803 (2002).

[216]J. A. Schuller, S. Karaveli, T. Schiros, K. He, S. Yang, I. Kymissis, J. Shan, and R. Zia, "Orientation of luminescent excitons in layered nanomaterials", Nature nanotechnology **8**, 271–276 (2013).

[217]J. J. Armao IV, P. Rabu, E. Moulin, and N. Giuseppone, "Long-range energy transport via plasmonic propagation in a supramolecular organic waveguide", Nano letters **16**, 2800–2805 (2016).

[218]Y. J. Li, Y. Yan, Y. S. Zhao, and J. Yao, "Construction of nanowire heterojunctions: photonic function-oriented nanoarchitectonics", Advanced Materials **28**, 1319–1326 (2016).

[219]S. J. Brown, R. A. Schlitz, M. L. Chabinyc, and J. A. Schuller, "Morphology-dependent optical anisotropies in the n-type polymer p (ndi2od-t2)", Physical Review B **94**, 165105 (2016).

[220]K. Takazawa, J.-i. Inoue, and K. Mitsuishi, "Optical waveguiding along a sub-100-nm-width organic nanofiber: significant effect of cooling on waveguiding properties", The Journal of Physical Chemistry C **120**, 1186–1192 (2016).

[221]K. Takazawa, J.-i. Inoue, K. Mitsuishi, and T. Kuroda, "Ultracompact asymmetric mach–zehnder interferometers with high visibility constructed from exciton polariton waveguides of organic dye nanofibers", Advanced Functional Materials **23**, 839–845 (2013).

[222]D. Venkatakrishnarao, M. A. Mohiddon, N. Chandrasekhar, and R. Chandrasekar, "Photonic microrods composed of photoswitchable molecules: erasable heterostructure waveguides for tunable optical modulation", Advanced Optical Materials **3**, 1035–1040 (2015).

[223]D. G. Lidzey, D. D. Bradley, A. Armitage, S. Walker, and M. S. Skolnick, "Photon-mediated hybridization of frenkel excitons in organic semiconductor microcavities", Science **288**, 1620–1623 (2000).

[224]S Blumstengel, S Sadofev, C Xu, J Puls, and F Henneberger, "Converting wannier into frenkel excitons in an inorganic/organic hybrid semiconductor nanostructure", Physical review letters **97**, 237401 (2006).

[225]O.-P. Kwon, M. Jazbinsek, J.-I. Seo, P.-J. Kim, E.-Y. Choi, Y. S. Lee, and P. Günter, "First hyperpolarizability orientation in asymmetric pyrrole-based polyene chromophores", Dyes and Pigments **85**, 162–170 (2010).

[226]R. Badugu, H. Szmacinski, K. Ray, E. Descrovi, S. Ricciardi, D. Zhang, J. Chen, Y. Huo, and J. R. Lakowicz, "Metal–dielectric waveguides for high-efficiency coupled emission", ACS photonics **2**, 810–815 (2015).

[227]S. Dutta Choudhury, R. Badugu, and J. R. Lakowicz, "Directing fluorescence with plasmonic and photonic structures", Accounts of chemical research **48**, 2171–2180 (2015).

[228]J. A. Hollingsworth, H. Htoon, A. Piryatinski, S. Götzinger, and V. Sandoghdar, "When excitons and plasmons meet: emerging function through synthesis and assembly", MRS Bulletin **40**, 768–776 (2015).

[229]Y. B. Zheng, B. Kiraly, S. Cheunkar, T. J. Huang, and P. S. Weiss, "Incident-angle-modulated molecular plasmonic switches: a case of weak exciton–plasmon coupling", Nano letters **11**, 2061–2065 (2011).

[230]G. A. Wurtz, P. R. Evans, W. Hendren, R. Atkinson, W. Dickson, R. J. Pollard, A. V. Zayats, W. Harrison, and C. Bower, "Molecular plasmonics with tunable exciton-plasmon coupling strength in j-aggregate hybridized au nanorod assemblies", Nano letters **7**, 1297–1303 (2007).

[231]J. Lee, P. Hernandez, J. Lee, A. O. Govorov, and N. A. Kotov, "Exciton–plasmon interactions in molecular spring assemblies of nanowires and wavelength-based protein detection", Nature materials **6**, 291–295 (2007).

[232]J. Claudon, J. Bleuse, N. S. Malik, M. Bazin, P. Jaffrennou, N. Gregersen, C. Sauvan, P. Lalanne, and J.-M. Gérard, "A highly efficient single-photon source based on a quantum dot in a photonic nanowire", Nature Photonics **4**, 174–177 (2010).

[233]D. Pacifici, H. J. Lezec, and H. A. Atwater, "All-optical modulation by plasmonic excitation of cdse quantum dots", Nature photonics **1**, 402–406 (2007).

[234]F. Xia, H. Wang, D. Xiao, M. Dubey, and A. Ramasubramaniam, "Two-dimensional material nanophotonics", Nature Photonics **8**, 899–907 (2014).

[235]N. T. Fofang, T.-H. Park, O. Neumann, N. A. Mirin, P. Nordlander, and N. J. Halas, "Plexcitonic nanoparticles: plasmon- exciton coupling in nanoshell- j-aggregate complexes", Nano letters **8**, 3481–3487 (2008).

[236]J. R. Lakowicz, "Radiative decay engineering 3. surface plasmon-coupled directional emission", Analytical biochemistry **324**, 153–169 (2004).

[237]D. Tedeschi, M. De Luca, H. A. Fonseka, Q. Gao, F. Mura, H. H. Tan, S. Rubini, F. Martelli, C. Jagadish, M. Capizzi, et al., "Long-lived hot carriers in iii–v nanowires", Nano letters **16**, 3085–3093 (2016).

[238]M. Salvador, B. A. MacLeod, A. Hess, A. P. Kulkarni, K. Munechika, J. I. Chen, and D. S. Ginger, "Electron accumulation on metal nanoparticles in plasmon-enhanced organic solar cells", Acs Nano **6**, 10024–10032 (2012).

[239]E. Eizner, O. Avayu, R. Ditcovski, and T. Ellenbogen, "Aluminum nanoantenna complexes for strong coupling between excitons and localized surface plasmons", Nano letters **15**, 6215–6221 (2015).

[240]P. Chantharasupawong, L. Tetard, and J. Thomas, "Coupling enhancement and giant rabi-splitting in large arrays of tunable plexcitonic substrates", The Journal of Physical Chemistry C **118**, 23954–23962 (2014).

[241]Q. Li, J. Y. Zheng, Y. Yan, Y. S. Zhao, and J. Yao, "Electrogenerated chemiluminescence of metal–organic complex nanowires: reduced graphene oxide enhancement and biosensing application", Advanced Materials **24**, 4745–4749 (2012).

[242]P. Simesen, T. Søndergaard, E. Skovsen, J. Fiutowski, H.-G. Rubahn, S. I. Bozhevolnyi, and K. Pedersen, "Surface plasmon polariton excitation by second harmonic generation in single organic nanofibers", Optics express **23**, 16356–16363 (2015).

[243]B. Rogez, R. Horeis, E. Le Moal, J. Christoffers, K. Al-Shamery, G. Dujardin, and E. Boer-Duchemin, "Optical and electrical excitation of hybrid guided modes in an organic nanofiber–gold film system", The Journal of Physical Chemistry C **119**, 22217–22224 (2015).

[244]S Mokkapati and C Jagadish, "Review on photonic properties of nanowires for photovoltaics [invited]", Optics Express **24**, 17345–17358 (2016).

[245]W. S. Ko, T.-T. D. Tran, I. Bhattacharya, K. W. Ng, H. Sun, and C. Chang-Hasnain, "Illumination angle insensitive single indium phosphide tapered nanopillar solar cell", Nano letters **15**, 4961–4967 (2015).

[246]D. G. Zhang, X. Yuan, and A. Bouhelier, "Direct image of surface-plasmon-coupled emission by leakage radiation microscopy", Applied optics **49**, 875–879 (2010).

[247]J. Yang, J.-P. Hugonin, and P. Lalanne, "Near-to-far field transformations for radiative and guided waves", ACS Photonics **3**, 395–402 (2016).

[248]L. Novotny and B. Hecht, *Principles of nano-optics* (Cambridge university press, 2012).

[249]L. Novotny, "Allowed and forbidden light in near-field optics. i. a single dipolar light source", JOSA A **14**, 91–104 (1997).

[250]A. Yurt, A. Uyar, T. B. Cilingiroglu, B. B. Goldberg, and M. S. Ünlü, "Evanescent waves in high numerical aperture aplanatic solid immersion microscopy: effects of forbidden light on subsurface imaging", Optics express **22**, 7422–7433 (2014).

[251]H. Yang, M. Qiu, and Q. Li, "Identification and control of multiple leaky plasmon modes in silver nanowires", Laser & Photonics Reviews (2015).

[252]J.-Y. Zheng, H. Xu, J. J. Wang, S. Winters, C. Motta, E. Karademir, W. Zhu, E. Varrla, G. S. Duesberg, S. Sanvito, et al., "Vertical single-crystalline organic nanowires on graphene: solution-phase epitaxy and optical microcavities", Nano Letters **16**, 4754–4762 (2016).

[253]M. Ono, H. Taniyama, H. Xu, M. Tsunekawa, E. Kuramochi, K. Nozaki, and M. Notomi, "Deep-subwavelength plasmonic mode converter with large size reduction for si-wire waveguide", Optica **3**, 999–1005 (2016).

[254]N Kalfagiannis, P. Karagiannidis, C Pitsalidis, N. Panagiotopoulos, C Gravalidis, S Kassavetis, P Patsalas, and S Logothetidis, "Plasmonic silver nanoparticles for improved organic solar cells", Solar Energy Materials and Solar Cells **104**, 165–174 (2012).

[255]I. Friedler, C. Sauvan, J.-P. Hugonin, P. Lalanne, J. Claudon, and J.-M. Gérard, "Solid-state single photon sources: the nanowire antenna", Optics express **17**, 2095–2110 (2009).

[256]T. B. Hoang, G. M. Akselrod, and M. H. Mikkelsen, "Ultrafast room-temperature single photon emission from quantum dots coupled to plasmonic nanocavities", Nano letters **16**, 270–275 (2015).

[257]E Altewischer, M. Van Exter, and J. Woerdman, "Plasmon-assisted transmission of entangled photons", Nature **418**, 304–306 (2002).

[258]F. Todisco, M. Esposito, S. Panaro, M. De Giorgi, L. Dominici, D. Ballarini, A. I. Fernandez-Dominguez, V. Tasco, M. Cuscunà, A. Passaseo, et al., "Towards cavity quantum electrodynamics with hybrid photon gap-plasmon states", ACS Nano (2016).

[259]Y. Yin, Y. Lu, B. Gates, and Y. Xia, "Template-assisted self-assembly: a practical route to complex aggregates of monodispersed colloids with well-defined sizes, shapes, and structures", Journal of the American Chemical Society **123**, 8718–8729 (2001).

[260]M. Rycenga, P. H. Camargo, and Y. Xia, "Template-assisted self-assembly: a versatile approach to complex micro-and nanostructures", Soft Matter **5**, 1129–1136 (2009).

[261]Y. Xia, Y. Yin, Y. Lu, and J. McLellan, "Template-assisted self-assembly of spherical colloids into complex and controllable structures", Advanced Functional Materials **13**, 907–918 (2003).

[262]J. W. Goodman, *Introduction to fourier optics* (Roberts and Company Publishers, 2005).

[263]O. K. Ersoy, *Diffraction, fourier optics and imaging*, Vol. 30 (John Wiley & Sons, 2006).

[264]L. K. van Vugt, "Optical properties of semiconducting nanowires", PhD thesis (Utrecht University, 2007).

[265]J. Hopfield, "Theory of the contribution of excitons to the complex dielectric constant of crystals", Physical Review **112**, 1555 (1958).

[266]J. Hopfield and D. Thomas, "Theoretical and experimental effects of spatial dispersion on the optical properties of crystals", Physical Review **132**, 563 (1963).

[267]J Lagois, "Dielectric theory of interacting excitonic resonances", Physical Review B **16**, 1699 (1977).

[268]C. F. Klingshirn, *Semiconductor optics* (Springer Science & Business Media, 2012).

[269]K. J. Vahala, "Optical microcavities", Nature **424**, 839–846 (2003).

[270]K. Vahala, *Optical microcavities*, Vol. 5 (World Scientific, 2004).

[271]Q. J. Wang, C. Yan, N. Yu, J. Unterhinninghofen, J. Wiersig, C. Pflügl, L. Diehl, T. Edamura, M. Yamanishi, H. Kan, et al., "Whispering-gallery mode resonators for highly unidirectional laser action", Proceedings of the National Academy of Sciences **107**, 22407–22412 (2010).

[272]T. Kippenberg, S. Spillane, and K. Vahala, "Kerr-nonlinearity optical parametric oscillation in an ultrahigh-q toroid microcavity", Physical review letters **93**, 083904 (2004).

[273]T. J. A. Kippenberg, "Nonlinear optics in ultra-high-q whispering-gallery optical microcavities", PhD thesis (California Institute of Technology, 2004).

[274]M. R. Foreman, J. D. Swaim, and F. Vollmer, "Whispering gallery mode sensors", Advances in optics and photonics **7**, 168–240 (2015).

[275]A. Darafsheh, G. F. Walsh, L. Dal Negro, and V. N. Astratov, "Optical super-resolution by high-index liquid-immersed microspheres", Applied Physics Letters **101**, 141128 (2012).

[276]M. Gerlach, Y. P. Rakovich, and J. F. Donegan, "Nanojets and directional emission in symmetric photonic molecules", Optics express **15**, 17343–17350 (2007).

[277]S. Lecler, S. Haacke, N. Lecong, O. Crégut, J.-L. Rehspringer, and C. Hirlimann, "Photonic jet driven non-linear optics: example of two-photon fluorescence enhancement by dielectric microspheres", Optics express **15**, 4935–4942 (2007).

[278]T. Bilici, S. Isci, A. Kurt, and A Serpenguzel, "Microsphere-based channel dropping filter with an integrated photodetector", IEEE Photonics Technology Letters **16**, 476–478 (2004).

[279]A. Serpengüzel, A. Kurt, and U. K. Ayaz, "Silicon microspheres for electronic and photonic integration", Photonics and Nanostructures-Fundamentals and Applications **6**, 179–182 (2008).

[280]A. Serpengüzel and A. Demir, "Silicon microspheres for near-ir communication applications", Semiconductor Science and Technology **23**, 064009 (2008).

[281]S. Horoche and D. Kleppner, "Cavity quantum electrodynamics", Phys. Today **42**, 24 (1989).

[282]L. Rayleigh, "The problem of the whispering gallery", The London, Edinburgh, and Dublin Philosophical Magazine and Journal of Science **20**, 1001–1004 (1910).

[283]L. Rayleigh, "Ix. further applications of bessel's functions of high order to the whispering gallery and allied problems", The London, Edinburgh, and Dublin Philosophical Magazine and Journal of Science **27**, 100–109 (1914).

[284]G. Righini, Y. Dumeige, P. Féron, M. Ferrari, G Nunzi Conti, D. Ristic, and S. Soria, "Whispering gallery mode microresonators: fundamentals and applications", Rivista del Nuovo Cimento **34**, 435–488 (2011).

[285]C. F. Bohren and D. R. Huffman, *Absorption and scattering of light by small particles* (John Wiley & Sons, 2008).